iScience

CellPress
OPEN ACCESS

Article

Computational modeling of unphosphorylated CtrA:*Cori* binding in the *Caulobacter* cell cycle

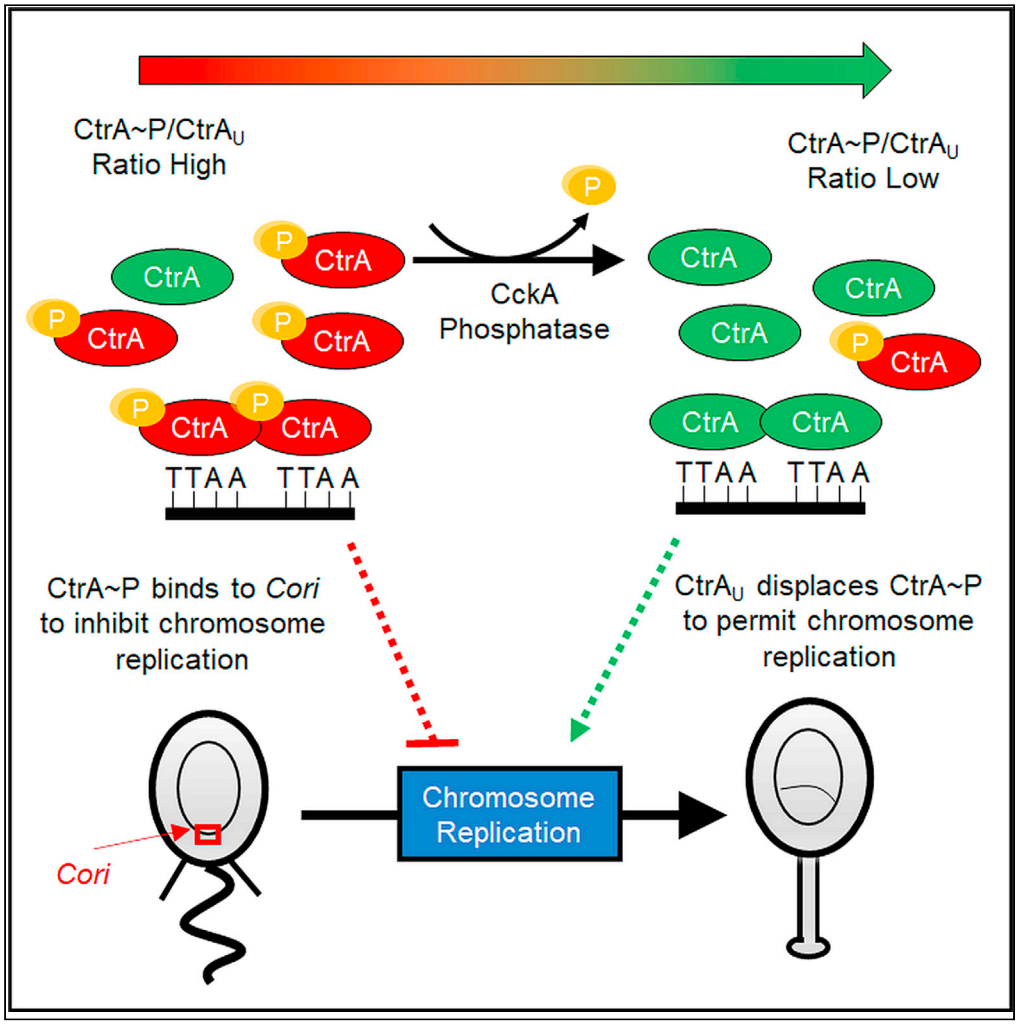

Bronson R. Weston, John J. Tyson, Yang Cao

ycao@cs.vt.edu

Highlights

CtrA$_U$ displaces CtrA~P from *Cori* at physiologically relevant concentrations

CtrA$_U$:*Cori* binding impacts chromosome replication timing by displacing CtrA~P

The viability of numerous mutant strains is dependent on CtrA$_U$:*Cori* binding

CtrA:*Cori* binding dynamics illustrates a novel motif within cellular physiology

Weston et al., iScience 24, 103413
December 17, 2021
https://doi.org/10.1016/j.isci.2021.103413

iScience

CellPress
OPEN ACCESS

Article

Computational modeling of unphosphorylated CtrA:*Cori* binding in the *Caulobacter* cell cycle

Bronson R. Weston,[1] John J. Tyson,[2] and Yang Cao[3,4,*]

SUMMARY

In the alphaproteobacterium, *Caulobacter crescentus*, phosphorylated CtrA (CtrA∼P), a master regulatory protein, binds directly to the chromosome origin (*Cori*) to inhibit DNA replication. Using a mathematical model of CtrA binding at *Cori* site [d], we provide computational evidence that $CtrA_U$ can displace CtrA∼P from *Cori* at the G1-S transition. Investigation of this interaction within a detailed model of the *C. crescentus* cell cycle suggests that CckA phosphatase may clear *Cori* of CtrA∼P by altering the [$CtrA_U$]/[CtrA∼P] ratio rather than by completely depleting CtrA∼P. Model analysis reveals that the mechanism allows for a speedier transition into S phase, stabilizes the timing of chromosome replication under fluctuating rates of CtrA proteolysis, and may contribute to the viability of numerous mutant strains. Overall, these results suggest that $CtrA_U$ enhances the robustness of chromosome replication. More generally, our proposed regulation of CtrA:*Cori* dynamics may represent a novel motif for molecular signaling in cell physiology.

INTRODUCTION

The accurate duplication of chromosomes and their exact partitioning to daughter cells are foundational to the perpetuation of life. In the freshwater bacterium, *Caulobacter crescentus*, the cycle of chromosome replication and partitioning is inextricably linked to an asymmetric cytokinesis process that divides a motile 'swarmer' cell from its parental, sessile 'stalked' cell. The processes of DNA replication, cell differentiation and division are managed by four master regulators: CtrA, GcrA, CcrM and DnaA (Laub et al., 2007). These proteins influence each other and the chromosome origin (*Cori*), both directly and indirectly, to coordinate progression through the cell cycle (Figure 1A). Specifically, CtrA∼P binds to *Cori* to inhibit the initiation of DNA replication (Jacobs et al., 1999; Quon et al., 1998), whereas DnaA-ATP binds to *Cori* to activate DNA replication (Wargachuk and Marczynski, 2015). DnaA and CtrA are indispensable for proper regulation of DNA synthesis. CcrM methylates *Cori*, perhaps to increase its activity, although this interaction is not essential for chromosome replication (Gonzalez et al., 2014). The fourth master regulator, GcrA, does not directly interact with *Cori*, but regulates numerous genes involved with the replication machinery (Holtzendorff et al., 2004). While GcrA is not essential for viability, Δ*gcrA* mutants have significantly slower cell cycles (Murray et al., 2013).

The activities of DnaA and CtrA are tightly regulated by three mechanisms: Gene expression, post-translational modifications, and proteolysis. First, the promoters of *ctrA* and *dnaA* are regulated, in part, by methylation sites. Upon DNA replication, the chromosome becomes hemi-methylated resulting in reduced activity of the *dnaA* promoter and increased activity of the *ctrA* P1 promoter (Laub et al., 2007; Reisenauer and Shapiro, 2002). CcrM, in turn, re-methylates these gene-promoter regions in G2 phase of the cell cycle (Stephens et al., 1996). Additionally, GcrA directly interacts with the *ctrA* P1 promoter to activate transcription (Holtzendorff et al., 2004) and with the *dnaA* promoter to inhibit transcription (Holtzendorff et al., 2004). CtrA, in turn, binds to its own P1 promoter to inhibit transcription, but activates transcription from its P2 promoter (Domian et al., 1999). Second, both CtrA and DnaA have active forms (CtrA∼P and DnaA-ATP) and inactive forms ($CtrA_U$ and DnaA-ADP). DnaA-ATP induces chromosome replication (Wargachuk and Marczynski, 2015); and, promptly after replication is initiated, the active DNA polymerase complex recruits an enzyme, HdaA, that hydrolyzes DnaA-ATP to DnaA-ADP to ensure that the chromosome replicates only once per cell cycle (Fernandez-Fernandez et al., 2011, 2013). In the pre-replicative phase, CtrA∼P binds with *Cori* to block chromosome replication (Quon et al., 1998; Reisenauer et al., 1999). At the G1-S transition, a bifunctional kinase/phosphatase, CckA, dephosphorylates CtrA∼P to enable

[1]Program in Genetics, Bioinformatics, and Computational Biology, Virginia Tech, Blacksburg, VA, USA

[2]Department of Biological Sciences, Virginia Tech, Blacksburg, VA, USA

[3]Department of Computer Science, Virginia Tech, Blacksburg, VA, USA

[4]Lead contact

*Correspondence: ycao@cs.vt.edu

https://doi.org/10.1016/j.isci.2021.103413

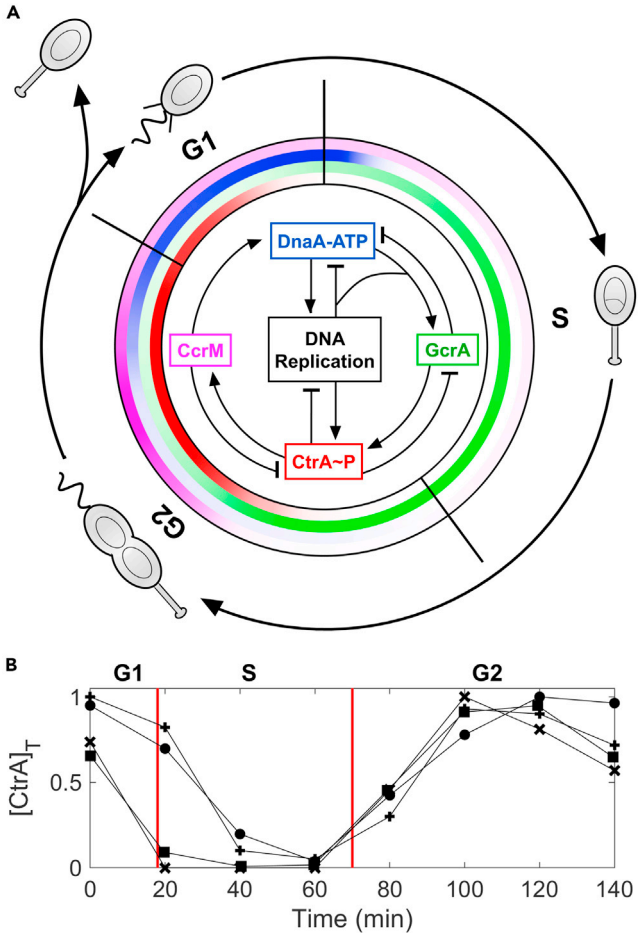

Figure 1. Master regulators control progression through the *C. crescentus* cell cycle

(A) The dimorphic lifestyle of *C. crescentus* is divided into three phases (G1, S, and G2). G1 is characterized by a swarmer phenotype, expressing a flagellum and pili. When DNA replication is initiated, the cell transitions into S phase, simultaneously releasing its swarmer organelles and synthesizing a stalk. As the cell completes DNA replication, the cell transitions into G2 and synthesizes a flagellum at the new pole. When the cell divides, the stalked daughter cell immediately enters S phase and the swarmer cell enters G1. This process is orchestrated by the cyclical expression of four master regulators (DnaA, GcrA, CcrM, and CtrA) and their interactions with each other and with DNA. Barbed arrows designate positive interactions and blunt connectors represent inhibition. The inner circle indicates the timing of expression of each master regulator (according to its color code).

(B) The expression pattern of normalized CtrA level at the G1-S transition varies significantly between experiments, but not much at the S-G2 transition. Vertical red lines separate phases of the cell cycle. Data points represent western blot data from synchronized populations, quantified with ImageJ (x, Collier et al., 2006, Figure 5A) (■, Holtzendorff et al., 2004, Figure 3B) (●, McGrath et al., 2006, Figure 3A) (+, Domian et al., 1997, Figure 1A).

chromosome replication (Chen et al., 2009). The third strategy by which *Caulobacter* regulates DnaA and CtrA is proteolysis. DnaA is degraded by Lon and ClpP proteases (Gorbatyuk and Marczynski, 2005; Jonas et al., 2013) while CtrA is degraded by ClpXP with the help of its associated adaptors, cyclic-di-GMP (cdG), PopA, RcdA and CpdR (Smith et al., 2014).

Given the variety of regulatory mechanisms governing the activities of DnaA and CtrA, one might expect consistent, tight control over DnaA and CtrA levels. While this is true for DnaA, it seems not to be so for CtrA. Comparison of CtrA western blots from different synchronization experiments (Figure 1B) reveals that CtrA expression at the G1-S transition varies dramatically between populations. While for some synchronized populations CtrA is mostly cleared by 20 min (Collier et al., 2006; Holtzendorff et al., 2004; Mignolet et al., 2016), in other populations it is not cleared until 40–60 min after birth of the swarmer

cell (Domian et al., 1997; McGrath et al., 2006; Radhakrishnan et al., 2008). Importantly, these experiments all indicate similar timing in the re-accumulation of CtrA (~80 min), in the timing of swarmer-to-stalk differentiation (~30–40 min), and in total cell cycle times of ~140–160 min, suggesting consistency in the timing of chromosome replication despite inconsistency in CtrA levels at the G1-S transition. It appears that chromosome replication may be initiated at CtrA concentrations ranging from 0–80% of maximal expression in wild type cells. Assuming a swarmer cell volume of 1 μm^3 (Harris and Theriot, 2016; Spencer et al., 2009; Terrana and Newton, 1975) and peak CtrA expression levels of ~20,000 molecules (Judd et al., 2003; Spencer et al., 2009), this corresponds to a range of 0–24 μM. In agreement with this conclusion, an experiment that simultaneously tracked DNA methylation and CtrA concentration in a synchronized population showed that chromosome replication was initiated when the CtrA concentration was approximately 50% of maximal (Quon et al., 1998). These observations contradict the typical narrative of *Caulobacter* cell-cycle progression, which posits rapid and complete proteolysis of CtrA at the G1-S transition (Domian et al., 1997; Hung and Shapiro, 2002; Ryan et al., 2002; Skerker and Laub, 2004).

Various studies report that chromosome replication begins approximately 15 min into the swarmer cell cycle (Brassinga and Marczynski, 2001; Jensen, 2006; Quon et al., 1998). The observed facts of (1) great consistency in the timing of the G1-S transition and (2) inconsistency in CtrA concentration at the G1-S transition suggest that the timely onset of S phase is primarily a consequence of CtrA~P dephosphorylation rather than proteolysis. However, CtrA~P has an extremely strong affinity for *Cori*, $K_d \approx 0.006$ μM (Siam and Marczynski, 2000), which suggests that a very active phosphatase would be required to clear CtrA~P from *Cori*. For example, if total CtrA concentration were half maximal (~15 μM), then 50% occupancy of *Cori* binding sites by CtrA~P would correspond to a 1/2500 ratio of CtrA~P to $CtrA_U$. While the threshold occupancy required to inhibit DNA replication is unclear, one study suggests that it may lie somewhere between 57% and 13% (Taylor et al., 2011). If so, then, under prior conceptions of *Cori* regulation, CckA phosphatase would consistently have to achieve a CtrA~P/$CtrA_U$ ratio of 1:2500 (and this is a modest estimate) at the G1-S transition. One may consider that CtrA~P could cling to other DNA binding sites during the G1-S transition, providing protection for *Cori*. However, a mathematical analysis of CtrA:DNA binding suggests that other DNA binding sites would make a relatively negligible impact on CtrA binding to *Cori* (see "Considering Increased Complexity of CtrA:DNA Binding" in STAR Methods).

Such an intense demand on CckA phosphatase seems far-fetched for three reasons. First, CckA is a bifunctional kinase/phosphatase, and it is unlikely that CckA could be partitioned so completely toward the phosphatase form to result in such an extreme CtrA~P/$CtrA_U$ ratio. Indeed, evidence suggests that detectable levels of phosphorylated CckA and CtrA persist throughout the G1-S transition (Beroual et al., 2019; Domian et al., 1997; Jacobs et al., 2003). Second, assuming a swarmer cell volume of 1 μm^3 (Harris and Theriot, 2016; Spencer et al., 2009; Terrana and Newton, 1975), a concentration of 0.006 μM corresponds to 3 or 4 CtrA~P molecules per cell. However, there are five CtrA binding sites on *Cori*, each of which has two CtrA binding sequences (a total of 10 CtrA binding recognition sequences) (Siam and Marczynski, 2000), so the *Cori* binding sites would be less than half occupied at 0.006 μM even if the binding were infinitely strong. In other words, the physiology of the *Cori* locus suggests that CtrA~P levels greater than 0.006 μM are required to saturate *Cori*. Third, if CtrA~P were to be depleted to such low levels to clear *Cori*, we would likely observe highly stochastic timing of chromosome replication, especially considering the variability in the expression pattern of CtrA among experiments, as even one CtrA~P molecule would make a significant difference in *Cori* binding. However, as mentioned earlier, the initiation of chromosome replication seems to be quite tightly regulated.

The incongruencies among these experimental observations merit a closer look into the regulation of CtrA and its interaction with *Cori*. In this article, we build a mathematical model to simulate the interactions of CtrA at *Cori* site [d] (one of the five CtrA binding sites). We identify a new role for the unphosphorylated form of CtrA at the G1-S transition; specifically, we propose that $CtrA_U$ interacts with *Cori* (dubbed $CtrA_U$:*Cori* binding) to interfere with CtrA~P:*Cori* binding. Our simulations suggest that this competitive inhibition would substantially alleviate the demand on CckA phosphatase (by ~70 fold) at the G1-S transition. We extend our study by developing a detailed mathematical model of the *Caulobacter* cell cycle to investigate how the interaction of $CtrA_U$ with *Cori* might impact cell cycle progression. Our model suggests that the $CtrA_U$:*Cori* interaction (1) enables a more prompt entry into S phase, (2) ensures consistent timing of chromosome replication given variations in CtrA proteolysis rates, and (3) enhances the robustness of the cell cycle to various mutations. In the Discussion, we suggest that the roles played by CtrA~P and $CtrA_U$ in

regulating DNA replication may be representative of a more general motif for molecular signaling within cells.

RESULTS

While CtrA∼P is known to repress chromosome replication, how unphosphorylated CtrA fits into the regulatory picture is not clear. Several mutant strains that eliminate CtrA proteolysis, such as Δ*rcdA*, Δ*popA*, and *ctrA*Δ*3*Ω, each have normal cell cycles (Domian et al., 1997; Duerig et al., 2009; McGrath et al., 2006). In contrast, a mutant strain that expresses non-proteolizable CtrA that cannot be inactivated via dephosphorylation, *ctrAD51E*Δ*3*Ω, exhibits G1 arrest (Domian et al., 1997). Thus, CtrA proteolysis-null strains must be viable as a consequence of CtrA dephosphorylation at the G1-S transition. However, evidence suggests that unphosphorylated CtrA binds strongly to *Cori*. Studying the association of $CtrA_U$ with the five *Cori* binding sites [a-e], Siam and Marczynski (2000) measured K_d values of 0.2–0.6 μM. In comparison, typical CtrA expression levels reach ∼25 μM in pre-divisional cells and ∼12.5 μM in swarmer cells (Harris and Theriot, 2016; Judd et al., 2003; Spencer et al., 2009; Terrana and Newton, 1975). Furthermore, CtrA levels are likely to be higher than normal in CtrA proteolysis-null mutant strains. Intuitively, $CtrA_U$ must be bound to *Cori* throughout the G1-S transition in these strains. Therefore, we conclude that $CtrA_U$:*Cori* binding does not arrest chromosome replication. (See the "Discussion" section for a more extensive evaluation of the literature.)

As discussed previously, we find it unlikely that in the absence of CtrA proteolysis CckA phosphatase could reduce CtrA∼P to concentrations well below the experimentally measured dissociation constant. However, given our conclusion that $CtrA_U$:*Cori* binding does not impair chromosome replication and that CckA phosphatase activity must somehow be sufficient for the G1-S transition in CtrA proteolysis-null mutants, we propose that $CtrA_U$ competes with CtrA∼P for *Cori* binding sites to promote chromosome replication. To investigate this hypothesis, we set out to build a mathematical model of CtrA:*Cori* binding. We find that sufficient experimental data from Siam and Marczynski (2000) is available to build a detailed model at site [d], but not other *Cori* binding sites. Specifically, the half-site mutation analysis at site [d] provides us with the necessary data to build a realistic model of site [d] (see STAR Methods "CtrA:*Cori* Binding"). As *Cori* binding sites are generally very similar (see Discussion for an in depth reflection), an analysis of site [d] will also provide key insight into the binding dynamics at other *Cori* binding sites.

$CtrA_U$ competes with CtrA∼P for *Cori* binding sites

CtrA recognizes the nucleic acid sequence TTAA. Each *Cori* binding site has two CtrA recognition sequences, generally characterized as TTAA-N7-TTAA. Mutation experiments at site [d] indicate that the affinity of a single CtrA molecule for a single *Cori* binding site is not affected by phosphorylation, but the cooperative binding of CtrA molecules to bipartite sites is affected by phosphorylation (Siam and Marczynski, 2000). Figure 2A illustrates the different possibilities of CtrA binding to a TTAA-N7-TTAA motif along with their corresponding equilibrium relationships. Note: we assume that the number of CtrA molecules bound to DNA relative to freely diffusing molecules is negligible, as justified in the STAR Methods.

Using Siam and Marczynski's experiments on site [d] to parameterize our *Cori* binding model (see STAR Methods), we find that our model agrees quite well with their data (Figure S1). We find that the first binding step of CtrA molecules to site [d] is weak ($K_{d1} \approx$ 1.06 μM) and independent of phosphorylation. If the first occupant is $CtrA_U$, then binding of the second molecule of $CtrA_U$ is weakly cooperative ($K_{d2} \approx$ 39 nM); however, if the first occupant is CtrA∼P, then binding of the second molecule of CtrA∼P is strongly cooperative ($K_{d3} \approx$ 0.085 nM). That is to say, the level of cooperativity between CtrA∼P molecules is ∼460-fold stronger than between $CtrA_U$ molecules ($K_{d3} = K_{d2}/460$). In the absence of data to determine the cooperativity between CtrA∼P and $CtrA_U$ for bipartite sites, we assume that the cooperativity is equivalent to the binding between two $CtrA_U$ molecules (K_{d2}).

Because $K_{d3} << K_{d2}$, it might seem unlikely that $CtrA_U$ competes significantly with CtrA∼P for *Cori* binding sites at the G1-S transition, but this expectation is unfounded. Using a range of physiologically relevant concentrations of $CtrA_U$ and CtrA∼P, we simulate the relative occupancy of the *Cori* site [d]-states depicted in Figure 2A. The patterns illustrated by the heat maps in Figure 2B show that the concentration of *Cori* site [d] saturated by CtrA∼P (i.e., [DNA:CtrA∼P_2]) decreases significantly as the concentration of $CtrA_U$ increases. Meanwhile, the concentration of $CtrA_U$ bound DNA (i.e., [DNA:$CtrA_{U2}$]) increases. The

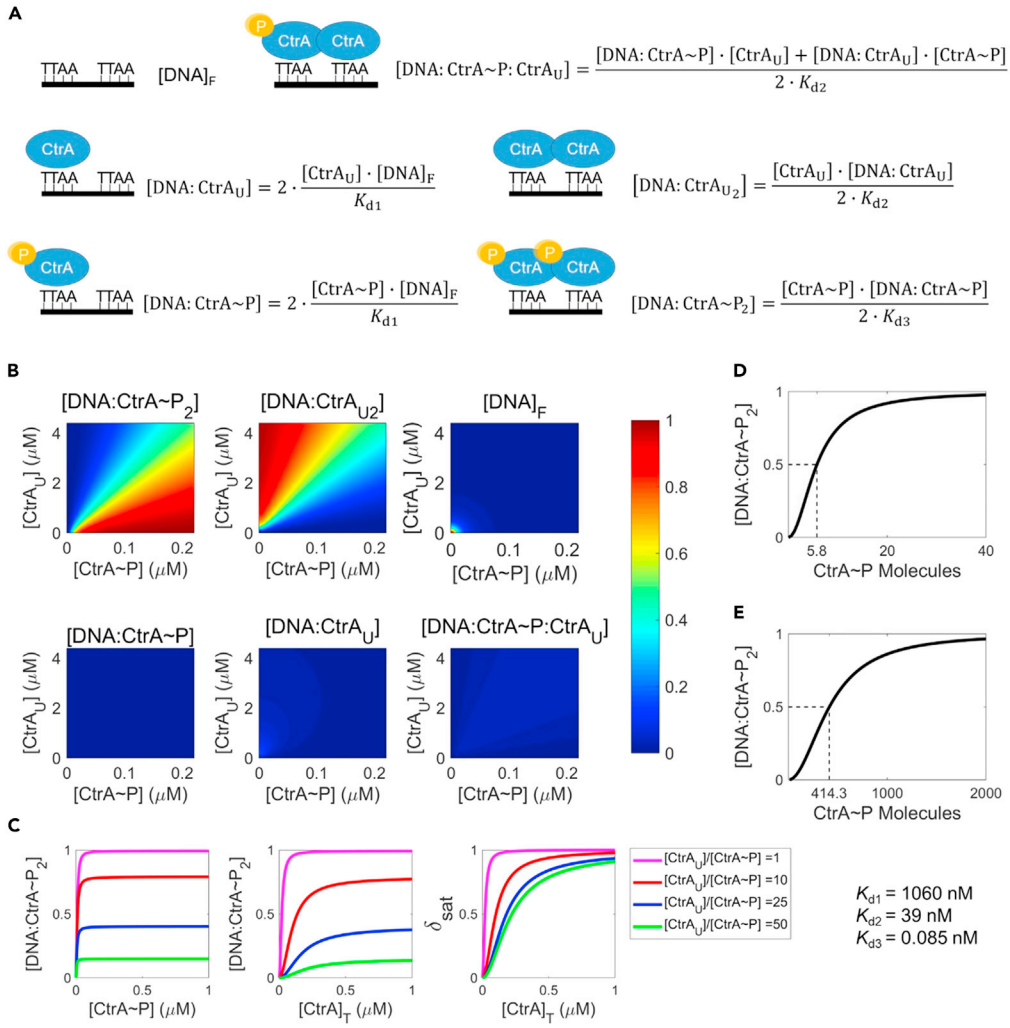

Figure 2. Unphosphorylated CtrA competes with CtrA~P for *Cori* binding sites

(A) CtrA (unphosphorylated) and CtrA~P bind to Cori site [d] in different combinations. Each combination (or state) is defined by an equilibrium expression, and the sum of all the different occupation states of Cori ≡ $[DNA]_T$ = 1 (by definition). Estimated values for the dissociation constants are presented in the lower-right corner.

(B) The probability of each possible state (from A) was calculated over a range of concentrations,$[CtrA_U]$ and [CtrA~P]. Results are represented by a heatmap, where the color corresponds to the fractional occupancy of the state, as depicted by the color bar on the right.

(C) $[DNA:CtrA\sim P_2]$ is a function of the $[CtrA_U]$/[CtrA~P] ratio and the concentration of all CtrA species (unphosphorylated and phosphorylated), $[CtrA]_T = [CtrA_U] + [CtrA\sim P]$. δ_{sat} reflects the current concentration of $DNA:CtrA\sim P_2$ divided by the maximum level possible at the given $[CtrA_U]$/[CtrA~P].

(D) Simulation of the $[DNA:CtrA\sim P_2]$ state as a function of CtrA~P molecules per cell when all CtrA molecules are phosphorylated. Assumed volume of cell is 1 μm^3.

(E) Simulation of $[DNA:CtrA\sim P_2]$ as a function of CtrA~P molecules per cell when unphosphorylated CtrA molecules are present. In these calculations, $[CtrA]_T$ = 15 μM. For an assumed volume of cell of 1 μm^3, the number of unphosphorylated CtrA molecules = 10,000 –number of CtrA~P molecules.

See also Figures S1 and S2.

concentrations of the other forms (e.g.,[DNA:CtrA~P:$CtrA_U$]) are negligible. These results support our hypothesis that $CtrA_U$ can displace CtrA~P at *Cori* binding sites at physiologically relevant concentrations.

To further investigate how the ratio of $CtrA_U$ to CtrA~P, $[CtrA_U]$/[CtrA~P], impacts *Cori*, we simulate site [d]-binding over a range of CtrA~P concentrations while holding the ratio constant (Figure 2C, left panel). We find that $[DNA:CtrA\sim P_2]$ is relatively independent of [CtrA~P] but is highly dependent on $[CtrA_U]$/

[CtrA∼P]. This statement remains true until concentrations of CtrA∼P are very low (<0.02 μM), at which point *Cori* is rapidly freed from CtrA binding. This result is consistent with the patterns in Figure 2B, as the shading is relatively constant when moving away from the graph origin in a radial direction. This behavior emphasizes the importance of $CtrA_U$:*Cori* binding. While decreasing CtrA∼P concentration (short of complete depletion) has a negligible impact on CtrA∼P binding to *Cori*, adjusting the $[CtrA_U]$/[CtrA∼P] ratio has a large effect, due to the competition between $CtrA_U$ and CtrA∼P for *Cori* binding sites.

Next, we compare how [DNA:CtrA∼P_2] depends on the total CtrA level, $[CtrA]_T$, at several fixed $[CtrA_U]$/[CtrA∼P] ratios (Figure 2C middle panel). Similar to the [DNA:CtrA∼P_2] *vs* [CtrA∼P] curve (Figure 2C left panel), [DNA:CtrA∼P_2] saturates with increasing $[CtrA]_T$, and the saturation limit (or maximum) of [DNA:CtrA∼P_2] decreases as $[CtrA_U]$/[CtrA∼P] increases. We also find that at higher $[CtrA_U]$/[CtrA∼P] ratios, the approach of [DNA:CtrA∼P_2] to maximum levels is less responsive to increasing $[CtrA]_T$ concentrations. However, correct interpretation of these curves is difficult because the maximum value of [DNA:CtrA∼P_2] depends on the $[CtrA_U]$/[CtrA∼P] ratio. To resolve this complication, we define a new metric, δ_{sat}, which measures [DNA:CtrA∼P_2] relative to the maximum [DNA:CtrA∼P_2] for a given $[CtrA_U]$/[CtrA∼P] ratio:

$$\delta_{sat} = \frac{[\mathrm{DNA} : \mathrm{CtrA} \sim P_2]}{\max([\mathrm{DNA} : \mathrm{CtrA} \sim P_2])},$$

where max([DNA:CtrA∼P_2]) is the limiting concentration of DNA:CtrA∼P_2 at sufficiently large $[CtrA]_T$ and fixed $[CtrA_U]$/[CtrA∼P] ratio. We estimate the max([DNA:CtrA∼P_2]) by calculating [DNA:CtrA∼P_2] when $[CtrA]_T$ = 100 μM. The δ_{sat} *vs* $[CtrA]_T$ curve (Figure 2C right panel) clearly shows that as $[CtrA]_T$ decreases, CtrA∼P saturation of *Cori* binding sites (relative to the maximum possible saturation) is cleared at a faster rate at higher $[CtrA_U]$/[CtrA∼P] ratios. Given that max([DNA:CtrA∼P_2]) is also much lower at higher ratios, there is a clear synergy between proteolysis (i.e., reducing $[CtrA]_T$) and dephosphorylation (i.e., increasing the $[CtrA_U]$/[CtrA∼P] ratio) in determining CtrA∼P binding to *Cori*.

Next, we compare our results to those of Siam and Marczynski, who estimated dissociation constants by fitting hyperbolic curves, i.e., $K_d/(K_d + [CtrA])$, to their experimental data. As mentioned, they estimated that CtrA∼P interacts with site [d] with K_d = 0.006 μM, which translates to 3 or 4 CtrA∼P molecules per cell, given a cell volume of 1 μm^3. The estimation produced by our model is very similar when $CtrA_U$ is absent, suggesting that site [d] is 50% saturated by CtrA∼P at concentrations corresponding to approximately 6–12 molecules per cell (Figures 2D and S2). However, when we fix $[CtrA]_T$ = 15 μM = 10^4 molecules per cell, and vary CtrA∼P level (Figure 2E), we find that site [d] is ∼50% occupied at CtrA∼P ≈ 414 molecules per cell (∼0.7 μM). This translates to a [CtrA∼P]/$[CtrA_U]$ ratio of approximately 1:20, which seems far more achievable for the bifunctional CckA kinase/phosphatase than the ratio of 1:2500 estimated earlier.

Caulobacter cell cycle model is extended to include $CtrA_U$:*Cori* interaction

In consideration of our findings in the previous section, we now investigate the potential roles of $CtrA_U$:*Cori* binding on cell cycle progression in *C. crescentus*. Inspired by earlier computational models of Li et al. (2009) and Subramanian et al. (2013), we develop a new mathematical model, based on ordinary differential equations (ODEs), to capture the dynamics of the molecular mechanism governing progression through the *Caulobacter* cell cycle. As with Li's model, our model encompasses protein-protein interactions, protein phosphorylation, DNA methylation, protein-DNA interactions, genetic expression, proteolysis, cytokinesis, and chromosome replication. We also introduce bifunctionality to the histidine kinase/phosphatase enzymes, PleC and CckA, as was done previously by Subramanian et al. We improve the model's representation of CtrA degradation by adding important molecular components, most notably the second-messenger molecule, cdG, which is an essential component to the CtrA proteolysis complex and interacts with CckA to induce its phosphatase state. Figure 3 details the regulatory interactions of the model. For a full description of the model, see STAR Methods.

In light of the experimental diversity of CtrA expression (Figure 1B), we study two different parameterizations of our model: 'Slow' parameter sets, characterized by sluggish CtrA proteolysis extending well into S phase (Figure 4A, top panel), and 'Quick' parameter sets, characterized by rapid proteolysis of CtrA at the G1-S transition (Figure 4B, top panel). Using the fitting procedure explained in STAR Methods, we obtained 918 and 1,151 sets of Slow and Quick parameters, respectively. Briefly, these parameter sets were optimized by fitting simulations of seventeen variables (Table S1) to time course data for wild-type (WT)

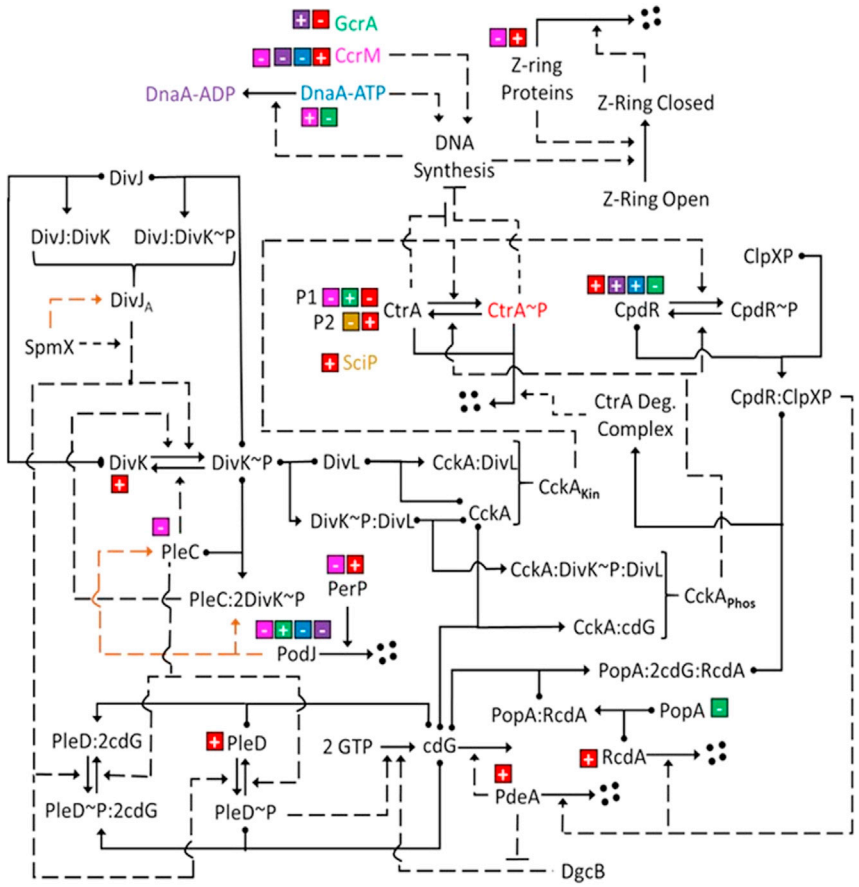

Figure 3. Wiring diagram of the molecular mechanisms underlying the cell cycle model of *C. crescentus*

Genetic regulation is depicted by a color-coded scheme: for each protein that interacts with a promoter, a box with a plus or minus sign indicates whether the protein activates or inhibits expression of the gene, respectively, and the color of the box identifies the regulatory protein (e.g., green = GcrA). Proteins that combine to form complexes are marked by solid dots on the arms of a T-shaped arrow pointing to the resulting complex (e.g., PopA and RcdA form the PopA:RcdA complex). The chemical conversion of one molecular species to another is indicated by an arrow (e.g., CtrA to CtrA~P). Proteolysis is depicted by an arrow from a protein to four black circles. Dashed arrows indicate an 'influence' (e.g., catalysis) of a protein on a chemical reaction (e.g., PleC dephosphorylates DivK~P). A dashed orange arrow indicates that one molecule influences the localization of another (e.g., PodJ affects the location of PleC).

swarmer cells, plotted in Figures 4A, 4B, S3, and S4, and to the phenotypes (viable or arrested) of swarmer and stalked cells in a collection of 11 mutant strains (red font in Figure 5A).

To assess the predictive power of our model, we simulated swarmer and stalked phenotypes for 24 additional mutant strains (black font in Figure 5A) and evaluated whether our model correctly predicts the cell cycle to be viable or arrested. Notably, the viability of certain mutants (such as Δ*gcrA* and Δ*ccrM*) varies depending on the cell culture medium and the corresponding growth rate. In such scenarios, we consider the case of slow growth conditions in M2G medium. Details of each mutant strain are found in Table S2. Figure 5A reports the fraction of simulations that fail to correctly predict strain viability or non-viability for each mutant strain. Considering mutant strain simulations that correctly predict cell viability more than 75% of the time to be successful predictions, we find that the QUICK and SLOW parameter sets perform equally well (88.9% strain success rate in Figure 5B).

Unphosphorylated CtrA interacts with *Cori* to ensure timely initiation of chromosome replication

To investigate the impact of $CtrA_U$:*Cori* binding on cell cycle progression, we first examine the effects of removing the $CtrA_U$:*Cori* interaction from WT cells (referred to as a 'WT−$CtrA_U$:*Cori*' simulation) on the

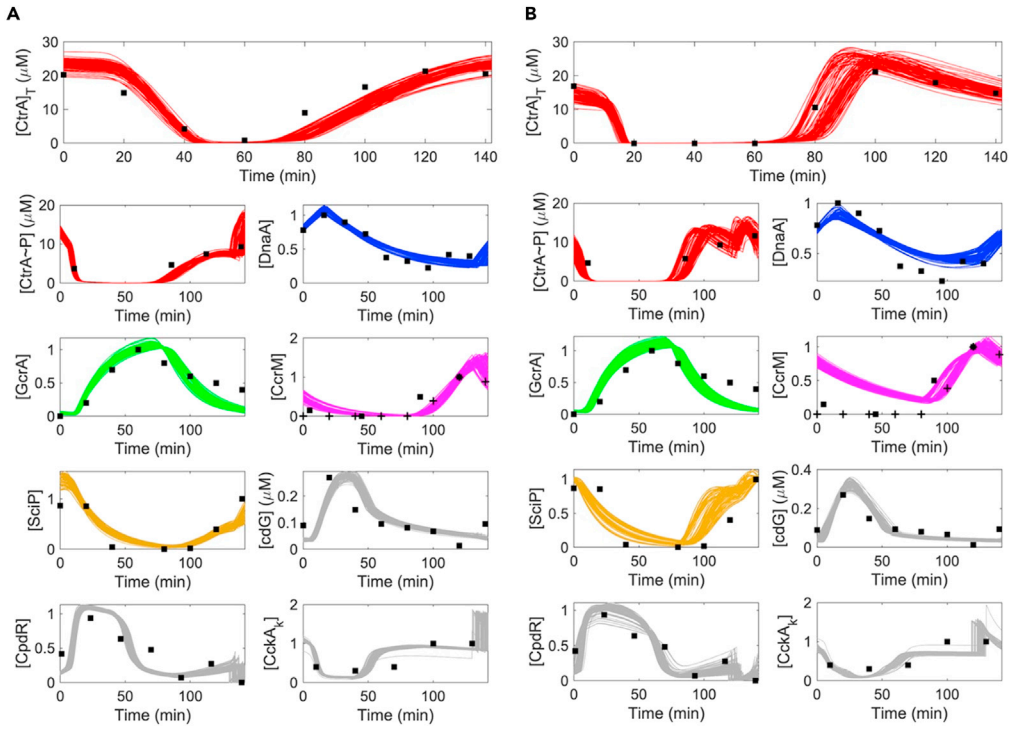

Figure 4. Swarmer cell simulations with both Slow and Quick parameter sets fit experimental data well

(A) For 100 randomly selected Slow parameter sets, we plot swarmer-cell simulations in comparison to experimental data, using the same color code as in Figure 3. The large spikes in [CckA$_K$] and [CpdR] near the end of the cell cycle (when the Z-ring closes) are artifacts of our modeling methodology (see STAR Methods for details). Data collected as follows:[CckA$_K$]: Jacobs et al., (2003), Figure 3A; [CpdR]: Iniesta et al., (2006), Figure 5A;[cdG]: Abel et al., (2013), Figure 7;[SciP]: Tan et al. 2010, Figure 1B;[CcrM]:+, Zhou and Shapiro, 2018, Figure 2A;[CcrM]: ■, Grünenfelder et al., 2001, Figure 2;[GcrA]: Holtzendorff et al., (2004), Figure 3B;[DnaA]: Cheng and Keiler (2009), Figure 2C;[CtrA~P]: Jacobs et al., (2003), Figure 3A (second data point removed);[CtrA]$_T$: McGrath et al., 2006, Figure 2C. In most graphs, protein concentrations are plotted relative to the maximum abundance observed in the experimental data. cdG concentration is not normalized, because absolute concentration was measured in the experiments. CtrA$_T$ and CtrA~P concentrations in μM are predictions of our model; the experimental data (in terms of relative abundances) are scaled by a common factor to align with the predicted waveform.

(B) Same as (A), for 100 Quick parameter sets. Experimental data are the same, except for [CtrA]$_T$ acquired from Collier et al., (2006), Figure 5A.

See also Table S1 and Figures S3, S4, and S6.

timing of chromosome replication (t^{cr}) (see STAR Methods "Chromosome replication" on details of modeling chromosome replication). We observe large differences in t^{cr} between our WT and WT−CtrA$_U$:*Cori* simulations (Figures 6A and 6C) for the Slow parameter sets (Δt^{cr} = 23 min) and smaller delays for the Quick parameter sets (Δt^{cr} = 2 min). These delays indicate that CtrA$_U$:*Cori* binding influences the timing of the G1-S transition, but the degree of influence is a function of the proteolysis rate.

To investigate these findings further, we decreased the rate of proteolysis in Quick WT simulations to find that proteolysis makes very little difference in t^{cr} in WT cells (Figure 6D). However, in the WT−CtrA$_U$:*Cori* simulations, t^{cr} increases substantially as the proteolysis rate decreases. This suggests that CtrA$_U$:*Cori* binding stabilizes the timing of chromosome replication when proteolysis is perturbed.

Next, we investigate the timing of cell division (t^{div}) of WT and WT−CtrA$_U$:*Cori* simulations. We find that Slow and Quick parameter sets predict average delays (Δt^{div}) of approximately 15 and 0.53 min, respectively (Figure 6C). The fact that delays in cell division are shorter than delays in chromosome replication (Δt^{cr}) suggests that delays in the G1-S transition are partially compensated in the S and G2 stages of the cell cycle. Upon inspection, we found that no single interaction of the model is responsible for this

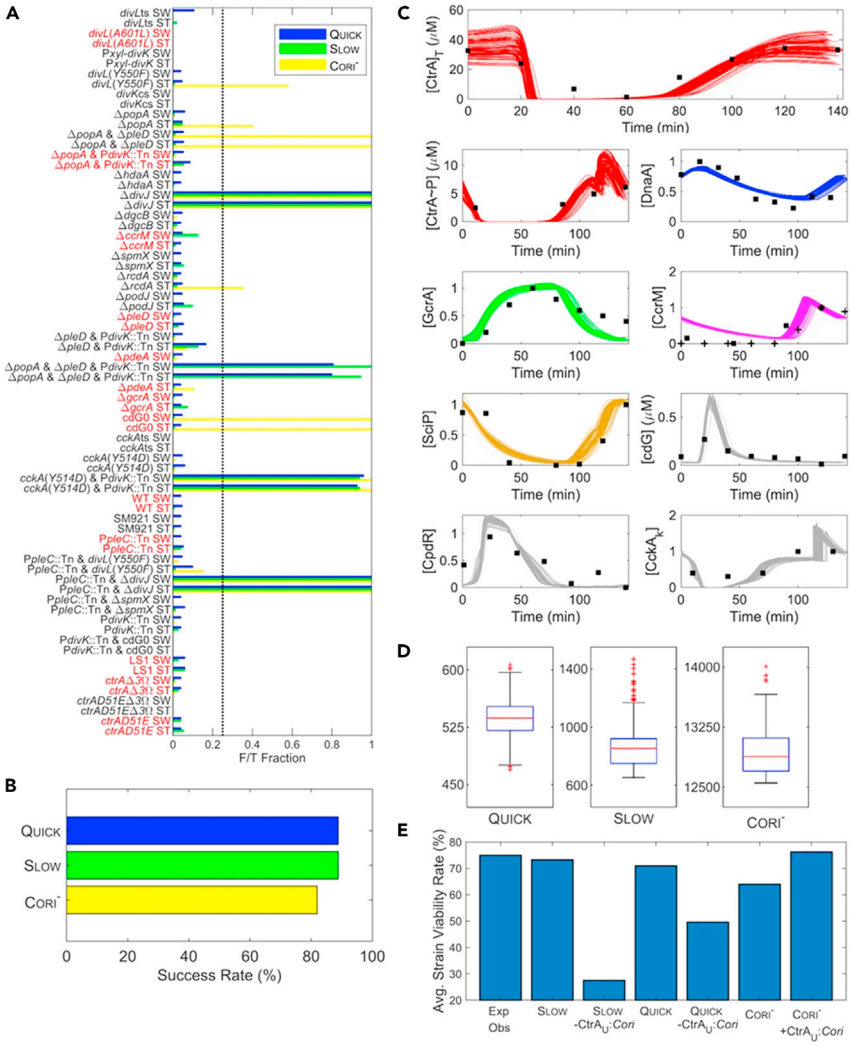

Figure 5. Parameter sets agree well with experimentally observed viability of mutant strains

(A) For three distinct parameter-set collections (QUICK, SLOW and CORI⁻), we plot the fraction (F/T) of total simulations that failed to correctly predict the phenotype (viable or inviable) of swarmer (SW) and stalked (ST) cells for 34 mutant strains and wild-type (WT) cells. See Table S2 for details on mutant simulations. For each strain, 150 parameter sets were chosen at random from each parameter-set collection and simulated for both swarmer and stalked cells. The dotted vertical line corresponds to an arbitrary threshold (25%) that we use to compute the success rate of predictions for the QUICK, SLOW, and CORI⁻ parameter sets. Strains labeled with red font were included in the cost function for estimating parameter values in the three collections of parameter sets.

(B) QUICK and SLOW parameter sets successfully capture strain viability behavior in 88.6% of all simulated strains; CORI⁻ parameter sets are successful in 81.4% of cases. A strain simulation is considered successful if 75% or more of simulations agree with experimental observations of strain viability/inviability.

(C) Plot of 100 swarmer cell simulations from the CORI⁻ parameter sets. Experimental data and methodology is the same as Figure 4A.

(D) Box plots of the cost distribution for each parameter-set collection. Red horizontal line indicates median cost, blue box indicates the interquartile range (IQR), whiskers are set to 1.5×IQR, and outliers are indicated by red '+' markers. Medians values are approximately 540, 850, and 12,900 for the QUICK, SLOW, and CORI⁻ parameter sets, respectively. The range of the vertical axis hides some outliers of the SLOW and CORI⁻ boxplots; the greatest costing outliers are ~3,600 and ~15,700 for the SLOW and CORI⁻ parameter sets, respectively.

(E) The average strain viability rate is calculated as the sum of all viable simulations divided by the total number of simulations for all strains in (A). Simulations were run with and without the $CtrA_U$:*Cori* interaction as indicated. The fraction of strains that are reported as viable experimentally (Exp Obs) is reported for comparison.

See also Tables S1 and S2, as well as Figures S5 and S6.

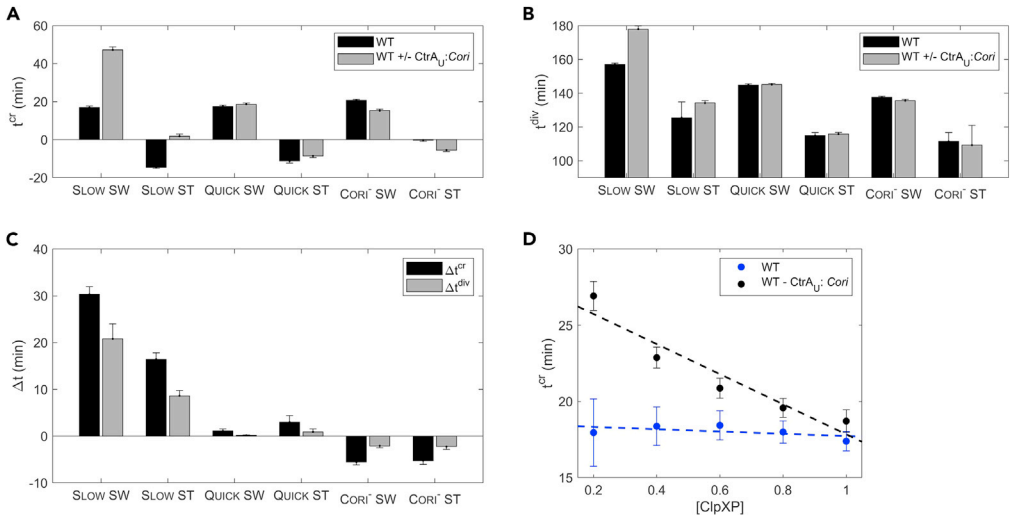

Figure 6. Chromosome replication and cell division times are influenced by the interaction of unphosphorylated CtrA with *Cori* binding sites

(A and B) Bar graphs report the average time from cell division to the initiation of chromosome replication (t^{cr}) and to cell division (t^{div}) in simulations of WT cells, with and without the CtrA$_U$:*Cori* interaction. Gray bars represent WT–CtrA$_U$:*Cori* for Slow and Quick parameter sets and represent WT + CtrA$_U$:*Cori* for Cori$^-$ parameter sets. t^{cr} and t^{div} are calculated as the time difference between the end of the previous cell cycle and the corresponding event time. Negative times for t^{cr} indicates that chromosome replication begins after the Z-ring closes but before the daughter cells separate. The error bars indicate standard deviations.

(C) For each cell we compare the WT and WT+/−CtrA$_U$:*Cori* simulations (as indicated in A and B) and plot the average differences in chromosome replication time and cell division. Error bars indicate standard deviations.

(D) Timing of chromosome replication was recorded for 150 randomly chosen Quick parameter sets under different ClpXP activity levels for WT and WT−CtrA$_U$:*Cori* simulations. [ClpXP] = 1 represents the basal level in simulations of WT cells. Simulations were performed by adjusting $k_{d,CtrA1}$ in accordance with the basal ClpXP activity. Dashed lines and corresponding equations illustrate the line of best fit for the simulated data points. Error bars indicate the standard deviations in t^{cr} of each simulation.

compensation, and we attribute it to synergies within the molecular mechanism driving cell cycle progression and its inherent robustness.

Given that perturbing CtrA$_U$:*Cori* binding results in heightened dependency of t^{cr} on the CtrA proteolysis rate, we speculate that removing CtrA$_U$:*Cori* interactions will induce G1 arrest in mutants that impair CtrA proteolysis. To evaluate this hypothesis, we simulate each mutant strain without CtrA$_U$:*Cori* binding and calculate strain-specific viability (File S1) and the average viability of all strains (Figure 5E). While original Slow and Quick simulations have average strain viability rates of 73% and 71%, respectively, removal of CtrA$_U$:*Cori* binding results in average strain viability rates of 28% and 50%, respectively. Thus, our simulations suggest that CtrA$_U$:*Cori* binding contributes significantly to mutant strain viability, especially in parameter sets with slow degradation of CtrA. Closer inspection (File S1) reveals that cell-cycle arrest is consistently induced in mutant strains that directly influence CtrA proteolysis, such as Δ*popA*, *ctrA*Δ3Ω and cdG^0 (a mutant strain depleted of cdG). However, the Slow parameters also exhibit cell-cycle arrest in several mutants that do not directly influence CtrA proteolysis, such as Δ*pleD* and P*pleC*:Tn. These latter simulations also predict G1 arrest (File S1), likely because these mutations influence proteolysis indirectly. The observation that Quick−CtrA$_U$:*Cori* simulations are more stable than Slow−CtrA$_U$:*Cori* simulations is likely a consequence of a more robust CtrA proteolysis response in Quick parameter sets. Overall, these results suggest that the CtrA$_U$:*Cori* interaction makes the cell cycle more robust to mutations that influence proteolysis, both directly and indirectly, and therefore contributes to the stability of the cell cycle control mechanism.

Parameter sets tuned without the CtrA$_U$:*Cori* interaction alleviate high rates of cell-cycle arrest but deviate from experimental observations

Because CtrA$_U$:*Cori* binding makes a significant difference for the timing of chromosome replication and the stability of the G1-S transition in simulations of mutant strains using both the Quick and Slow parameter

sets, we decided to investigate how the model might behave if we parameterized it without $CtrA_U$:*Cori* binding. Thus, we created a new collection of parameter sets, dubbed the CORI$^-$ parameter sets, that are selected with the same cost function as the SLOW parameter sets but without the $CtrA_U$:*Cori* interaction. In Figure 5C, we plot simulations of WT swarmer cells using 100 parameter sets randomly chosen from the CORI$^-$ collection. We find that while the CORI$^-$ parameter sets fit the experimental data reasonably well, the cost of CORI$^-$ parameter sets are ~20 times higher than the cost of QUICK and SLOW parameter sets (Figure 5D). Indeed, investigation of CORI$^-$ simulations reveals some unusual characteristics.

First, we observe that the CORI$^-$ parameter sets express high levels of total CtrA, with an average peak concentration of 36 μM in swarmer simulations (Figures 5C and S6A). In comparison, SLOW and QUICK parameter sets have an average swarmer cell peak of 24 μM and 25 μM, respectively (Figures 4A, 4B, and S6A). As experimental observations report peak CtrA levels approaching 20–30 μM (Spencer et al., 2009), CORI$^-$ parameter sets do not perform quite as well as the SLOW and QUICK parameter sets, especially when considering that the cost function's targeted peak concentration for $[CtrA]_T$ was 25 μM for swarmer cell simulations. While SLOW and QUICK parameter sets, on average, come within 1 μM of the targeted concentration, the average CORI$^-$ simulation is approximately 11 μM (~44%) higher than the target concentration. Despite having higher total CtrA levels, CtrA~P concentrations are lower in CORI$^-$ simulations than in QUICK and SLOW simulations (Figure S6B). These discrepancies suggest that the CORI$^-$ parameter sets struggle to sufficiently phosphorylate CtrA, and therefore require an exaggerated expression of total CtrA to increase the level of CtrA~P. If true, this would suggest that phosphatase activity of the bifunctional CckA kinase/phosphatase is overly emphasized in CORI$^-$ parameter sets. This concern is validated by two observations. (1) Comparing parameter values among the three parameter-set collections (File S2: Parameter Values), we find that the activity of CckA phosphatase on CtrA~P is far stronger (by 4- to 8-fold) in the CORI$^-$ parameter sets than in the QUICK and SLOW parameter sets. (2) The level of CckA kinase, i.e., $[CckA_K]$, is completely depleted at the G1-S transition in CORI$^-$ simulations, which contradicts experimental observations (Figure 5C). In contrast, QUICK and SLOW simulations show detectable levels of $[CckA_K]$ throughout the G1-S transition (Figures 4A and B).

We further observe that CORI$^-$ simulations exhibit a large spike in cdG at the G1-S transition, with an average peak of 0.67 μM in swarmer cell simulations (Figures 5C and S6D). In contrast, QUICK and SLOW parameter sets have average swarmer simulation peaks of 0.32 μM and 0.28 μM at the G1-S transition, respectively (Figures 4A, 4B, and S6D). As the peak cdG concentration in swarmer cells reaches approximately 0.27 μM at the G1-S transition (Abel et al., 2013), it is clear that CORI$^-$ parameter sets over emphasize cdG synthesis.

The last discrepancy we observe is that the total concentration of CtrA, $[CtrA]_T$, depletes far faster in the CORI$^-$ simulations than in the SLOW simulations (Figures 5C *vs.* 4A), despite being parameterized against the same experimental data. We conclude that this is a consequence of the dramatic cdG response in CORI$^-$ parameter sets, which results in extreme partitioning of CckA toward the phosphatase state, causing rapid accumulation of unphosphorylated CpdR, the active form of CpdR (Smith et al., 2014). As levels of RcdA and PopA are already sufficiently high in G1 (Figures S3 and S4), the exaggerated synthesis of cdG in CORI$^-$ simulations results in rapid accumulation of the CtrA degradation complex (Figures 3 and S5) and speedy proteolysis of CtrA.

Next, we investigate the performance of CORI$^-$ parameter sets on mutant strains. We find that 82% of simulated strains agree with experimentally observed cell viability (Figure 5B). In comparison, SLOW parameter sets had an 89% success rate. Notably, CORI$^-$ parameter sets predict cell-cycle arrest of the cdG^0 mutant (Figure 5A), i.e., cells that lack cdG. This was a surprising result, as cdG^0 is a strain that is penalized by the cost function. Attempts were made to acquire CORI$^-$ parameter sets that predict viable cdG^0 mutants, but none were successful (see STAR Methods). This implies that despite the heavy penalty, the parameterization algorithm favors parameter sets with 'non-viable' cdG^0 simulations, indicating that parameter sets that predict viable cdG^0 cells incur greater costs elsewhere. As this was not an issue with QUICK and SLOW parameter sets, cdG must be acting as an essential crutch to compensate for the absence of the $CtrA_U$:*Cori* interaction in CORI$^-$ parameter sets.

Additional investigation of Δ*rcdA* and Δ*popA* (Figure 5A) suggests that when CtrA proteolysis is impaired, the CORI$^-$ parameter sets have difficulty (failure rates >25%) simulating the cell cycle of stalked cells but not

of swarmer cells. Moreover, for the Δ*popA*&Δ*pleD* strain, the CORI$^-$ parameter sets fail completely (100%) for both swarmer and stalked simulations. We conclude that when proteolysis is impaired, the G1-S transition in simulations of CORI$^-$ parameter sets depends on excessive cdG synthesis (via PleD) to induce a dramatic CckA phosphatase response in order to sufficiently dephosphorylate CtrA.

In summary, the same parameterization algorithm that provided high-quality parameter sets for the QUICK and SLOW collections was unable to train the model to fit all of the biological constraints when the CtrA$_U$:*Cori* interaction was removed. The incongruencies between experimental observations and CORI$^-$ simulations point to a dependence on an excessive shift in the ratio of CckA kinase to CckA phosphatase to sufficiently deplete CtrA∼P at the G1-S transition. This result supports our previous conclusion that the competition between CtrA$_U$ and CtrA∼P for *Cori* binding sites is an essential interaction for robust regulation of the G1-S transition.

Introducing CtrA$_U$:*Cori* interactions improves the behavior of CORI$^-$ simulations

We extend our study by introducing the CtrA$_U$:*Cori* interaction to the CORI$^-$ simulations (see General Simulation Methodology in STAR Methods), and find that the interaction increases overall strain viability from 64% to 76% (Figure 5E). Closer investigation reveals that adding the CtrA$_U$:*Cori* interaction to CORI$^-$ simulations results in 100% rescue of cdG^0 cells from G1 arrest. We further find that previously mentioned strains (Δ*rcdA*, Δ*popA* and Δ*popA*&Δ*pleD*) are all rescued from G1 arrest as well (File S1: Viability and Arrest Data). These results support our previous conclusion that the CtrA$_U$:*Cori* interaction makes a significant contribution toward the robustness of the G1-S transition.

Next, we evaluate the timing of chromosome replication in CORI$^-$ simulations with the addition of CtrA$_U$:*Cori* (Figures 6A and 6C). We find that chromosome replication begins approximately 5–6 min earlier in the presence of CtrA$_U$:*Cori* binding than in its absence. The cell cycle duration was also ∼2 min shorter in WT+CtrA$_U$:*Cori* (CORI$^-$) simulations (Figures 6B and 6C). These results also agree with our findings from the QUICK and SLOW parameter sets that the CtrA$_U$:*Cori* interaction enables an earlier transition into S phase and a quicker cell cycle.

By every measure, we find that the discrepancies between the SLOW/QUICK simulations and SLOW–CtrA$_U$:*Cori*/QUICK–CtrA$_U$:*Cori* simulations are qualitatively the same as the discrepancies between the CORI$^-$ and CORI$^-$+CtrA$_U$:*Cori* simulations. As each parameter set collection is tuned to different experimental data or under different conditions, this suggests that our results are unlikely to be a consequence of parameter choice but are a consequence of the underlying interactions of the model (i.e., the fundamental biology).

DISCUSSION

In 1998, it was established that CtrA∼P inhibits chromosome replication by interacting with five *Cori* binding sites, designated [a]-[e] (Quon et al., 1998). More than 20 years later, the role of unphosphorylated CtrA (CtrA$_U$) on *Cori* regulation has yet to be determined. Utilizing a mathematical model, trained by experimental data, we demonstrate that CtrA$_U$ interacts with *Cori* binding site [d] to displace CtrA∼P at physiologically relevant concentrations. Although sufficient experimental data were not available to build accurate models for sites [a], [b], [c] and [e], we contend that CtrA$_U$ should influence CtrA∼P binding at all *Cori* binding sites. First, we note that sites [b]-[e] all exhibit the TTAA-N7-TTAA consensus sequence necessary for cooperative binding of CtrA molecules. Site [a] only differs from the consensus sequence by one base pair, i.e., TTAA-N7-CTAA (Siam and Marczynski, 2000). Second, affinities measured by Siam and Marczynski suggest that binding sites [a]-[e] have similar dissociation constants for both CtrA$_U$ (0.2–0.6 μM) and CtrA∼P (0.003–0.015 μM). Moreover, the CtrA∼P binding affinity was consistently ∼40-fold stronger than CtrA$_U$ binding for sites [a], [c], [d], and [e]. Site [b], however, measured 100-fold stronger for CtrA∼P than CtrA$_U$. Nonetheless, we expect this difference to be of a quantitative nature while maintaining the same qualitative behavior. For instance, our results suggest that CtrA$_U$ can reasonably displace CtrA∼P from site [d] when the [CtrA∼P]/[CtrA$_U$] ratio is greater than 1:20. Based on the binding affinities reported by Siam and Marczynski, we may roughly extrapolate our results to predict that CtrA$_U$ can displace CtrA∼P from site [b] at ratios greater than 1:60 (∼3× greater than site [d]). In comparison, if CtrA$_U$ did not compete with CtrA∼P for *Cori* binding sites, CckA would have to achieve a CtrA∼P:CtrA$_U$ ratio of roughly 1:5000 to clear site [b], given a total CtrA concentration of ∼15 μM.

Given that $CtrA_U$ competes with CtrA∼P for *Cori* binding sites, what then is the significance of this interaction? We propose that the initiation of chromosome replication is far more likely when *Cori* is bound by $CtrA_U$ than when bound by CtrA∼P, and thereby $CtrA_U$ can enhance *Cori* activity by displacing CtrA∼P. Although no experiment, to the best of our knowledge, has explicitly investigated if chromosome replication can be initiated while *Cori* is occupied by unphosphorylated CtrA, we raise three arguments, based on the *Caulobacter* literature, that $CtrA_U$ does not impair chromosome replication.

1) CtrA proteolysis-null mutants (e.g., Δ*rcdA*, Δ*popA*, and *ctrA*Δ3Ω) progress through the cell cycle normally by means of dephosphorylating CtrA at the G1-S transition (Domian et al., 1997; Duerig et al., 2009; McGrath et al., 2006). In the absence of CtrA proteolysis, we would expect the concentration of CtrA at the G1-S transition in these mutants to be similar to or greater than the peak WT CtrA level of 20–30 μM (Spencer et al., 2009). Because $CtrA_U$ binds very strongly to *Cori* binding sites ($K_d \approx$ 0.2–0.6 μM) (Siam and Marczynski, 2000), they should be nearly 100% occupied by $CtrA_U$ when [$CtrA_U$] > 4 μM and [CtrA∼P] < 0.4 μM (Figure 2B). This reasoning suggests that $CtrA_U$ should completely occupy *Cori* binding sites at the G1-S transition in CtrA proteolysis-null mutants, thus suggesting that chromosome replication is not impeded by $CtrA_U$:*Cori* binding.

2) This first argument would be discredited if some other molecule competes with $CtrA_U$ and CtrA∼P for *Cori* binding sites and displaces $CtrA_U$ at the G1-S transition in proteolysis-null mutants. To the best of our knowledge, there are no known competitors of CtrA binding at sites [a], [b] and [d], but DnaA is known to compete for binding at sites [c] and [e]. Nonetheless, binding studies (Siam and Marczynski, 2000; Spencer et al., 2009; Taylor et al., 2011) suggest that DnaA does not interact strongly enough with sites [c] and [e] to displace $CtrA_U$ (see "CtrA/DnaA Competitive Binding" in STAR Methods for detailed explanation).

3) Flow cytometry on a population of PxylX:*ctrA* cells (which express WT CtrA from a xylose-inducible promoter) reveals an even distribution of cells with one and two chromosomes, indicating a normal cell cycle, and a similar distribution was observed for PxylX:*ctrA*Δ3Ω cells that overexpress CtrAΔ3Ω, a non-proteolizable form of CtrA (Domian et al., 1997). Despite the overexpression, CtrAΔ3Ω does not impede chromosome replication because it is dephosphorylated at the G1-S transition. In comparison, PxylX:*ctrAD51E*Δ3Ω cells are arrested in G1 (Domian et al., 1997), because they are expressing a constitutively active form of CtrA (CtrAD51E) that cannot be degraded. Importantly, while CtrAD51E behaves like CtrA∼P in terms of activity, CtrAD51E was shown to bind with similar affinity as $CtrA_U$ to *Cori* binding sites (Siam and Marczynski, 2003). Thus, we expect CtrAD51EΔ3Ω to bind with similar affinity as $CtrA_U$ but behave like CtrA∼P when bound to *Cori*. Given that PxylX:*ctrAD51E*Δ3Ω and PxylX:*ctrA*Δ3Ω were exposed to the same concentration of xylose, we can also assume that the concentrations of CtrAD51EΔ3Ω and CtrAΔ3Ω in their respective mutants were very similar. Since CtrAD51EΔ3Ω and unphosphorylated CtrAΔ3Ω interact with *Cori* with similar affinity and should have similar concentrations, and since PxylX:*ctrAD51E*Δ3Ω mutant cells are clearly arrested in G1, we conclude that CtrA molecules must be interacting strongly with *Cori* in both mutants and that true differences exist between the activity of $CtrA_U$ and CtrA∼P bound *Cori*. Moreover, the distribution of chromosomes of PxylX:*ctrA*Δ3Ω cells is indistinguishable from pXylX:*ctrA* cells (which degrade CtrA via proteolysis at the G1-S transition), which suggests that the difference in activity between $CtrA_U$ bound *Cori* and CtrA-free *Cori* is negligible.

How might $CtrA_U$ bind to *Cori* without disrupting chromosome replication? To address this question, we first review the physiology of the *Cori* locus (Figure 7A). As previously mentioned, CtrA∼P represses *Cori* by attaching to five binding sites, designated [a]-[e] (Quon et al., 1998). The activity of *Cori* is promoted via the strong promoter Ps, which controls downstream *hemE* activity and is essential for chromosome replication (Marczynski et al., 1995; Siam and Marczynski, 2000). DnaA-ATP interacts with two moderately strong 'G' boxes and five weak 'W' boxes to unwind DNA and recruit other proteins (e.g., helicase) to initiate chromosome replication (Taylor et al., 2011). It is known that CtrA∼P binds to sites [a] and [b] to inhibit the essential strong promoter Ps and repress chromosome replication (Quon et al., 1998; Siam and Marczynski, 2000). However, $CtrA_U$ must not impair chromosome replication; otherwise, the *ctrA*Δ3Ω mutant (and similar mutants) would exhibit G1 arrest. Similar behavior has been documented before. At the *ctrA* promoter, P1, it was shown that CtrA∼P binds to inhibit transcription, while $CtrA_U$ binds to P1 with similar affinity without disrupting transcription (Spencer et al., 2009). Site [c] overlaps with the DnaA G2 box and a binding site for integration host factor (IHF), a protein that presumably promotes chromosome

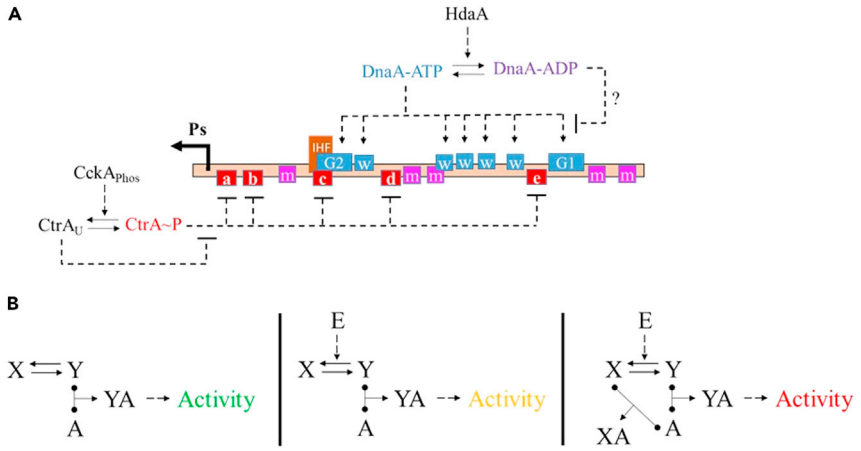

Figure 7. *Cori* physiology and regulation

(A) The *Cori* locus consists of five methylation sites (m), five weak DnaA binding sites (w), two moderate affinity G boxes (G1 and G2), five CtrA binding sites ([a]-[e]) and an IHF binding site overlapping G2 and site [c]. The strong promoter (Ps) is regulated via binding of CtrA~P to sites [a]-[c]. CtrA~P inhibits *Cori* activity while DnaA-ATP promotes activity. Dashed lines indicate influencing interactions, arrow heads designate activation and flat heads designate inhibition. Solid arrows pointing from one molecular species to another designate molecular transformation (i.e., a chemical reaction). HdaA converts DnaA-ATP to DnaA-ADP while CckA phosphatase (CckA$_{Phos}$) converts CtrA~P to CtrA$_U$. We provide computational evidence that CtrA$_U$ displaces CtrA~P for *Cori* binding sites to promote chromosome replication. We suspect that DnaA-ADP displaces DnaA-ATP to inhibit a second round of chromosome replication but do not provide computation evidence (uncertainty indicated with '?').

(B) For any pair of species X and Y, where Y binds with A to induce some activity but X does not, enzyme E can inhibit this activity by converting Y to X. Intuitively, the efficiency of E for inhibiting activity is enhanced if X can also bind with A without inducing activity. Thus, E simultaneously reduces the concentration of Y and A to deplete the YA complex. Binding interactions are illustrated as lines with solid bulbs pointing to the binding partners and arrows pointing to the resulting complex. Solid arrows indicate conversion of one species to another and dashed arrows indicate influential interactions. Green, yellow, and red color coded 'Activity' indicate high, medium, and low activity, respectively.

replication. It was shown that active CtrA can displace both IHF and DnaA from site [c] (Siam et al., 2003; Taylor et al., 2011). If CtrA$_U$ can displace CtrA~P from site [c], we might expect CtrA$_U$ to displace IHF and DnaA as well, which would make CtrA$_U$ a repressor at site [c]. One study showed that mutations at site [c] resulted in significant increases in Ps transcription (i.e., enhances *Cori* activity), while a site [c] knock-out strain is viable but cell proliferation slows down significantly (Siam et al., 2003). It is unclear if the cell cycle defects in the site [c] knock-out strain are a consequence of reduced Ps activity or impaired binding of DnaA and IHF. However, neither IHF nor DnaA binding to G2 are essential for chromosome replication (Siam et al., 2003; Taylor et al., 2011). Based on these results, we propose two scenarios. (1) CtrA$_U$ may prohibit binding of IHF and DnaA at site [c] but does allow transcription from Ps. In contrast, CtrA~P must repress Ps activity via site [c]. In this scenario, CtrA$_U$ displacement of CtrA~P would alleviate repression of Ps but would continue to repress IHF and DnaA binding in the neighborhood of site [c]. (2) CtrA$_U$ interacts differently than CtrA~P with DnaA and IHF to allow them to bind at site [c]. More research will be necessary to understand the binding of these proteins in the neighborhood of site [c]. Site [d] is also a mystery, as the mechanism by which CtrA~P inhibits chromosome replication at site [d] is not documented, to the best of our knowledge. However, *Caulobacter* cells expressing *Cori*-cloned plasmids showed a significant increase in plasmid replication when site [d] was knocked out (Bastedo and Marczynski, 2009), indicating that site [d] is important to repress *Cori* activity. Site [e] is located ~4 bp from the essential DnaA box G1. It was shown that active CtrA displaces DnaA from G1 and adjacent W sites (Taylor et al., 2011). As binding of DnaA to the G1 box is essential for the initiation of chromosome replication, and the *ctrA*Δ3Ω strain has a normal cell cycle, CtrA$_U$ must not impair DnaA binding to G1. Somehow, the phosphorylation of CtrA must cause a conformational change that blocks DnaA from binding to G1, either directly or indirectly.

Regardless of the mechanisms involved, the cumulative evidence from the literature and this work suggest that CtrA$_U$ competes with CtrA~P for *Cori* binding sites at physiologically relevant concentrations to

promote chromosome replication. Indeed, we find that the $CtrA_U$:*Cori* interaction dramatically influences CtrA∼P:*Cori* binding dynamics. Our model suggests that the fraction of CtrA∼P saturated *Cori* binding sites, [DNA:CtrA∼P_2], is relatively independent of the cellular concentration of CtrA∼P but strongly dependent on the [$CtrA_U$]/[CtrA∼P] ratio (Figure 2C), due to the competition between CtrA∼P and $CtrA_U$ for *Cori* binding sites. This result has profound implications for the role of CckA at the G1-S transition. It was previously thought that CtrA dephosphorylation and proteolysis are redundant mechanisms and that the function of CckA phosphatase was simply to clear CtrA∼P at the G1-S transition (Abel et al., 2011; Taylor et al., 2009). Yet, our calculations (Figure 2C) indicate that falling concentrations of CtrA∼P have a negligible impact on CtrA∼P:*Cori* binding until [CtrA∼P] is extremely low (<0.02 μM). We propose that such complete dephosphorylation of CtrA would be challenging for CckA, as it is a bifunctional enzyme and retains some kinase activity at the G1-S transition (Jacobs et al., 2003). Instead, due to the competitive binding of $CtrA_U$ and CtrA∼P to *Cori*, CckA can dramatically relieve *Cori* from inhibition by CtrA∼P by manipulating the [$CtrA_U$]/[CtrA∼P] ratio, and this effect is relatively independent of the total concentration of CtrA (unless $[CtrA]_T$< 0.5 μM). This result provides new insights into the efficiency of CtrA regulation and further explains why a wide range of CtrA expression patterns are observed at the G1-S transition (Figure 1B). By manipulating the ratio of CckA kinase to CckA phosphatase, *Caulobacter* can adjust the ratio of $CtrA_U$ to CtrA∼P independently of the total concentration of CtrA. Thus, we suspect that the total concentration of CtrA at the G1-S transition has a minimal impact on cell cycle progression when CckA is functioning normally.

To further investigate the implications of $CtrA_U$:*Cori* binding, we developed a detailed mathematical model of the molecular mechanisms driving events of the *Caulobacter* cell cycle. We parameterized our model to three separate conditions (i.e., Slow, Quick and $Cori^-$). Both Slow and Quick parameter sets include $CtrA_U$:*Cori* binding, but they are tuned separately to expression patterns with slow and quick proteolysis of CtrA at the G1-S transition. The $Cori^-$ parameter sets were parameterized without $CtrA_U$:*Cori* binding and with slow CtrA proteolysis data. Despite being parameterized to the same data, we find that the Slow parameter sets fit the 'slow' CtrA degradation pattern very well, but the $Cori^-$ parameter sets demand rapid degradation of CtrA at the G1-S transition. Additionally, we find that the $Cori^-$ parameter sets require supra-physiological levels of cdG in order to induce supra-physiological activity of CckA phosphatase (Figures 4A and 5C). These results support our contention that the total concentration of CtrA at the G1-S transition has a negligible impact on cell cycle progression due to $CtrA_U$:*Cori* binding and normal CckA functioning. The fact that $Cori^-$ parameter sets have distinct abnormalities also suggests that the competition of $CtrA_U$ with CtrA∼P for *Cori* binding sites is an essential interaction to explain the cumulative observations of cell cycle progression in *C. crescentus*.

When we remove $CtrA_U$:*Cori* binding from Slow and Quick parameter sets, we find that the timing of chromosome replication is consistently delayed, but these delays are significantly greater in the Slow parameter sets ($\Delta t^{cr} \approx$ 23 min) than in Quick parameter sets ($\Delta t^{cr} \approx$ 2 min). The large difference in delays is evidence that the timing of the G1-S transition is highly dependent on CtrA proteolysis when $CtrA_U$:*Cori* binding is compromised. However, the fact that Quick parameter sets, characterized by rapid proteolysis of CtrA, still exhibit consistent delays in the onset of chromosome replication when the $CtrA_U$:*Cori* interaction is removed suggests one of two scenarios: either (1) $CtrA_U$ displacement of CtrA∼P at *Cori* typically precedes proteolysis; or (2) CtrA dephosphorylation and proteolysis act cooperatively, in a $CtrA_U$:*Cori* dependent manner, to disrupt CtrA∼P:*Cori* binding. In support of the second scenario, our analysis of CtrA binding to *Cori* site [d] did suggest some cooperativity between reducing $[CtrA]_T$ to low levels and manipulating the [$CtrA_U$]/[CtrA∼P] ratio (Figure 2C). However, when we decreased the rate of proteolysis in Quick WT simulations, we found very mild delays in chromosome replication ($\Delta t^{cr} \approx$ 0.5 min), suggesting that the timing of chromosome replication is relatively independent of proteolysis under normal conditions. In contrast, the removal of $CtrA_U$:*Cori* binding resulted in a roughly 2 min delay in chromosome replication. This result supports the first scenario, where $CtrA_U$ displaces CtrA∼P at *Cori* prior to significant proteolysis (even if proteolysis is very quick). This scenario makes sense when considering the biochemistry of *C. crescentus*. CckA kinase/phosphatase dictates the phosphorylation of both CtrA and CpdR (Biondi et al., 2006a; Chen et al., 2009). Thus, CtrA∼P and CpdR∼P are simultaneously dephosphorylated at the G1-S transition. CpdR, in its unphosphorylated state, localizes to the old pole where it interacts with ClpXP (Iniesta et al., 2006). The CpdR:ClpXP complex must then recruit other adaptors (PopA, RcdA and cdG) before CtrA proteolysis can begin (Duerig et al., 2009; Smith et al., 2014), and then it takes several minutes before CtrA levels are completely depleted (Domian et al., 1997; Smith et al., 2014). In contrast, there is no lag between the dephosphorylation of CtrA and its ability to compete with CtrA∼P for *Cori* binding sites.

Therefore, since CtrA∼P and CpdR∼P are dephosphorylated simultaneously, $CtrA_U$ should have ample time to displace CtrA∼P from *Cori* binding sites before proteolysis dominates CtrA behavior.

Investigation of mutant simulations of all three parameter set categories (i.e., Slow, Quick and Cori$^-$) revealed that the $CtrA_U$:*Cori* interaction is necessary for the viability of several mutant strains, including cdG^0, Δ*popA* and Δ*rcdA*. We report that when $CtrA_U$:*Cori* binding was removed from simulations, overall strain viability dropped by 46% in Slow parameter sets and 21% in Quick parameter sets. Additionally, overall strain viability increased by 12% when adding $CtrA_U$:*Cori* binding to Cori$^-$ simulations (Figure 5E). We point out that the Slow and Quick results are likely more accurate in terms of predicting viability than the Cori$^-$parameter sets, given that Cori$^-$ simulations do not fit biological observations quite as well. Importantly, despite the cdG^0 mutant being a penalized strain of the cost function, 100% of Cori$^-$parameter sets failed to capture cdG^0 viability. However, simply introducing the $CtrA_U$:*Cori* interaction to Cori$^-$ simulations resulted in recovery of the cdG^0 mutant from G1 arrest. A closer investigation into other mutant simulations revealed that the absence of the $CtrA_U$:*Cori* interaction frequently led to G1 arrest in mutants that have impaired proteolysis. Conclusively, these results suggest that the $CtrA_U$:*Cori* interaction is necessary to explain observed mutant viability behavior. As pointed out previously, the competition of $CtrA_U$ and CtrA∼P for *Cori* binding sites changes the dynamics of CtrA∼P:*Cori* binding from being a simple function of CtrA∼P concentration to being a function of the [$CtrA_U$]/[CtrA∼P] ratio. This leads to greater efficiency of CckA phosphatase at the G1-S transition, which seems to be necessary for a dephosphorylation-dependent G1-S transition. In other words, the competitive binding of $CtrA_U$ to *Cori* is necessary for CckA phosphatase to sufficiently clear *Cori* of CtrA∼P in the absence of total proteolysis. Thus, the $CtrA_U$:*Cori* interaction significantly enhances the robustness of the G1-S transition.

In conclusion, we have provided computational evidence that $CtrA_U$ contributes to a speedier and more robust G1-S transition by competing with CtrA∼P for binding to *Cori* sites [a]-[e]. This competitive interaction between $CtrA_U$ and CtrA∼P dramatically increases the efficacy of CckA phosphatase in regulating DNA replication. While this study has focused on CtrA:*Cori* binding dynamics, we suggest that similar molecular interactions may have been overlooked for other molecular species within *Caulobacter* and other organisms as well. Thus, we propose in Figure 7B a general motif for molecular signaling in cell physiology. A molecule X is converted to molecule Y which binds with an activator A to induce its activity. An enzyme E converts Y back to X which does not associate with A. In this scenario, enzyme E reduces the 'activity' by depleting Y and reducing the concentration of the Y:A complex. However, the efficiency of E in impairing A's activity can be enhanced if X competes with Y for A-binding sites, but does not induce activity. In this case, E (the signal) depletes the Y:A complex by simultaneously reducing the availability of both Y and A. As biological systems are pruned for efficiency by natural selection, we propose that for a signal-response motif like the central panel of Figure 7B, there may be selective pressure for molecule X to bind competitively to A.

In addition to the case {X, Y, A, E} = {$CtrA_U$, CtrA∼P, *Cori*, CckA phosphatase} considered in detail here, we can think of two additional examples in *C. crescentus* that have not yet been investigated. First, *ctrA* promoters P1 and P2 have similar binding affinities for CtrA∼P and $CtrA_U$, yet $CtrA_U$ does not influence *ctrA* activity in the same manner as CtrA∼P (Spencer et al., 2009). No one, to the best of our knowledge, has investigated the dynamics of competition between $CtrA_U$ and CtrA∼P for *ctrA* promoters P1 and P2. But if $CtrA_U$ and CtrA∼P have similar binding affinities for *ctrA* promoters then they should compete for binding sites on P1 and P2. Because $CtrA_U$ does not directly affect *ctrA* P1 or P2 activity and CtrA∼P does, $CtrA_U$ is likely a competitive inhibitor of CtrA∼P with regards to *ctrA* regulation. In a similar vein, it is known that both DnaA-ADP and DnaA-ATP can bind to *Cori* with comparable affinity (Taylor et al., 2011), but *Cori* is less active after DnaA-ATP hydrolysis (Collier and Shapiro, 2009), suggesting that DnaA-ADP does not promote chromosome replication. As HdaA hydrolyzes DnaA-ATP to DnaA-ADP immediately after DNA replication is initiated in order to avoid a second round of chromosome replication (Collier and Shapiro, 2009), DnaA-ADP should displace DnaA-ATP from *Cori* binding sites as the ratio shifts in favor of DnaA-ADP. Therefore, we suspect that DnaA-ADP may act as a competitive inhibitor to DnaA-ATP at *Cori* just as $CtrA_U$ does with CtrA∼P. In our model, we do not simulate DnaA-ADP binding to *Cori*, because we could not find quantitative experiments necessary to estimate kinetic constants. In our model, DnaA-ATP must be hydrolyzed extremely quickly by HdaA to ensure that a second round of chromosome replication does not begin (Figures S3–S5). We suspect that, in reality, DnaA-ATP is not hydrolyzed as quickly as in our model. Just as parameterizing our model without the $CtrA_U$:*Cori* interaction (i.e., the Cori$^-$ parameter sets) resulted in the

dubiously high activity of CckA phosphatase, the improbably high rate of DnaA-ATP hydrolysis in our model may be a consequence of neglecting the DnaA-ADP:*Cori* interaction. Competitive displacement of DnaA-ATP from *Cori* by DnaA-ADP should increase the efficiency of the HdaA enzyme, just as our model suggests that the $CtrA_U$:*Cori* interaction enhances the efficiency of CckA. We urge experimental biologists to consider such potential interactions in the future and emphasize the need for investigation of the roles of unphosphorylated CtrA in the *Caulobacter* cell cycle. We point out that the validity of our results and analysis hinges on our assumption that CtrA~P and $CtrA_U$ have different effects when interacting with *Cori*, and we encourage experimental biologists to test this assumption in *Caulobacter* cells.

Limitations of study

As with any systems biology study, the accuracy of our predictions is limited by the underlying assumptions of our model. The most notable assumption is that $CtrA_U$ does not impair chromosome replication in the same manner as CtrA~P when interacting with *Cori*. While much indirect evidence supports this key assumption (see Discussion) there is no direct evidence to support it. If future experimental studies validate this assumption, then our conclusions pertaining to the role of $CtrA_U$ in the G1-S transition will be increasingly secure. Another notable assumption is that DnaA cannot compete with CtrA~P or $CtrA_U$ for *Cori* binding sites at physiological concentrations. Again, while indirect evidence may support this assumption, direct evidence is lacking. Moreover, the way that we model the timing of chromosome replication relies on the integration of a threshold function that in itself relies on assumptions on the quantitative nature by which CtrA and DnaA influence the probability of chromosome replication (See "Chromosome replication" in STAR Methods). Our approach may provide a reasonable estimate for the timing of chromosome replication, but a more detailed mechanistic model could improve its accuracy. With this said, further experimental research concerning the mechanisms regulating chromosome replication in *Caulobacter* is needed to derive a more accurate mechanistic model.

Other limitations of theoretical studies like ours pertain to the methods whereby the model is parameterized and analyzed. Limitations due to parameter choices are largely mitigated by including thousands of parameter sets and three different classes of parameterization criteria (i.e., SLOW, QUICK and $CORI^-$) in our analysis. However, as our model is parameterized to timescales pertaining to growth on nutrient-limited media (e.g., M2G), our results regarding the timing of chromosome replication and mutant viability should be generalized to other conditions with caution.

STAR★METHODS

Detailed methods are provided in the online version of this paper and include the following:

- KEY RESOURCES TABLE
- RESOURCE AVAILABILITY
  - Lead contact
  - Materials availability
  - Data and code availability
- METHOD DETAILS
  - General simulation methodology
  - General ODE structure
  - Protein complexes and phosphorylation
  - Localization
  - Swarmer vs. stalked simulations
  - CtrA:*Cori* binding
  - CtrA/DnaA competitive binding
  - Considering increased complexity of CtrA:DNA binding
  - Biological mechanisms
  - Parameter estimation
  - Equations and simulation events governing the cell cycle model
  - Events and switches
  - Concentration shifts due to cytokinesis
- QUANTIFICATION AND STATISTICAL ANALYSIS

SUPPLEMENTAL INFORMATION

Supplemental information can be found online at https://doi.org/10.1016/j.isci.2021.103413.

ACKNOWLEDGMENTS

This work was partially supported by the National Science Foundation (NSF) under awards CCF-1526666, MCB-1613741, and CCF-1909122. The funding sources played no role in the design of the study, in the collection, analysis, and interpretation of data, and in writing the manuscript.

AUTHOR CONTRIBUTIONS

BRW conducted the research. BRW and JJT wrote the manuscript. All authors contributed to the conceptualization of the project and to the development of the model, and all authors approve the final manuscript.

DECLARATION OF INTERESTS

The authors declare no competing interests.

Received: May 4, 2021
Revised: September 17, 2021
Accepted: November 5, 2021
Published: December 17, 2021

SUPPORTING CITATIONS

The following reference appears in the Supplemental information: Biondi et al., 2006b; Christen et al., 2010; Jonas et al., 2011; Sanselicio et al., 2015; Schredl et al., 2012; Viollier et al., 2002a; Viollier et al., 2002b; Wheeler and Shapiro, 1999; Zweiger and Shapiro, 1994.

REFERENCES

Abel, S., Chien, P., Wassmann, P., Schirmer, T., Kaever, V., Laub, M.T., Baker, T.A., and Jenal, U. (2011). Regulatory cohesion of cell cycle and cell differentiation through interlinked phosphorylation and second messenger networks. Mol. Cell *43*, 550–560. https://doi.org/10.1016/j.molcel.2011.07.018.

Abel, S., Bucher, T., Nicollier, M., Hug, I., Kaever, V., Abel zur Wiesch, P., and Jenal, U. (2013). Bimodal distribution of the second messenger c-di-GMP controls cell fate and asymmetry during the Caulobacter cell cycle. PLOS Genet. *9*, e1003744. https://doi.org/10.1371/journal.pgen.1003744.

Adhikari, S., and Curtis, P.D. (2016). DNA methyltransferases and epigenetic regulation in bacteria. FEMS Microbiol. Rev. *40*, 575–591. https://doi.org/10.1093/femsre/fuw023.

Aldridge, P., Paul, R., Goymer, P., Rainey, P., and Jenal, U. (2003). Role of the GGDEF regulator PleD in polar development of Caulobacter crescentus. Mol. Microbiol. *47*, 1695–1708. https://doi.org/10.1046/j.1365-2958.2003.03401.x.

Allard, J.F., and Cytrynbaum, E.N. (2009). Force generation by a dynamic Z-ring in Escherichia coli cell division. Proc. Natl. Acad. Sci. U S A *106*, 145–150. https://doi.org/10.1073/pnas.0808657106.

Ardissone, S., and Viollier, P.H. (2015). Interplay between flagellation and cell cycle control in Caulobacter. Curr. Opin. Microbiol. *28*, 83–92. https://doi.org/10.1016/j.mib.2015.08.012.

Bastedo, D.P., and Marczynski, G.T. (2009). CtrA response regulator binding to the Caulobacter chromosome replication origin is required during nutrient and antibiotic stress as well as during cell cycle progression. Mol. Microbiol. *72*, 139–154. https://doi.org/10.1111/j.1365-2958.2009.06630.x.

Beroual, W., Lalaouna, D., Zaina, N.B., Valette, O., Prévost, K., Denis, Y., Djendli, M., Brilli, M., Marta, R., Jose-Ignacio, J.-Z., et al. (2019). CcnA, a novel non-coding RNA regulating the bacterial cell cycle. BioRxiv, 756452. https://doi.org/10.1101/756452.

Biondi, E.G., Reisinger, S.J., Skerker, J.M., Arif, M., Perchuk, B.S., Ryan, K.R., and Laub, M.T. (2006a). Regulation of the bacterial cell cycle by an integrated genetic circuit. Nature *444*, 899–904. https://doi.org/10.1038/nature05321.

Biondi, E.G., Skerker, J.M., Arif, M., Prasol, M.S., Perchuk, B.S., and Laub, M.T. (2006b). A phosphorelay system controls stalk biogenesis during cell cycle progression in Caulobacter crescentus. Mol. Microbiol. *59*, 386–401. https://doi.org/10.1111/j.1365-2958.2005.04970.x.

Brassinga, A.K., and Marczynski, G.T. (2001). Replication intermediate analysis confirms that chromosomal replication origin initiates from an unusual intergenic region in Caulobacter crescentus. Nucleic Acids Res. *29*, 4441–4451. https://doi.org/10.1093/nar/29.21.4441.

Campos, M., Surovtsev, I.V., Kato, S., Paintdakhi, A., Beltran, B., Ebmeier, S.E., and Jacobs-Wagner, C. (2014). A constant size extension drives bacterial cell size homeostasis. Cell *159*, 1433–1446. https://doi.org/10.1016/j.cell.2014.11.022.

Cha, S. (1970). Kinetic behavior at high enzyme concentrations magnitude of errors of michaelis-menten and other approximations. J. Biol. Chem. *245*, 4814–4818. https://doi.org/10.1016/S0021-9258(18)62865-0.

Chan, C., Paul, R., Samoray, D., Amiot, N.C., Giese, B., Jenal, U., and Schirmer, T. (2004). Structural basis of activity and allosteric control of diguanylate cyclase. Proc. Natl. Acad. Sci. U S A *101*, 17084–17089. https://doi.org/10.1073/pnas.0406134101.

Chen, J.C., Hottes, A.K., McAdams, H.H., McGrath, P.T., Viollier, P.H., and Shapiro, L. (2006). Cytokinesis signals truncation of the PodJ polarity factor by a cell cycle-regulated protease. EMBO J. *25*, 377–386. https://doi.org/10.1038/sj.emboj.7600935.

Chen, Y.E., Tsokos, C.G., Biondi, E.G., Perchuk, B.S., and Laub, M.T. (2009). Dynamics of two phosphorelays controlling cell cycle progression in Caulobacter crescentus. J. Bacteriol. *191*, 7417–7429. https://doi.org/10.1128/JB.00992-09.

Cheng, L., and Keiler, K.C. (2009). Correct timing of dnaA transcription and initiation of DNA replication requires trans translation. J. Bacteriol. *191*, 4268–4275. https://doi.org/10.1128/JB.00362-09.

Childers, W.S., Xu, Q., Mann, T.H., Mathews, I.I., Blair, J.A., Deacon, A.M., and Shapiro, L. (2014).

Cell fate regulation governed by a repurposed bacterial histidine kinase. PLoS Biol. *12*, e1001979. https://doi.org/10.1371/journal.pbio.1001979.

Christen, B., Christen, M., Paul, R., Schmid, F., Folcher, M., Jenoe, P., Meuwly, M., and Jenal, U. (2006). Allosteric control of cyclic di-GMP signaling. J. Biol. Chem. *281*, 32015–32024. https://doi.org/10.1074/jbc.M603589200.

Christen, B., Fero, M.J., Hillson, N.J., Bowman, G., Hong, S.-H., Shapiro, L., and McAdams, H.H. (2010). High-throughput identification of protein localization dependency networks. Proc. Natl. Acad. Sci. U S A *107*, 4681–4686. https://doi.org/10.1073/pnas.1000846107.

Collier, J. (2012). Regulation of chromosomal replication in Caulobacter crescentus. Plasmid *67*, 76–87. https://doi.org/10.1016/j.plasmid.2011.12.007.

Collier, J., and Shapiro, L. (2009). Feedback control of DnaA-mediated replication initiation by replisome-associated HdaA protein in Caulobacter. J. Bacteriol. *191*, 5706–5716. https://doi.org/10.1128/JB.00525-09.

Collier, J., Murray, S.R., and Shapiro, L. (2006). DnaA couples DNA replication and the expression of two cell cycle master regulators. EMBO J. *25*, 346–356. https://doi.org/10.1038/sj.emboj.7600927.

Collier, J., McAdams, H.H., and Shapiro, L. (2007). A DNA methylation ratchet governs progression through a bacterial cell cycle. Proc. Natl. Acad. Sci. U S A *104*, 17111–17116. https://doi.org/10.1073/pnas.0708112104.

Domian, I.J., Quon, K.C., and Shapiro, L. (1997). Cell type-specific phosphorylation and proteolysis of a transcriptional regulator controls the G1-to-S transition in a bacterial cell cycle. Cell *90*, 415–424. https://doi.org/10.1016/S0092-8674(00)80502-4.

Domian, I.J., Reisenauer, A., and Shapiro, L. (1999). Feedback control of a master bacterial cell-cycle regulator. Proc. Natl. Acad. Sci. U S A *96*, 6648–6653. https://doi.org/10.1073/pnas.96.12.6648.

Dubey, B.N., Lori, C., Ozaki, S., Fucile, G., Plaza-Menacho, I., Jenal, U., and Schirmer, T. (2016). Cyclic di-GMP mediates a histidine kinase/phosphatase switch by noncovalent domain cross-linking. Sci. Adv. *2*, e1600823. https://doi.org/10.1126/sciadv.1600823.

Duerig, A., Abel, S., Folcher, M., Nicollier, M., Schwede, T., Amiot, N., Giese, B., and Jenal, U. (2009). Second messenger-mediated spatiotemporal control of protein degradation regulates bacterial cell cycle progression. Genes Dev. *23*, 93–104. https://doi.org/10.1101/gad.502409.

Erickson, H.P. (2009). Modeling the physics of FtsZ assembly and force generation. Proc. Natl. Acad. Sci. U S A *106*, 9238–9243. https://doi.org/10.1073/pnas.0902258106.

Fernandez-Fernandez, C., Gonzalez, D., and Collier, J. (2011). Regulation of the activity of the dual-function DnaA protein in Caulobacter crescentus. PLoS One *6*, e26028. https://doi.org/10.1371/journal.pone.0026028.

Fernandez-Fernandez, C., Grosse, K., Sourjik, V., and Collier, J. (2013). The β-sliding clamp directs the localization of HdaA to the replisome in Caulobacter crescentus. Microbiology *159*, 2237. https://doi.org/10.1099/mic.0.068577-0.

Gonzalez, D., and Collier, J. (2013). DNA methylation by CcrM activates the transcription of two genes required for the division of C aulobacter crescentus. Mol. Microbiol. *88*, 203–218. https://doi.org/10.1111/mmi.12180.

Gonzalez, D., and Collier, J. (2015). Genomic adaptations to the loss of a conserved bacterial DNA methyltransferase. MBio *6*, e00952. https://doi.org/10.1128/mBio.00952-15.

Gonzalez, D., Kozdon, J.B., McAdams, H.H., Shapiro, L., and Collier, J. (2014). The functions of DNA methylation by CcrM in Caulobacter crescentus: a global approach. Nucleic Acids Res. *42*, 3720–3735. https://doi.org/10.1093/nar/gkt1352.

Gorbatyuk, B., and Marczynski, G.T. (2005). Regulated degradation of chromosome replication proteins DnaA and CtrA in Caulobacter crescentus. Mol. Microbiol. *55*, 1233–1245. https://doi.org/10.1111/j.1365-2958.2004.04459.x.

Grünenfelder, B., Rummel, G., Vohradsky, J., Röder, D., Langen, H., and Jenal, U. (2001). Proteomic analysis of the bacterial cell cycle. Proc. Natl. Acad. Sci. U S A *98*, 4681–4686. https://doi.org/10.1073/pnas.071538098.

Harris, L.K., and Theriot, J.A. (2016). Relative rates of surface and volume synthesis set bacterial cell size. Cell *165*, 1479–1492. https://doi.org/10.1016/j.cell.2016.05.045.

Hengge, R. (2009). Principles of c-di-GMP signalling in bacteria. Nat. Rev. Microbiol. *7*, 263–273. https://doi.org/10.1038/nrmicro2109.

Hinz, A.J., Larson, D.E., Smith, C.S., and Brun, Y.V. (2003). The Caulobacter crescentus polar organelle development protein PodJ is differentially localized and is required for polar targeting of the PleC development regulator. Mol. Microbiol. *47*, 929–941. https://doi.org/10.1046/j.1365-2958.2003.03349.x.

Holtzendorff, J., Hung, D., Brende, P., Reisenauer, A., Viollier, P.H., McAdams, H.H., and Shapiro, L. (2004). Oscillating global regulators control the genetic circuit driving a bacterial cell cycle. Science *304*, 983–987. https://doi.org/10.1126/science.1095191.

Hung, D.Y., and Shapiro, L. (2002). A signal transduction protein cues proteolytic events critical to Caulobacter cell cycle progression. Proc. Natl. Acad. Sci. U S A *99*, 13160–13165. https://doi.org/10.1073/pnas.202495099.

Iniesta, A.A., McGrath, P.T., Reisenauer, A., McAdams, H.H., and Shapiro, L. (2006). A phospho-signaling pathway controls the localization and activity of a protease complex critical for bacterial cell cycle progression. Proc. Natl. Acad. Sci. U S A *103*, 10935–10940. https://doi.org/10.1073/pnas.0604554103.

Iniesta, A.A., Hillson, N.J., and Shapiro, L. (2010). Polar remodeling and histidine kinase activation, which is essential for Caulobacter cell cycle progression, are dependent on DNA replication initiation. J. Bacteriol. *192*, 3893–3902. https://doi.org/10.1128/JB.00468-10.

Jacobs, C., Domian, I.J., Maddock, J.R., and Shapiro, L. (1999). Cell cycle–dependent polar localization of an essential bacterial histidine kinase that controls DNA replication and cell division. Cell *97*, 111–120. https://doi.org/10.1016/S0092-8674(00)80719-9.

Jacobs, C., Ausmees, N., Cordwell, S.J., Shapiro, L., and Laub, M.T. (2003). Functions of the CckA histidine kinase in Caulobacter cell cycle control. Mol. Microbiol. *47*, 1279–1290. https://doi.org/10.1046/j.1365-2958.2003.03379.x.

Jenal, U. (2009). The role of proteolysis in the Caulobacter crescentus cell cycle and development. Res. Microbiol. *160*, 687–695. https://doi.org/10.1016/j.resmic.2009.09.006.

Jenal, U., and Fuchs, T. (1998). An essential protease involved in bacterial cell-cycle control. EMBO J. *17*, 5658–5669. https://doi.org/10.1093/emboj/17.19.5658.

Jensen, R.B. (2006). Coordination between chromosome replication, segregation, and cell division in Caulobacter crescentus. J. Bacteriol. *188*, 2244–2253. https://doi.org/10.1128/JB.188.6.2244-2253.2006.

Jonas, K., Chen, Y.E., and Laub, M.T. (2011). Modularity of the bacterial cell cycle enables independent spatial and temporal control of DNA replication. Curr. Biol. *21*, 1092–1101. https://doi.org/10.1016/j.cub.2011.05.040.

Jonas, K., Liu, J., Chien, P., and Laub, M.T. (2013). Proteotoxic stress induces a cell-cycle arrest by stimulating Lon to degrade the replication initiator DnaA. Cell *154*, 623–636. https://doi.org/10.1016/j.cell.2013.06.034.

Joshi, K.K., Bergé, M., Radhakrishnan, S.K., Viollier, P.H., and Chien, P. (2015). An adaptor hierarchy regulates proteolysis during a bacterial cell cycle. Cell *163*, 419–431. https://doi.org/10.1016/j.cell.2015.09.030.

Judd, E.M., Ryan, K.R., Moerner, W.E., Shapiro, L., and McAdams, H.H. (2003). Fluorescence bleaching reveals asymmetric compartment formation prior to cell division in Caulobacter. Proc. Natl. Acad. Sci. U S A *100*, 8235–8240. https://doi.org/10.1073/pnas.1433105100.

Kozdon, J.B., Melfi, M.D., Luong, K., Clark, T.A., Boitano, M., Wang, S., Zhou, B., Gonzalez, D., Collier, J., Turner, S.W., et al. (2013). Global methylation state at base-pair resolution of the Caulobacter genome throughout the cell cycle. Proc. Natl. Acad. Sci. U S A *110*, E4658–E4667. https://doi.org/10.1073/pnas.1319315110.

Lan, G., Wolgemuth, C.W., and Sun, S.X. (2007). Z-ring force and cell shape during division in rod-like bacteria. Proc. Natl. Acad. Sci. U S A *104*, 16110–16115. https://doi.org/10.1073/pnas.0702925104.

Lasker, K., Schrader, J.M., Men, Y., Marshik, T., Dill, D.L., McAdams, H.H., and Shapiro, L. (2016a). CauloBrowser: a systems biology resource for Caulobacter crescentus. Nucleic Acids Res. *44*, D640–D645. https://doi.org/10.1093/nar/gkv1050.

Lasker, K., Mann, T.H., and Shapiro, L. (2016b). An intracellular compass spatially coordinates cell cycle modules in Caulobacter crescentus. Curr. Opin. Microbiol. *33*, 131–139. https://doi.org/10.1016/j.mib.2016.06.007.

Laub, M.T., McAdams, H.H., Feldblyum, T., Fraser, C.M., and Shapiro, L. (2000). Global analysis of the genetic network controlling a bacterial cell cycle. Science *290*, 2144–2148. https://doi.org/10.1126/science.290.5499.2144.

Laub, M.T., Shapiro, L., and McAdams, H.H. (2007). Systems biology of Caulobacter. Annu. Rev. Genet. *41*, 429–441. https://doi.org/10.1146/annurev.genet.41.110306.130346.

Lawler, M.L., Larson, D.E., Hinz, A.J., Klein, D., and Brun, Y.V. (2006). Dissection of functional domains of the polar localization factor PodJ in Caulobacter crescentus. Mol. Microbiol. *59*, 301–316. https://doi.org/10.1111/j.1365-2958.2005.04935.x.

Li, S., Brazhnik, P., Sobral, B., and Tyson, J.J. (2009). Temporal controls of the asymmetric cell division cycle in Caulobacter crescentus. PLoS Comput. Biol. *5*, e1000463. https://doi.org/10.1371/journal.pcbi.1000463.

Liu, J., Francis, L.I., Jonas, K., Laub, M.T., and Chien, P. (2016). ClpAP is an auxiliary protease for DnaA degradation in Caulobacter crescentus. Mol. Microbiol. *102*, 1075–1085. https://doi.org/10.1111/mmi.13537.

Lori, C., Ozaki, S., Steiner, S., Böhm, R., Abel, S., Dubey, B.N., Schirmer, T., Hiller, S., and Jenal, U. (2015). Cyclic di-GMP acts as a cell cycle oscillator to drive chromosome replication. Nature *523*, 236. https://doi.org/10.1038/nature14473.

Lott, T., Ohta, N., and Newton, A. (1987). Order of gene replication in Caulobacter crescentus; use of in vivo labeled genomic DNA as a probe. Mol. Gen. Genet. *210*, 543–550. https://doi.org/10.1007/BF00327210.

Mann, T.H., and Shapiro, L. (2018). Integration of cell cycle signals by multi-PAS domain kinases. BioRxiv, 323444. https://doi.org/10.1101/323444.

Marczynski, G.T., Lentine, K., and Shapiro, L. (1995). A developmentally regulated chromosomal origin of replication uses essential transcription elements. Genes Dev. *9*, 1543–1557. https://doi.org/10.1101/gad.9.12.1543.

Martin, M.E., Trimble, M.J., and Brun, Y.V. (2004). Cell cycle-dependent abundance, stability and localization of FtsA and FtsQ in Caulobacter crescentus. Mol. Microbiol. *54*, 60–74. https://doi.org/10.1111/j.1365-2958.2004.04251.x.

Matroule, J.-Y., Lam, H., Burnette, D.T., and Jacobs-Wagner, C. (2004). Cytokinesis Monitoring during development: rapid Pole-to-Pole shuttling of a signaling protein by localized kinase and phosphatase in Caulobacter. Cell *118*, 579–590. https://doi.org/10.1016/j.cell.2004.08.019.

McGrath, P.T., Iniesta, A.A., Ryan, K.R., Shapiro, L., and McAdams, H.H. (2006). A dynamically localized protease complex and a polar specificity factor control a cell cycle master regulator. Cell *124*, 535–547. https://doi.org/10.1016/j.cell.2005.12.033.

Mignolet, J., Holden, S., Berge, M., Panis, G., Eroglu, E., Theraulaz, L., Manley, S., and Viollier, P.H. (2016). Functional dichotomy and distinct nanoscale assemblies of a cell cycle-controlled bipolar zinc-finger regulator. Elife *5*, e18647. https://doi.org/10.7554/eLife.18647.001.

Miraldi, E.R., Thomas, P.J., and Romberg, L. (2008). Allosteric models for cooperative polymerization of linear polymers. Biophys. J. *95*, 2470–2486. https://doi.org/10.1529/biophysj.107.126219.

Murray, S.M., Panis, G., Fumeaux, C., Viollier, P.H., and Howard, M. (2013). Computational and genetic reduction of a cell cycle to its simplest, primordial components. PLoS Biol. *11*, e1001749. https://doi.org/10.1371/journal.pbio.1001749.

Paul, R., Jaeger, T., Abel, S., Wiederkehr, I., Folcher, M., Biondi, E.G., Laub, M.T., and Jenal, U. (2008). Allosteric regulation of histidine kinases by their Cognate response regulator determines cell fate. Cell *133*, 452–461. https://doi.org/10.1016/j.cell.2008.02.045.

Quon, K.C., Yang, B., Domian, I.J., Shapiro, L., and Marczynski, G.T. (1998). Negative control of bacterial DNA replication by a cell cycle regulatory protein that binds at the chromosome origin. Proc. Natl. Acad. Sci. U S A *95*, 120–125. https://doi.org/10.1073/pnas.95.1.120.

Radhakrishnan, S.K., Thanbichler, M., and Viollier, P.H. (2008). The dynamic interplay between a cell fate determinant and a lysozyme homolog drives the asymmetric division cycle of Caulobacter crescentus. Genes Dev. *22*, 212–225. https://doi.org/10.1101/gad.1601808.

Reisenauer, A., and Shapiro, L. (2002). DNA methylation affects the cell cycle transcription of the CtrA global regulator in Caulobacter. EMBO J. *21*, 4969–4977. https://doi.org/10.1093/emboj/cdf490.

Reisenauer, A., Quon, K., and Shapiro, L. (1999). The CtrA response regulator mediates temporal control of gene expression during the Caulobacter cell cycle. J. Bacteriol. *181*, 2430–2439. https://doi.org/10.1128/JB.181.8.2430-2439.1999.

Ryan, K.R., Judd, E.M., and Shapiro, L. (2002). The CtrA response regulator essential for Caulobacter crescentus cell-cycle progression requires a bipartite degradation signal for temporally controlled proteolysis. J. Mol. Biol. *324*, 443–455. https://doi.org/10.1016/S0022-2836(02)01042-2.

Sanselicio, S., Bergé, M., Théraulaz, L., Radhakrishnan, S.K., and Viollier, P.H. (2015). Topological control of the Caulobacter cell cycle circuitry by a polarized single-domain PAS protein. Nat. Commun. *6*, 1–14. https://doi.org/10.1038/ncomms8005.

Schneider, C.A., Rasband, W.S., and Eliceiri, K.W. (2012). NIH Image to ImageJ: 25 years of image analysis. Nat. Methods *9*, 671–675. https://doi.org/10.1038/nmeth.2089.

Schredl, A.T., Mora, Y.G.P., Herrera, A., Cuajungco, M.P., and Murray, S.R. (2012). The Caulobacter crescentus ctrA P1 promoter is essential for the coordination of cell cycle events that prevent the overinitiation of DNA replication. Microbiology *158*, 2492. https://doi.org/10.1099/mic.0.055285-0.

Siam, R., and Marczynski, G.T. (2000). Cell cycle regulator phosphorylation stimulates two distinct modes of binding at a chromosome replication origin. EMBO J. *19*, 1138–1147. https://doi.org/10.1093/emboj/19.5.1138.

Siam, R., and Marczynski, G.T. (2003). Glutamate at the phosphorylation site of response regulator CtrA provides essential activities without increasing DNA binding. Nucleic Acids Res. *31*, 1775–1779. https://doi.org/10.1093/nar/gkg271.

Siam, R., Brassinga, A.K.C., and Marczynski, G.T. (2003). A dual binding site for integration host factor and the response regulator CtrA inside the Caulobacter crescentus replication origin. J. Bacteriol. *185*, 5563–5572. https://doi.org/10.1128/JB.185.18.5563-5572.2003.

Skerker, J.M., and Laub, M.T. (2004). Cell-cycle progression and the generation of asymmetry in Caulobacter crescentus. Nat. Rev. Microbiol. *2*, 325–337. https://doi.org/10.1038/nrmicro864.

Smith, S.C., Joshi, K.K., Zik, J.J., Trinh, K., Kamajaya, A., Chien, P., and Ryan, K.R. (2014). Cell cycle-dependent adaptor complex for ClpXP-mediated proteolysis directly integrates phosphorylation and second messenger signals. Proc. Natl. Acad. Sci. U S A *111*, 14229–14234. https://doi.org/10.1073/pnas.1407862111.

Spencer, W., Siam, R., Ouimet, M.-C., Bastedo, D.P., and Marczynski, G.T. (2009). CtrA, a global response regulator, uses a distinct second category of weak DNA binding sites for cell cycle transcription control in Caulobacter crescentus. J. Bacteriol. *191*, 5458–5470. https://doi.org/10.1111/j.1365-2958.2009.06630.x.

Stephens, C., Reisenauer, A., Wright, R., and Shapiro, L. (1996). A cell cycle-regulated bacterial DNA methyltransferase is essential for viability. Proc. Natl. Acad. Sci. U S A *93*, 1210–1214. https://doi.org/10.1073/pnas.93.3.1210.

Subramanian, K., Paul, M.R., and Tyson, J.J. (2013). Potential role of a bistable histidine kinase switch in the asymmetric division cycle of Caulobacter crescentus. PLoS Comput. Biol. *9*, e1003221. https://doi.org/10.1371/journal.pcbi.1003221.

Takacs, C.N., Hocking, J., Cabeen, M.T., Bui, N.K., Poggio, S., Vollmer, W., and Jacobs-Wagner, C. (2013). Growth medium-dependent glycine incorporation into the peptidoglycan of Caulobacter crescentus. PLoS One *8*, e57579. https://doi.org/10.1371/journal.pone.0057579.

Taylor, J.A., Wilbur, J.D., Smith, S.C., and Ryan, K.R. (2009). Mutations that alter RcdA surface residues decouple protein localization and CtrA proteolysis in Caulobacter crescentus. J. Mol. Biol. *394*, 46–60. https://doi.org/10.1016/j.jmb.2009.08.076.

Tan, M.H., Kozdon, J.B., Shen, X., Shapiro, L., and McAdams, H.H. (2010). An essential transcription factor, SciP, enhances robustness of Caulobacter cell cycle regulation. Proceedings of the National Academy of Sciences *107*, 18985–18990. https://doi.org/10.1073/pnas.1014395107.

Taylor, J.A., Ouimet, M., Wargachuk, R., and Marczynski, G.T. (2011). The Caulobacter

crescentus chromosome replication origin evolved two classes of weak DnaA binding sites. Mol. Microbiol. *82*, 312–326. https://doi.org/10.1111/j.1365-2958.2011.07785.x.

Terrana, B., and Newton, A. (1975). Pattern of unequal cell division and development in Caulobacter crescentus. Dev. Biol. *44*, 380–385. https://doi.org/10.1016/0012-1606(75)90409-1.

Thanbichler, M., and Shapiro, L. (2006). MipZ, a spatial regulator coordinating chromosome segregation with cell division in Caulobacter. Cell *126*, 147–162. https://doi.org/10.1016/j.cell.2006.05.038.

Tsokos, C.G., and Laub, M.T. (2012). Polarity and cell fate asymmetry in Caulobacter crescentus. Curr. Opin. Microbiol. *15*, 744–750. https://doi.org/10.1016/j.mib.2012.10.011.

Tsokos, C.G., Perchuk, B.S., and Laub, M.T. (2011). A dynamic complex of signaling proteins uses polar localization to regulate cell-fate asymmetry in Caulobacter crescentus. Dev. Cell *20*, 329–341. https://doi.org/10.1016/j.devcel.2011.01.007.

Viollier, P.H., Sternheim, N., and Shapiro, L. (2002a). Identification of a localization factor for the polar positioning of bacterial structural and regulatory proteins. Proc. Natl. Acad. Sci. U S A *99*, 13831–13836. https://doi.org/10.1073/pnas.182411999.

Viollier, P.H., Sternheim, N., and Shapiro, L. (2002b). A dynamically localized histidine kinase controls the asymmetric distribution of polar pili proteins. EMBO J. *21*, 4420–4428. https://doi.org/10.1093/emboj/cdf454.

Wargachuk, R., and Marczynski, G.T. (2015). The Caulobacter crescentus homolog of DnaA (HdaA) also regulates the proteolysis of the replication initiator protein DnaA. J. Bacteriol. *197*, 3521–3532. https://doi.org/10.1128/JB.00460-15.

Wheeler, R.T., and Shapiro, L. (1999). Differential localization of two histidine kinases controlling bacterial cell differentiation. Mol. Cell *4*, 683–694. https://doi.org/10.1016/S1097-2765(00)80379-2.

Williams, B., Bhat, N., Chien, P., and Shapiro, L. (2014). ClpXP and ClpAP proteolytic activity on divisome substrates is differentially regulated following the C aulobacter asymmetric cell division. Mol. Microbiol. *93*, 853–866. https://doi.org/10.1111/mmi.12698.

Wright, R., Stephens, C., Zweiger, G., Shapiro, L., and Alley, M.R. (1996). Caulobacter Lon protease has a critical role in cell-cycle control of DNA methylation. Genes Dev. *10*, 1532–1542. https://doi.org/10.1101/gad.10.12.1532.

Xu, C., Weston, B.R., Tyson, J.J., and Cao, Y. (2020). Cell cycle control and environmental response by second messengers in Caulobacter crescentus. BMC Bioinformatics *21*, 1–19. https://doi.org/10.1186/s12859-020-03687-z.

Zhou, B., Schrader, J.M., Kalogeraki, V.S., Abeliuk, E., Dinh, C.B., Pham, J.Q., Cui, Z.Z., Dill, D.L., McAdams, H.H., and Shapiro, L. (2015). The global regulatory architecture of transcription during the Caulobacter cell cycle. PLoS Genet. *11*, e1004831. https://doi.org/10.1371/journal.pgen.1004831.

Zweiger, G., and Shapiro, L. (1994). Expression of Caulobacter dnaA as a function of the cell cycle. J. Bacteriol. *176*, 401–408. https://doi.org/10.1128/jb.176.2.401-408.1994.

Zhou, X., and Shapiro, L. (2018). Cell cycle-controlled clearance of the CcrM DNA methyltransferase by Lon is dependent on DNA-facilitated proteolysis and substrate polar sequestration. bioRxiv *293738*. https://doi.org/10.1101/293738.

Zweiger, G., Marczynski, G., and Shapiro, L. (1994). A Caulobacter DNA methyltransferase that functions only in the predivisional cell. J. Mol. Biol. *235*, 472–485. https://doi.org/10.1006/jmbi.1994.1007.

STAR★METHODS

KEY RESOURCES TABLE

REAGENT or RESOURCE	SOURCE	IDENTIFIER
Software and algorithms		
ImageJ	Schneider et al. (2012)	https://imagej.net
MATLAB	The MathWorks Inc.	R2019a
Caulobrowser	Lasker et al. (2016a)	http://web.stanford.edu/group/golden_gate_clon/cgi-bin/index/index.py
Modeling and analysis scripts	This Paper	https://github.com/bronsonweston/CaulobacterModel

RESOURCE AVAILABILITY

Lead contact

Further information and requests for resources should be directed to and will be fulfilled by the lead contact, Yang Cao (ycao@cs.vt.edu).

Materials availability

This study did not generate new unique reagents.

Data and code availability

- No raw data was collected for this study. All results were produced from deterministic simulations. Our results, tables, and figures can be reproduced by running our data and figure generating pipelines, which are easily accessible through our publically available code.
- All of the code used for simulations and figure generation can be found at https://github.com/bronsonweston/CaulobacterModel.
- Any additional information required to reanalyze the data reported in this paper is available from the lead contact upon request.

METHOD DETAILS

General simulation methodology

All simulations and quantitative analyses were conducted with customized MATLAB R2019a scripts, unless otherwise stated. Each cell cycle simulation was carried out utilizing MATLAB's ode15s for 1600 simulated minutes. A full list of equations governing the cell cycle model is specified in the section "Equations and Simulation Events Governing Cell Cycle Model". The presence/absence of $CtrA_U$:*Cori* binding in each simulation is dictated by the parameter, $\sigma_{CtrAU:Cori}$. For Quick, Slow and $Cori^-$+$CtrA_U$:*Cori* simulations, $\sigma_{CtrAU:Cori}$ is set to zero. For Quick–$CtrA_U$:*Cori*, Slow–$CtrA_U$:*Cori*, and $Cori^-$ simulations, $\sigma_{CtrAU:Cori}$ is set to one.

In the following text we specify the biology and methodology behind our cell cycle equations. As precise concentrations of most *Caulobacter* proteins are unknown, we do not assign specific concentration units to each variable. Notable exceptions are CtrA and cdG, which do have experimentally measured concentrations.

General ODE structure

We gather information on the promoters of each gene from the online database CauloBrowser (Lasker et al., 2016a). Since CauloBrowser indicates whether a protein binds to a promoter site, but often does not specify the nature of the protein's influence over the gene's activity, we determine the nature of a given gene-protein interaction by referring to the literature, when possible, and comparing the expression of

mRNA (via the CauloBrowser tool) with the expression of proteins that influence the gene of interest. It is often straightforward to determine if a transcription factor inhibits or activates a gene.

The differential equation for the rate of change of a protein, P, takes the standard form:

$$\frac{d[\mathrm{P}]}{dt} = k_{s,\mathrm{P}} \cdot h \cdot \left(\prod\nolimits_{a \epsilon A} \frac{[\mathrm{TF}]_a^n + \varepsilon_{\mathrm{P,a}} \cdot J_{\mathrm{P,a}}^n}{[\mathrm{TF}]_a^n + J_{\mathrm{P,a}}^n} \right) \left(\prod\nolimits_{i \epsilon I} \frac{\varepsilon_{\mathrm{P,i}} \cdot [\mathrm{TF}]_i^n + J_{\mathrm{P,i}}^n}{[\mathrm{TF}]_i^n + J_{\mathrm{P,i}}^n} \right) - (k_{d,\mathrm{P}} + \mu)[\mathrm{P}] + f,$$

where the first term dictates the rate of synthesis, the second term dictates the rate of degradation/dilution and the third term, f, represents the rates of all other interactions that influence the production and removal of the protein. Synthesis and degradation rate constants are denoted k_s and k_d, respectively, and μ denotes the specific rate of dilution of a component due to cell growth. When several different proteins interact at a promoter site to regulate the synthesis of P, we assume that the total promoter activity is the product of individual protein contributions (AND logic rather than OR logic). Here, A and I represent the collection of all proteins that activate and inhibit the gene, respectively. $J_{\mathrm{P,a}}$ and $J_{\mathrm{P,i}}$ are the concentrations of the transcription factors 'a' and 'i' that correspond to half-maximal influence over synthesis of P. For transcription factors that do not have complete control over a gene's transcription we introduce a parameter ε, $0 \leq \varepsilon \leq 1$. We typically set ε to zero unless an alternative value is necessary to explain biologically observed behaviors. The parameter, n, dictates the degree of cooperativity of transcription factors in influencing promoter activity. Unless the literature suggests otherwise, we assume that each transcription factor has only one binding site on a given promoter, and set $n = 1$. However, promoter sites targeted by CtrA often have two binding sites that interact cooperatively. Such binding motifs are called "full", while promoters with only one CtrA binding site are called "half" (Zhou et al., 2015). The CauloBrowser online database designates each promoter site as a "full" or "half" motif (Lasker et al., 2016a), and we set $n = 1$ and $n = 2$ for "half" and "full" motifs, respectively. Finally, h represents the influence of methylation on promoter activity. For genes that are more active when hemi-methylated, $h = 1 - m_{\mathrm{P}}(2M_{\mathrm{P}}-1)$, and for genes that are more active when fully methylated, $h = 1 + 2m_{\mathrm{P}}(M_{\mathrm{P}}-1)$, Here, M_{P} represents the methylation state of the gene: $M_{\mathrm{P}} = 1$ when fully methylated and $M_{\mathrm{P}} = 0.5$ when hemi-methylated, and m_{P} is a parameter that dictates the degree by which the methylation state influences the promoter activity of P, where $0 < m_{\mathrm{P}} \leq 1$. For genes that do not have a methylation site and genes that do not seem to be influenced by methylation, we set $m_{\mathrm{P}} = 0$.

Importantly, the methylation state M_{P} of a gene acts like a switch. When CcrM is sufficiently active ([CcrM] = 0.65 in our simulations), all hemi-methylated genes become methylated. Because genes transition from fully methylated to hemi-methylated when the chromosome replication fork passes through the gene (Kozdon et al., 2013), we must keep track of the progression of the replication fork, by means of the variable Elong,

$$\frac{d[\mathrm{Elong}]}{dt} = k_{\mathrm{Elong}} \cdot RepSwitch.$$

RepSwitch = 1 or 0 when the chromosome is replicating or not replicating, respectively. [Elong] also ranges from 0 to 1, representing the fraction of the chromosome that has been replicated. When [Elong] = 1, chromosome replication has been completed, and *RepSwitch* and [Elong] are reset to 0. Referring to the CauloBrowser database (Lasker et al., 2016a), we note the location L_{G} of each gene containing a methylation site. (L_{G} = fractional location of gene G along the chromosome.) When [Elong] = L_{G}, the methylation status of the gene changes from 1 to $^1/_2$. L_{G} values are specified in the "Equations and Simulation Events Governing Cell Cycle Model" section.

Protein complexes and phosphorylation

Protein binding and phosphotransferase reactions are modeled with mass action kinetics. We assume that such reactions are at pseudo-steady state, as these reactions are much faster than those pertaining to genetic regulation and protein synthesis. Enzymatic reactions, such as phosphorylation and proteolysis, are typically described by:

$$\mathrm{S} + \mathrm{E} \rightleftarrows^{k_1}_{k_{-1}} \mathrm{S:E} \overset{k_{\mathrm{cat}}}{\rightarrow} \mathrm{E} + \mathrm{P},$$

where S is the substrate, E is the enzyme, and P is the product (although there is often no product worth tracking for proteolysis). If the substrate concentration is much greater than the enzyme concentration, then the rate of this reaction is given by the Michaelis-Menten equation,

$$\frac{d[P]}{dt} = k_{s,P}\frac{[E]_T[S]}{[S]+K_M}.$$

The Michaelis constant, $K_M = (k_{-1} + k_{cat})/k_1$, is defined in terms of the forward and reverse rate constants for the enzyme-substrate binding reaction, and the catalytic rate constant for the step S:E → E + P. Here, $k_{s,P} = k_{cat}$. However, in the context of several protein-protein reactions in the *Caulobacter* cell cycle control network, the concentrations of the 'substrate' and the 'enzyme' are similar, and the Michaelis-Menten rate law cannot be used (Cha, 1970). To simplify things in this context, we assume that $k_{cat}>>k_1>>k_{-1}$, in which case

$$\frac{d[P]}{dt} = k_{s,P}[E][S],$$

where $k_{s,P} = k_1$, i.e., the reaction is rate-limited by the enzyme-substrate binding step. An advantage of this assumption is that we can model different reactions independently, even if the same substrate is targeted by multiple enzymes or if the same enzyme targets multiple substrates. We use this approach for modeling DivJ and PleC phosphorylation/dephosphorylation of DivK and PleD.

Phosphotransferase kinetics take the form:

$$A \sim P + B \leftrightarrow A + B \sim P.$$

If A is a histidine kinase, such as CckA kinase, we can assume that the reaction is not reversible, and A is immediately re-phosphorylated by ATP after offering its phosphate group to B. In this scenario, [B ∼ P] accumulates at a rate of:

$$\frac{d[B \sim P]}{dt} = k_f[A]_T[B],$$

where k_f is the forward reaction rate constant and $[A]_T = [A \sim P] + [A] \approx [A \sim P]$. Similarly, if A is a histidine phosphatase, such as CckA phosphatase, we assume that A∼P is dephosphorylated immediately after it is phosphorylated and the reaction is non-reversible such that:

$$\frac{d[B]}{dt} = k_r[A]_T[B \sim P],$$

where k_r is the reverse reaction rate constant and $[A]_T = [A \sim P] + [A] \approx [A]$.

To model protein complexes, $A + B \leftrightarrow C$, we utilize two approaches. 1) If the binding is very strong, then the more dilute protein (say, B) is negligible in the free form compared to the bound form, such that:

$$[C] = \min([A]_T, [B]_T) = [B]_T,$$
$$[A]_F = [A]_T - [B]_T,$$
$$[B]_F = 0\ .$$

Here, [C] is the protein complex concentration, while $[A]_F$ and $[B]_F$ are the concentrations of the free forms of A and B, respectively. We utilize this method for modeling the interaction of DgcB with PdeA. Alternatively, 2) we solve for the equilibrium concentrations of the reaction

$$A + B \leftrightarrow C,$$

where $[A] = [A]_T - [C]$ and $[B] = [B]_T - [C]$. The solution for this system at equilibrium is:

$$[C] = \frac{[A]_T + [B]_T + \frac{1}{K_C} - \sqrt{\left([A]_T + [B]_T + \frac{1}{K_C}\right)^2 - 4\cdot[A]_T\cdot[B]_T}}{2}$$

where $K_C = k_f/k_r$, is the equilibrium binding constant of the complex. While this approach is more complicated than the previous approach, it is capable of capturing a range of system behaviors. We use it to model interactions that are key to regulating master regulator CtrA, such as [RcdA:PopA] and [CckA:DivL].

Localization

In many instances, enzymes localize to the poles of *C. crescentus*, while their substrates are freely diffusing. Although our model is based on ordinary differential equations (ODE), we are able to capture the effects of polar localization by assuming that diffusion of substrates in the cytoplasm is very fast. For an enzyme-catalyzed reaction occurring at a pole, we introduce a local volume V_L distinct from the volume V of the entire cell. For a molecule X that is freely diffusing, its local concentration $[X]_L$ is the same as its cellular concentration [X], but for a molecule that is entirely localized to V_L,$[X] = V_L[X]_L/V$. The rate that a product accumulates in the local volume is defined as

$$\frac{d[P]_L}{dt} = k_{s,P}\frac{[E]_L[S]_L}{[S]_L + K_M}.$$

If the substrate is freely diffusing but the enzyme is localized to V_L, then

$$\frac{d[P]_L}{dt} = k_{s,P}\cdot[E]\cdot\left(\frac{V}{V_L}\right)\cdot\frac{[S]}{[S]+K_M},$$

And, therefore, the rate that a freely diffusing product accumulates in the entire cell volume is:

$$\frac{d[P]}{dt} = k_{s,P}\cdot[E]\cdot\frac{[S]}{[S]+K_M}.$$

Thus, $d[P]/dt$ is independent of enzyme localization and cell volume. Therefore, in the case of a localized enzyme and a freely diffusing substrate, we can model as if there were no localization. (We are assuming in these cases that $[S]_L >> [E]_L$ so that the Michaelis-Menten rate law is valid.)

If we reverse the roles of substrate and enzyme in the previous scenario, such that the substrate is the localized agent and the enzyme is freely diffusing, then we get:

$$\frac{d[P]}{dt} = k_{s,P}\cdot[E]\cdot\frac{[S]}{[S]\cdot\left(\frac{V}{V_L}\right)+K_M}.$$

Since V_L is a constant, the equation works out to:

$$\frac{d[P]}{dt} = \widehat{k}_{s,P}\cdot[E]\cdot\frac{[S]}{[S]\cdot V+\widehat{K}}.$$

where $\widehat{K} = K_M\cdot V_L$ and $\widehat{k}_{s,P} = k_{s,P}\cdot V_L$. This case describes the dynamics of CtrA proteolysis, discussed later.

Finally, by the same logic, if both the enzyme and the substrate are localized, then

$$\frac{d[P]}{dt} = k_{s,P}\cdot[E]\cdot\frac{[S]}{[S]+\frac{\widehat{K}}{V}}.$$

This equation describes the dynamics of PleC/PodJ localization, discussed later.

Swarmer vs. stalked simulations

While swarmer and stalked cells have different phenotypes, the fundamental kinetics of molecular interactions are the same in both cell types, so we model both types of cells with the same set of ODEs. This small feature represents a large improvement over other ODE models of the *C. crescentus* cell cycle, which simulate stalked and swarmer cells with fundamentally different ODEs (Li et al., 2009; Murray et al., 2013). Instead, we keep track of the localized proteins of the cell, and where they end up after cytokinesis. Simulations designated SW or ST follow either the swarmer or stalked cell at the time of cell division.

Upon cytokinesis, the volume of the parent cell is divided between two daughter cells. For a given molecular species localized to a pole, the local concentration $[C]_L$ and volume V_L will remain the same, but the cellular concentration [C] will change as the cell volume V changes, as follows:

$$[C]_{new} = [C]_{old}\cdot\left(\chi_{dif} + \chi_{pole}\left(\frac{V_{old}}{V_{new}}\right)\right),$$

where $[C]_{old}$ is the concentration prior to cytokinesis and $[C]_{new}$ is the concentration in the cell of interest (ST or SW) after cytokinesis. χ_{pole} and χ_{dif} represent the fraction of species C that is located at the pole of interest and that is freely diffusing, respectively. V_{old} is the original volume of the cell and V_{new} is the volume of the daughter cell of interest. Given the characteristics of *Caulobacter* growth, we assume that the volume shift after cytokinesis is proportional to the change in length after cytokinesis. Because stalked cell length after cytokinesis is approximately 54% of the original cell length (Terrana and Newton, 1975), $V_{new} = 0.54 \cdot V_{old}$ when following the stalked cell and $V_{new} = 0.46 \cdot V_{old}$ when following the swarmer cell.

CtrA:*Cori* binding

CtrA∼P interacts with five binding sites at the chromosome origin (*Cori*), designated [a]-[e], to inhibit chromosome replication (Collier, 2012). CtrA molecules recognize the nucleotide motif, TTAA (half-site); however, *Cori* binding sites [a]-[e] have nucleotides in the arrangement of TTAA-N7-TTAA (full-site) (Siam and Marczynski, 2000). Hence, each CtrA binding site may recruit two CtrA molecules, and experiments suggest that pairs of CtrA molecules interact cooperatively to enhance their affinity for *Cori* (Siam and Marczynski, 2000, 2003). While CtrA∼P seems to have a higher affinity than $CtrA_U$ for sites [a]-[e], mutant experiments on site [d] suggest that $CtrA_U$ interacts with individual TTAA recognition sites with equal affinity as CtrA∼P (Siam and Marczynski, 2000); this suggests that the differences in affinity between unphosphorylated and phosphorylated forms of CtrA to sites [a]-[e] are a consequence of cooperativity. To investigate this mechanism further, we developed a mathematical model of CtrA interactions with DNA at site [d]. Figure 2A depicts each possible state of CtrA:DNA and the corresponding equilibrium expression. Table S3 presents binding/unbinding reactions at site [d] and corresponding steady-state kinetic expressions. In Table S3 we assume that the fraction of CtrA that is bound to DNA is negligible compared to freely diffusing CtrA. This assumption simplifies the model. Importantly, we also assume that the cooperativity between $CtrA_U$ and CtrA∼P when bound to DNA is equivalent to the cooperativity between two $CtrA_U$ molecules.

The concentration of Cori sites is normalized so that:

$$[DNA]_{Total} = [DNA]_F + [DNA : CtrA_U] + [DNA : CtrA_{U2}] + [DNA : CtrA \sim P] + [DNA : CtrA \sim P_2] + [DNA : CtrA \sim P : CtrA_U] = 1.$$

By plugging the equilibrium expressions from Table S3 into this equation, we obtain the expression:

$$[DNA]_F = K_{d1} \cdot \left(K_{d1} + 2 \cdot [CtrA_U] + 2 \cdot [CtrA \sim P] + \frac{[CtrA_U]^2}{K_{d2}} + \frac{[CtrA \sim P]^2}{K_{d3}} + 2 \cdot \frac{[CtrA_U] \cdot [CtrA \sim P]}{K_{d2}} \right)^{-1}.$$

Thus, for any combination of $[CtrA_U]$ and [CtrA∼P], the fraction of DNA in each state depicted in Figures 2A and Table S3 can be calculated. However, reasonable estimates for these states rely on reasonable parameter estimates for K_{d1}, K_{d2} and K_{d3}. To acquire these estimates, we compared our model simulations with experiments published by Siam and Marczynski (Siam and Marczynski, 2000), who measured how DNA footprinting band intensities vary over different concentrations of $CtrA_U$ and CtrA∼P. As Siam and Marczynski utilized excess CtrA (relative to DNA binding sites) in their experiments, our assumption that the concentration of free CtrA is unaffected by DNA binding is valid.

First we consider $CtrA_U$ binding to a site [d] mutant that has only one TTAA recognition sequence (Siam and Marczynski, 2000). In this scenario, the only two states possible are $[DNA]_F$ and $[DNA:CtrA_U]$. Thus, the solution becomes:

$$Intensity = [DNA]_F = \frac{K_{d1}}{K_{d1} + [CtrA_U]}.$$

Fitting the above equation to the band intensity depicted in Figure 4A of Siam and Marczynski, utilizing MATLAB's cftool, we estimate that $K_{d1} = 1.06$ μM (Figure S1A).

Next, we investigate Figure 4B of Siam and Marczynski, which displays the intensity of the DNase I footprinting assay on WT site [d]. As no CtrA∼P was present in the experiment, the following expression describes this scenario:

$$Intensity = [DNA]_F + \frac{[DNA : CtrA_U]}{2},$$
$$= \frac{K_{d1} + [CtrA_U]}{K_{d1} + 2 \cdot [CtrA_U] + \frac{[CtrA_U]^2}{K_{d2}}}.$$

In Figure S1B, we fit the corresponding data in Siam and Marczynski (utilizing MATLAB's cftool) to estimate K_{d2} = 0.039 μM. Similarly, when modeling [CtrA∼P] (with no $CtrA_U$ present), the readings for band intensity should be proportional to:

$$Intensity = [DNA]_F + \frac{[DNA : CtrA \sim P]}{2},$$
$$= \frac{K_{d1} + [CtrA \sim P]}{K_{d1} + 2 \cdot [CtrA \sim P] + \frac{[CtrA \sim P]^2}{K_{d3}}}.$$

While the authors do not provide data on [CtrA∼P], they do provide a K_d value that they determined by fitting the data to a hyperbolic function $K_d/(K_d + [CtrA\sim P])$. We utilized their K_d value to generate artificial data points and fit our equation using cftool, as shown in Figure S1C, to derive K_{d3} = 0.085 nM.

CtrA/DnaA competitive binding

It was shown that CtrA can bind to *Cori* to displace DnaA binding. However, we must consider if DnaA may displace CtrA from *Cori*; Between 0.001 μM and 0.01 μM of GST-CtrA, a dimerized active form of CtrA, is sufficient to displace 0.1 μM of DnaA from *Cori* (Taylor et al., 2011). GST-CtrA has a similar binding affinity as CtrA∼P for *Cori* (Spencer et al., 2009), and CtrA∼P binds to *Cori* binding sites with $K_d \approx$ 0.003–0.015. Since we would expect to witness considerable CtrA∼P binding at 0.001–0.01 μM in the absence of DnaA, this indicates that DnaA made a negligible impact on CtrA∼P binding.

Our results indicate that $CtrA_U$ can displace the majority of CtrA∼P at ratios of 25:1 (Figure 2C). Therefore, if CtrA∼P and $CtrA_U$ interact identically with DnaA, we would expect that 0.1 μM of DnaA can be displaced by 0.25 μM of $CtrA_U$. Compared to the estimated dissociation constant for $CtrA_U$, $K_d \approx$ 0.2–0.6 μM (Siam and Marczynski, 2000), this implies that DnaA would have a negligible impact on $CtrA_U$ binding as well. Since DnaA is unlikely to displace $CtrA_U$ and CtrA∼P for *Cori* binding sites, we do not consider DnaA in our calculations of CtrA:*Cori* binding.

Considering increased complexity of CtrA:DNA binding

There are three complications that we must consider when extending our model from the experiments of Siam and Marczynski to an *in vivo* system. First, the concentration of free CtrA may not be close to the total concentration of CtrA (i.e., DNA bound CtrA is non-negligible). Second, there are CtrA binding sites on DNA other than *Cori* sites [a]-[e], and these sites may compete with *Cori* for CtrA binding. Third, *Cori* sites [a]-[e] may compete with each other for CtrA. To investigate these concerns, we developed a set of ODEs to describe these interactions. We call this ODE model the "complex" model and the algebraic equation model (described previously) the "simple" model.

CtrA binds to 183 transcriptional start sites in *Caulobacter*: 54 full-sites (bind two CtrA molecules) and 124 half-sites (bind one CtrA molecule) (Zhou et al., 2015). Information on binding strength to these sites is extremely limited. We assume that the average dissociation constant at the half-sites (K_{dHS}) is equal to K_{d1}, as K_{d1} is an estimate for the affinity of a single CtrA molecule for the TTAA motif. The dissociation constants for the full-motif promoters of *fliQ* and *ccrM* have been estimated to be 0.2 μM and 3.5 μM, respectively (Reisenauer et al., 1999). We choose the stronger of the two, K_{dFS} = 0.2 μM. For the sake of simplicity, we also assume that binding at sites [a]-[e] is identical to binding at site [d]. The four ODEs and two algebraic equations that comprise this "complex" model are summarized as:

$$\frac{d[DNA_{HS}:CtrA \sim P]}{dt} = (([DNA_{HS}]_T - [DNA_{HS}:CtrA \sim P])) \cdot [CtrA \sim P]_F - K_{dHS} \cdot [DNA_{HS}:CtrA \sim P]$$
$$\frac{d[DNA_{FS}:CtrA \sim P_2]}{dt} = ([DNA_{FS}]_T - [DNA_{FS}:CtrA \sim P_2]) \cdot [CtrA \sim P]_F^2 - K_{dFS} \cdot [DNA_{FS}:CtrA \sim P_2]$$
$$\frac{d[DNA_{Cori}:CtrA \sim P]}{dt} = 2 \cdot [DNA_{Cori}]_F \cdot [CtrA \sim P]_F - K_{d1} \cdot [DNA_{Cori}:CtrA \sim P]$$

$$\frac{d[\mathrm{DNA_{Cori}{:}CtrA\sim P_2}]}{dt} = [\mathrm{DNA_{\mathit{Cori}}{:}CtrA\sim P}]\cdot[\mathrm{CtrA\sim P}]_F - 2\cdot K_{d3}\cdot[\mathrm{DNA_{\mathit{Cori}}{:}CtrA\sim P_2}]$$

$$[\mathrm{CtrA\sim P}]_F = [\mathrm{CtrA\sim P}]_T - [\mathrm{DNA_{HS}{:}CtrA\sim P}] - 2\cdot[\mathrm{DNA_{FS}{:}CtrA\sim P_2}] - [\mathrm{DNA_{Cori}{:}CtrA\sim P}] - 2\cdot[\mathrm{DNA_{Cori}{:}CtrA\sim P_2}]$$

$$[\mathrm{DNA_{\mathit{Cori}}}]_F = [\mathrm{DNA_{\mathit{Cori}}}]_T - [\mathrm{DNA_{\mathit{Cori}}{:}CtrA\sim P}] - [\mathrm{DNA_{\mathit{Cori}}{:}CtrA\sim P_2}]$$

$$[\mathrm{DNA_{HS}}]_T = 0.21\mu\mathrm{M};[\mathrm{DNA_{FS}}]_T = 0.09\mu\mathrm{M};[\mathrm{DNA_{\mathit{Cori}}}]_T = 0.0083\mu\mathrm{M}$$

Here, DNA_{HS} represents DNA half-sites, DNA_{FS} represents DNA full-sites, and DNA_{Cori} represents *Cori* binding sites. For a given species X, the concentration of free (unbound) X is represented as $[X]_F$ and $[X]_T$ is the total concentration of X (sum of bound and unbound). Notably, the "complex" model does not include binding of unphosphorylated CtrA, as it focuses on the binding dynamics of CtrA∼P.

We solve for the steady state solution of these equations (utilizing MATLAB solver ode15s) over a range of CtrA∼P concentrations. We find that at steady state (i.e., at chemical equilibrium), $[CtrA\sim P]_F$ values deviate significantly from $[CtrA\sim P]_T$ concentrations when total concentrations are low (Figure S2A). However, when we plot the fraction of $[DNA_{Cori}{:}CtrA\sim P_2]/[DNA_{Cori}]_T$ against $[CtrA\sim P]_T$ (Figure S2B), the shape of the curve is extremely similar to that of Figure 2D which describes binding of CtrA∼P to *Cori* in the simple model. The only distinguishing difference between the two figures is the CtrA concentration at half-maximal saturation of *Cori*. The simple and complex models predict 50% *Cori* saturation at CtrA∼P concentrations of 6 and 12 molecules per cell, respectively. Considering that there are ∼9,000 CtrA molecules in a swarmer cell (Spencer et al., 2009), the difference between the two models seems to be negligible in consideration of the G1-S transition. Thus, we conclude that the simple model is sufficient for studying the dynamics of CtrA:*Cori* binding and for use in our larger model of the *C. crescentus* cell cycle.

Biological mechanisms

Progression through the *Caulobacter crescentus* cell cycle is controlled by a complex molecular mechanism that involves genetic regulation, proteolysis, protein-protein interactions, protein phosphorylation and dephosphorylation, and protein localization. To capture the dynamics of these processes, we derived a set of nonlinear ODEs, using the procedures described above and based on observed biological facts stated below. In this section, we discuss the molecular mechanisms behind the larger model.

Chromosome replication. The initiation of chromosome replication is modeled with the variable, Ini, which considers the influence of DnaA, CtrA, and methylation on *Cori* activity. When Ini is equal to one, chromosome replication begins (see "Equations and simlation events governing the cell cycle model") and the corresponding time is marked as t^{cr}. A detailed description of *Cori* regulation is provided in the 'Discussion' of the main text.

Given that the mechanistic details of CtrA inhibition and DnaA activation of *Cori* are complex and not completely understood, attempting to create a detailed model of *Cori* activity would be challenging and likely inaccurate. Therefore, we take a simplistic approach to model the initiation of DNA replication via the variable Ini. First, we assume that $[DNA{:}CtrA\sim P_2]$ is the only relevant species to inhibit chromosome replication, as levels of $[DNA{:}CtrA\sim P]$ and $[DNA{:}CtrA\sim P{:}CtrA]$ are negligible compared to $[DNA{:}CtrA\sim P_2]$, as shown in Figure 2B. Next, we assume that all five CtrA binding sites cooperatively work together to impair chromosome replication. Thus, we assume that the inhibition of Ini by CtrA∼P is proportional to $(1-[CtrA{:}CtrA\sim P_2])^5$. DnaA-ATP binds with moderate affinity to two 'G' boxes and weakly to five 'W' boxes. Binding to the W boxes is dependent on cooperative interactions with DnaA at G boxes. Thus, we assume that if DnaA-ATP binds to the G boxes, the W boxes will follow. We further assume that DnaA-ATP binding at each G box is independent, but DnaA works cooperatively at each G site to initiate chromosome replication. Therefore, we model the binding of DnaA-ATP as a hyperbolic function, and square the function to capture cooperativity. *Cori* also has several methylation sites, but it was shown that Δ*ccrM* strains are viable (Collier, 2012; Gonzalez and Collier, 2013). Therefore, *Cori* methylation only partially influences DNA replication in this model.

Regulation of ccrM. The *ccrM* promoter has a methylation site of its own, and is upregulated by CtrA∼P and downregulated by DnaA (Collier et al., 2007; Lasker et al., 2016a). As *ccrM* is more active transcriptionally when hemi-methylated, chromosome replication primes the cell for CcrM expression. In G2, CtrA∼P levels accumulate, and DnaA levels decline, resulting in CcrM synthesis. When CcrM levels are high enough to methylate DNA, the gene shuts off until G2 of the next cell cycle. Additionally, CcrM is rapidly degraded

by Lon protease. As a result of these regulatory mechanisms, the window of CcrM expression is very short (Adhikari and Curtis, 2016; Wright et al., 1996). Given that Lon is reported to be constantly active (Wright et al., 1996), we model the degradation of CcrM as a simple first-order reaction with Lon activity folded into the rate constant.

Regulation of CtrA. Regulation of *ctrA* is discussed in depth in the main text. Here, we will expand upon the biology and mathematical modeling of CtrA proteolysis and phosphorylation. Effective proteolysis of CtrA requires the collaboration of several proteins, including ClpX, ClpP, CpdR, RcdA, and PopA. While unphosphorylated CpdR binds directly to ClpXP and localizes the protease to the old pole, RcdA interacts with both CpdR and PopA. PopA, however, does not recruit CtrA unless it is activated by two cyclic diguanosine monophosphate (cdG) molecules. Furthermore, PopA localization to the pole is dependent on cdG, but PopA can interact with RcdA independently of cdG (Smith et al., 2014). When these components all come together, they form a complex that effectively targets and degrades CtrA over other ClpXP substrates (Joshi et al., 2015). Since the concentration of ClpX and ClpP do not fluctuate with the cell cycle (Jenal and Fuchs, 1998), we do not explicitly model ClpXP. We also assume that unphosphorylated CpdR is always localized and bound to ClpXP at the old pole. Similarly, we assume that the PopA:cdG$_2$:RcdA complex is always localized at the old pole. Since PopA interacts with RcdA independently of cdG and vice versa (Smith et al., 2014), the concentration of the localized PopA:cdG$_2$:RcdA complex is equal to the total amount of RcdA bound to PopA times the fraction of PopA that is bound by cdG:

$$[\mathrm{PopA{:}cdG_2{:}RcdA}] = \frac{[\mathrm{PopA{:}cdG_2}]\cdot[\mathrm{RcdA{:}PopA}]_T}{[\mathrm{PopA{:}cdG_2}]+[\mathrm{PopA}]}.$$

We assume that the PopA:cdG$_2$:RcdA complex interacts with the localized CpdR:ClpXP complex (simply denoted by CpdR) by simple mass action kinetics, so the rate of change for the entire CtrA proteolytic complex, denoted as $[\mathrm{ClpXP}]_{\mathrm{Complex}}$ takes the form:

$$\frac{d[\mathrm{ClpXP}]_{\mathrm{Complex}}}{dt} = \frac{V_L}{V}\left(-k_1\frac{V}{V_L}[\mathrm{ClpXP}]_{\mathrm{Complex}} + k_2\left(\frac{V}{V_L}\right)^2[\mathrm{CpdR}][\mathrm{PopA{:}cdG_2{:}RcdA}]_F\right),$$

where $[\mathrm{PopA{:}cdG_2{:}RcdA}]_F$ designates the concentration of [PopA:cdG$_2$:RcdA] that is not bound to CpdR. As all participating complexes in this interaction are localized to the old pole, we must account for the changes in local concentration on the kinetics by incorporating volume conversions (see "localization" section for reference). Importantly, we assume that the concentration of CpdR is much larger the PopA:cdG$_2$:RcdA complex. Thus, $[\mathrm{PopA{:}cdG_2{:}RcdA}]_F = [\mathrm{PopA{:}cdG_2{:}RcdA}] - [\mathrm{ClpXP}]_{\mathrm{Complex}}$, and the steady state solution for $[\mathrm{ClpXP}]_{\mathrm{Complex}}$ is:

$$[\mathrm{ClpXP}]_{\mathrm{Complex}} = \frac{[\mathrm{CpdR}]}{[\mathrm{CpdR}]+\frac{J_{ClpXP:CpdR}}{V}}\cdot\frac{[\mathrm{PopA{:}2cdG}]\cdot[\mathrm{RcdA{:}PopA}]_T}{[\mathrm{PopA{:}2dG}]+[\mathrm{PopA}]},$$

where $J_{\mathrm{ClpXP:CpdR}} = V_L\cdot k_1/k_2$.

Phosphorylation of CtrA is regulated by the bifunctional histidine kinase/phosphatase CckA. CckA interacts with CtrA via the phosphotransferase enzyme, ChpT (Subramanian et al., 2013). As ChpT levels are relatively constant throughout the cell cycle (Chen et al., 2009), we assume that ChpT does not fluctuate and instantaneously passes a phosphate from CtrA to CckA and vice versa. Given these assumptions, we can model the phosphorylation and dephosphorylation of CtrA in the form expressed in the "Protein complexes and phosphorylation" section. The activity of CckA as a bifunctional phosphatase/kinase is regulated by a variety of mechanisms discussed in the next section.

CckA kinase/phosphatase regulation. CckA, which functions as both a kinase and a phosphatase, is regulated by several mechanisms. First, *in vitro* experiments suggest that when CckA is unperturbed by regulatory factors, it acts as a kinase (Mann and Shapiro, 2018). The tyrosine kinase, DivL, binds with the CckA PAS-B domain and is generally implicated in maintaining the kinase state of CckA (Iniesta et al., 2010; Subramanian et al., 2013). However, phosphorylated DivK (DivK∼P) can bind to DivL likely causing a change in conformation of DivL's PAS domains (Childers et al., 2014). As a result, the DivK∼P:DivL complex binds with CckA to induce phosphatase activity over kinase activity. Importantly, DivK (unphosphorylated) has a weak affinity for DivL (Childers et al., 2014; Mann and Shapiro, 2018), and on this basis we

assume that unphosphorylated DivK does not interact with DivL in our model. Alternatively, CckA is regulated by the signaling molecule, cdG, which binds to CckA's PAS-B domain to induce the phosphatase state (Dubey et al., 2016; Mann and Shapiro, 2018).

With these assumptions, we calculate the total CckA phosphatase concentration ($[CckA]_P$) as:

$$[CckA]_P = \frac{[CckA:DivL]_T \cdot [DivL:DivK \sim P]}{[DivL]_T} + [CckA:cdG] - \frac{[CckA:cdG] \cdot \frac{[CckA:DivL]_T \cdot [DivL:DivK \sim P]}{[DivL]_T}}{[CckA]_T},$$

where the first term represents the fraction of CckA that is bound by DivL:DivK∼P and the second term represents the total amount of CckA bound by cdG. As the amount of CckA bound by both cdG and DivL:DivK∼P ([cdG:CckA:DivL:DivK∼P]) is counted twice by the first two terms, the third term subtracts by [cdG:CckA:DivL:DivK∼P]. Finally, the difference between $[CckA]_P$ and $[CckA]_T$ is used to compute $[CckA]_K$.

$$[CckA]_K = [CckA]_T - [CckA]_P.$$

Regulation of DnaA and GcrA. Details of *dnaA* regulation are discussed in the main text. DnaA-ATP, the active form of DnaA, is converted to DnaA-ADP by the enzyme HdaA (Fernandez-Fernandez et al., 2013; Wargachuk and Marczynski, 2015). We could not find any data on temporal regulation of HdaA; however, DnaA-ATP and DnaA-ADP activate the *hdaA* promoter (Fernandez-Fernandez et al., 2011). Since DnaA levels are at their peak at the timing of chromosome replication, it is reasonable to assume that HdaA levels would also be sufficiently high to hydrolyze DnaA at this time as well. Therefore, we do not model HdaA explicitly but rather model DnaA-ATP hydrolysis as a function of the variable *RepSwitch*, which is set to 1 during chromosome replication and 0 when DNA synthesis is complete. Additionally, DnaA proteolysis is targeted by both the ClpAP and Lon proteases (Jonas et al., 2013; Liu et al., 2016). However, because our model can fit DnaA expression data well without explicitly modeling mechanisms regulating DnaA proteolysis, we assume that DnaA turnover as a simple first-order reaction.

The influence of DnaA-ATP and DnaA-ADP on DnaA-targeted genes seems to differ depending on the gene. As mentioned, *hdaA* is targeted by both DnaA-ATP and DnaA-ADP; however, DnaA mutant studies suggest that *gcrA, mipZ* and *ftsZ* may be influenced more strongly by DnaA-ADP (Fernandez-Fernandez et al., 2011). Thus, in our model only DnaA-ADP can stimulate *gcrA* activity. Given the uncertainty of regulation at other DnaA targets, we assume equivalent activity of DnaA-ATP and DnaA-ADP.

Intracellular concentrations of the master regulator GcrA are regulated by transcriptional controls and by proteolysis. The *gcrA* promoter is activated by DnaA and inhibited by CtrA (Collier et al., 2007; Lasker et al., 2016a). The CtrA binding motif is full, meaning that it has two CtrA binding recognition sequences (Lasker et al., 2016a). Cell cycle-dependent turnover rates of GcrA also suggest that GcrA is targeted for proteolysis; however, the mechanism of GcrA proteolysis has not been identified (Collier et al., 2006; Jenal, 2009). In the absence of this information, we use a simple linear degradation rate to model GcrA turnover.

PleC and DivJ. DivJ, which accumulates during the swarmer-to-stalked transition, is a histidine kinase that serves to phosphorylate both DivK and PleD (Paul et al., 2008). DivJ activation is regulated primarily by SpmX and DivK. DivK and DivK∼P bind to DivJ allosterically to induce its kinase activity (Childers et al., 2014; Paul et al., 2008), while SpmX activates DivJ by directly binding with the protein and recruiting it to the cell pole (Radhakrishnan et al., 2008). We assume that DivJ likely has some activity independent of SpmX, and thus model the activity of DivJ as

$$[DivJ]_A = ([DivJ:DivK \sim P] + [DivJ:DivK]) \cdot \left([SpmX] + \theta_{DivJ}\right),$$

where θ_{DivJ} represents the activity of DivJ without SpmX, and [SpmX] has a maximum activity of $1-\theta_{DivJ}$. Factors that influence *spmX* promoter activity and mRNA translation are complex and not fully understood (Radhakrishnan et al., 2008; Tsokos and Laub, 2012). Therefore, we develop a function for [SpmX] that is not derived from the biochemistry, but is convenient for our modeling methodology:

$$\frac{d[SpmX]}{dt} = k_{s,SpmX}\left(\frac{[SpmX]^3}{c^3 + [SpmX]^3}\right)\left(X_{cap} - [SpmX]\right),$$

where X_{cap} represents the non-zero steady state [SpmX] value and is set to $1-\theta_{DivJ}$ in all simulations unless otherwise stated. The parameter c determines the inflection point at which [SpmX] begins to accumulate rapidly. The rate constant $k_{s,SpmX}$ determines the overall rate of [SpmX] accumulation. Because SpmX localizes to the old pole, upon cytokinesis the [SpmX] value remains constant in the stalked cell, but is reset to 0.01 in the swarmer cell. Importantly, [SpmX] is not set to 0, because this would be a stable state of [SpmX] and therefore [SpmX] would never accumulate in the swarmer cell.

PleC acts as the primary antagonist to DivJ, as it can act as a phosphatase on DivK∼P. Interestingly, DivK∼P can also allosterically bind to PleC to induce its kinase state (Matroule et al., 2004; Paul et al., 2008). Thus, we assume that PleC operates as a phosphatase when not bound to DivK∼P, but otherwise operates as a kinase. Additionally, PleC regulates PleD activity (Aldridge et al., 2003), as discussed further in the "cdG" section.

PleC is recruited to the new pole by PodJ in the pre-divisional phase of the cell cycle (Hinz et al., 2003), however the mechanism of localization is unclear. We propose that the PleC and PodJ localization reaction takes the form, PleC + PodJ ↔ PodJ:PleC → $PleC_{pole}$ + PodJ, which is identical to the structure of Michaelis-Menten kinetics. The overall assumptions leading to the development of the Michaelis-Menten equation are that the substrate-enzyme complex bind and unbind much faster than product formation and that the substrate concentration is much greater than the enzyme concentration. In parallel, we assume that the rate that PodJ and PleC bind/unbind is much faster than [PleC] is converted to $[PleC]_{pole}$, and we assume that the localized concentration of PodJ is much greater than local [PleC]. Therefore, we derive the equation as specified in the "localization" section.

There are two forms of PodJ: $PodJ_L$ and $PodJ_S$. $PodJ_L$ is the active form of PodJ and is responsible for polar recruiting of PleC. PodJ is synthesized in the $PodJ_L$ form (Lawler et al., 2006), and the *podJ* promoter is regulated by GcrA, DnaA and methylation (Lasker et al., 2016a). $PodJ_L$ is converted to $PodJ_S$ by PerP (Chen et al., 2006), which has a promoter regulated by methylation and CtrA (Lasker et al., 2016a). Thus, PerP accumulates in the late pre-divisional cell to impair PodJ activity (Chen et al., 2006). In our model we do not track $PodJ_S$, and $PodJ_L$ is represented by the variable, [PodJ].

cdG. Diguanylate cyclase (DGC) enzymes, including PleD and DgcB, synthesize cdG from two GTP molecules. cdG, in turn, binds allosterically to the I-site of the DGC domain to inhibit activity (Hengge, 2009), which contributes to the steady decrease in cdG following the rapid spike during the G1-S transition (Xu et al., 2020). While it has been demonstrated that cdG binds to PleD allosterically (Chan et al., 2004), no experiments (to our knowledge) have investigated binding with DgcB. Since the I-site is highly conserved in DGC enzymes (Christen et al., 2006), we assume that cdG allosterically inhibits DgcB as well.

PleD can only synthesize cdG in its phosphorylated state. Furthermore, PleD∼P localizes to the stalked pole, while the unphosphorylated form does not (Ardissone and Viollier, 2015; Jenal, 2009). The phosphorylation state of PleD is regulated by PleC phosphatase and DivJ kinase (Jenal, 2009; Lasker et al., 2016b). Given that PleC phosphatase interacts with PleD∼P, but that these proteins localize to opposite poles, we assume that 10% of PleD∼P is freely diffusing and able to interact with PleC phosphatase at the swarmer pole, while the other 90% localizes at the stalked pole.

Phosphodiesterase (PDE) enzymes convert cdG to pGpG (Hengge, 2009). PdeA, the best studied PDE enzyme in *C. crescentus*, also regulates cdG by binding to and inhibiting DgcB (Abel et al., 2011; Ardissone and Viollier, 2015). PdeA synthesis is induced by CtrA and PdeA is degraded by the CpdR-ClpXP complex (Ardissone and Viollier, 2015).

Z-ring. Z-ring assembly and mechanics are complicated, and several models have been published on the dynamics of Z-ring assembly/contraction (Allard and Cytrynbaum, 2009; Erickson, 2009; Lan et al., 2007; Miraldi et al., 2008). Given that the Z-ring is just one small piece of our model, we want to keep the Z-ring component of the model as simple as possible, while accurately predicting the timing of cytokinesis. Figure S7 illustrates how normalized mRNA expression levels of Z-ring relevant genes peak around 120 min of a 150 min cell cycle. In comparison, the Z-ring should completely close around the 130 min mark of a 150 min cell cycle (Judd et al., 2003). Thus, many Z-ring proteins reach peak expression right around the time of Z-ring constriction. Furthermore, many of these genes are activated by CtrA (Lasker et al., 2016a).

Therefore, we model Z-ring proteins as a general variable, [Zproteins], whose synthesis is induced by CtrA∼P. To improve precision of our model, we designed our rate equation for [Zproteins] after a crucial Z-ring protein FtsA, which is responsible for anchoring FtsZ polymers to the cytoplasmic membrane and recruiting downstream Z-ring proteins. The *ftsA* promoter is upregulated by CtrA (Lasker et al., 2016a) and FtsA is quickly degraded in a ClpAP-dependent manner immediately after cytokinesis (Martin et al., 2004; Williams et al., 2014). Taking these facts into account, we write the following differential equation for [Zproteins]:

$$\frac{d[\text{Zproteins}]}{dt} = k_{s,Zp} \cdot \frac{[\text{CtrA} \sim \text{P}]^2}{J_{a,Zp-CtrA}{}^2 + [\text{CtrA} \sim \text{P}]^2} - (\mu + k_{d,Zp} + k_{d,ZP2} \cdot [\text{ClpAP}]) \cdot [\text{Zproteins}].$$

[ClpAP] is a binary variable such that [ClpAP] = 0 for the majority of the cell cycle, but is set to one from the point of Z-ring closure to the point of daughter cell segregation.

Given that multiple Z-ring proteins work together to form a functional Z-ring, it is reasonable to assume that Z-ring assembly and constriction is a cooperative process. Thus, we use a Hill function to model constriction of the Z-ring:

$$\frac{d[\text{Zring}]}{dt} = -k_{zconstrict} \cdot MipZswitch \cdot \frac{[\text{Zproteins}]^5}{(J_{Zring} + \theta_Z[\text{Zring}])^5 + [\text{Zproteins}]^5},$$

where [Zring] = 1 when the Z-ring is fully open and [Zring] = 0 when closed. Notably, the half-maximal rate of Z-ring constriction occurs when [ZProteins] is equal to $J_{Zring} + \theta_Z \cdot$[Zring]. Here, $J_{Zring} + \theta_Z$ dictates the resources needed to initiate cytokinesis (when [Zring] = 1) and J_{Zring} dictates the minimum resources needed to complete cytokinesis (when [Zring] ≈ 0). This feature was introduced for two reasons: 1) A detailed mathematical model of Z-ring constriction in *E. coli* provides evidence that the force required for Z-ring constriction is greatest at the beginning of cytokinesis, and gradually decreases from 8 pN to 3 pN as the Z-ring closes (Lan et al., 2007). 2) Local concentration of Z-ring proteins should increase as the circumference of the Z-ring decreases, which should further facilitate constriction. Thus, we assume that as the Z-ring closes, less total resources are required to maintain constriction. Finally, *MipZswitch* represents the impact of MipZ on Z-ring assembly. At the beginning of the cell cycle, the Z-ring scaffold, composed of FtsZ polymers, remains localized at the new pole. MipZ binds indirectly to DNA, near the *Cori* locus, and once chromosome replication is underway, MipZ migrates with the chromosome's *Cori* locus to the new pole. MipZ then initiates the depolymerization and re-localization of FtsZ. In this way, *C. crescentus* ensures that the Z-ring cannot re-assemble at mid-cell until after the replicating chromosome is well along in the segregation process (Thanbichler and Shapiro, 2006). To account for this activity, *MipZswitch* turns on ([MipZ switch] = 1) after chromosome replication is completed and turns off ([MipZ switch] = 0) after cytokinesis.

Cell growth. Cells grown in PYE and M2G media have the same average cell length and width despite having significantly different cell cycle times (Takacs et al., 2013). Thus, the growth rate and cell cycle time must be interrelated to maintain consistent cell size in different conditions. Since the molecular mechanism of cell size control in *Caulobacter* has not been elucidated and is outside the scope of this model, we do not attempt to accurately model cell growth and size control. However, because cell volume is a variable influencing several equations in our model, we must estimate changes in volume. We use the exponential growth function:

$$\frac{dV}{dt} = \mu V,$$

to model volume growth, and adjust the growth rate μ after each cell division such that:

$$\mu = T^{-1} \cdot \ln \frac{V_{div}}{V_{birth}},$$

where T is the time of the previous cell cycle, V_{birth} is the cell volume at birth, and V_{div} is the targeted volume at division ($V_{div} = 2$). When we run our parameter optimization algorithms, this method ensures that μ adjusts accordingly. In particular, it ensures that the volume of a mutant cell does not go to zero or infinity in mutant strains that have cell cycle times different from a WT cell. With that said, we also expect that *Caulobacter* should have an upper and lower bound for growth rate. Thus, we put a limit on μ such that:

$$0.0038 \leq \mu \leq 0.007.$$

If μ is calculated to be a value outside of these bounds, μ is set to the corresponding limit.

Notably, there is a difference between the timing that the Z-ring closes and the end/beginning of the cell cycle. It has been observed in *C. crescentus* that daughter cells separate approximately 18 $\pm$ 5 min after the Z-ring closes (Judd et al., 2003). In experiments with synchronized *Caulobacter* cells, newly isolated swarmer cells are considered to be at the beginning of a new cell cycle. Since these cells are isolated from the rest of the population (i.e., unseparated cells are excluded), these experiments consider the beginning of the cell cycle to be approximately 18 $\pm$ 5 min after the Z-ring closes. Therefore, we mark the beginning of the cell cycle as 20 min after the Z-ring closes.

Parameter estimation

Parameter values were initially estimated from published experimental sources whenever possible and the remainder were assigned by educated guesswork. To improve the model's performance, we implemented a random-walk algorithm to generate new sets of parameter values and to evaluate each set's performance based on certain criteria built into a 'cost function'. We implement the random-walk algorithm with two goals in mind. The first is to identify a 'best' parameter set with a dramatically smaller cost than the original parameter set. The second is to develop a collection of parameter sets that serve as a sample of 'acceptable' parameter sets close to the best parameter set. In this section, we first explain how we implemented the random-walk algorithm and then we discuss the details of our cost function.

Random-walk algorithm. To find improved parameter sets, we utilized the Monte-Carlo Markov-Chain/Simulated Annealing approach. We start with a 'current' parameter set,

$$\mathbf{p} = \begin{pmatrix} p_1 \\ p_2 \\ \vdots \\ p_x \end{pmatrix},$$

of length x and perturb it to generate a 'temporary' parameter set p', such that:

$$p_i' = p_i(1 + \delta_i \cdot N(0, \sigma)),$$

where $N(0,\sigma)$ is a random number drawn from a normal distribution with mean zero and standard deviation σ. δ_i is a Boolean variable (i.e., $\delta_i = 0$ or 1) that dictates whether or not a given parameter p_i will be subjected to random perturbation. To determine the values of δ_i, we randomly choose n parameters without replacement using MATLAB's built-in function, randsample. If p_i is selected, then δ_i is set to 1. Otherwise $\delta_i = 0$. Additionally, any p_i' that evaluates to a negative number is set to 0.

For a given iteration of the algorithm, the probability that the temporary parameter set replaces the 'current' parameter set is defined as:

$$\mathbf{p} = \mathbf{p}' \text{ if } g \leq Pr,$$
$$Pr = \min\left(\exp\left(\frac{f(\mathbf{p}) - f(\mathbf{p}')}{\tau}\right), 1\right),$$

where g is a random number selected from a uniform distribution between 0 and 1, f is the cost function for the parameter set, and τ is the 'cooling factor' for simulated annealing. Thus, any temporary parameter set that has a lower cost than the 'current' parameter set replaces the 'current' parameter set. Any temporary parameter set that has a higher cost than the 'current' parameter set has a probability Pr of replacing the current parameter set. This process of generating a new (temporary) parameter set and evaluating it compared to the current parameter set is considered one iteration (one step) of the random walk.

Ultimately, the efficiency of the algorithm is tied to the parameters σ, τ and n. A smaller σ corresponds to smaller perturbations from a given parameter set. If σ is very small, it is more likely to generate a p' that is an improvement over p. However, it may take much longer to make larger improvements. τ dictates the probability that a p' that has a higher cost than p will be accepted as the new p. A larger τ improves the algorithm's chances of escaping a local minimum but decreases the probability of identifying a new local minimum. When n is large, more parameters are perturbed in each iteration. As a result, each p' will be further

away (in parameter space) from p. The advantage to a large *n* is that less steps are needed to make a larger change; however, the chances that p' is an improvement over p decreases.

We use this algorithm to develop three collections of parameter sets: Slow, Quick, and Cori^{-}. Slow and Quick parameter sets are parameterized to different CtrA expression patterns (Table S1), while Cori^{-} is parameterized under the assumption that $CtrA_U$ does not bind to *Cori*. Each collection of parameter sets is intended to contain diverse sets of parameter values that adequately fit the biological constraints of the cost function. To create each collection, we first identified a 'best' or 'seed' parameter set for each collection. Starting from a parameter set that we obtained by manually fitting the model to some desired properties, we searched for a seed parameter set in three stages. First, pursue a local minimum using large perturbations and a moderate cooling temperature; second, hone in on a local minimum by making smaller perturbations at a cooler temperature; and third, escape the local minimum (in hopes of finding a radically new parameter set) by making large perturbations at high temperature. The settings for each stage and the number of iterations within each stage were as follows:

Stage #	n	σ	τ	Iterations
1	3	35	2.5	250
2	20	5	0.7	750
3	10	15	25	250

Finally, we repeated this process in a cyclical fashion (stage 1, stage 2, stage 3, stage 1, etc.) until the algorithm stops improving over two cycles. At that point, the parameter set with the best score is defined as the seed parameter set for deriving an entire collection of 'acceptable' parameter sets.

Once the seed parameter set is identified, the parameterization algorithm is run five separate times for 1500 iterations (with the seed parameter set as the initial p for each run) under the following conditions: n = 10, σ = 5, τ = 6. Here, we save each accepted, or 'current', parameter set to develop the parameter set collection. The small perturbations and medium cooling factor ensure that the algorithm stays close to the local minimum, yet frequently accepts randomly generated temporary parameter sets. Running the algorithm five separate times dramatically increases the diversity of the parameter sets within the collection, as each run of the algorithm takes a different randomized path.

Cost function. The cost function *f*(p) is a sum of the scores S of individual simulations of wild-type cells and a selection of mutant strains, simulated for both swarmer (SW) and stalked (ST) cells:

$$f(\mathbf{p}) = 4\cdot(S_{WT,ST} + S_{WT,SW}) + \sum_{m\in M}(S_{m,ST} + S_{m,SW}),$$

where M is the set of mutant strains {Δ*pdeA*, Δ*pleD*, Δ*ccrM*, Δ*gcrA*, Δ*popA*& P*divK*:Tn, P*pleC*:Tn, *divLA601L*, LS1, *ctrAD51E*, *ctrA*Δ*3*Ω, cdG^{0}} that contribute to the cost function. S_m is the score (defined below) for a given strain simulation. Each simulation was run for 1600 min and scores were calculated over the last three cycles of the simulation (discussed below). Both swarmer and stalked cells were simulated for each strain. Wild type (WT) simulation scores are multiplied by four to increase their weight in the parameter estimation process.

The score for a WT cell, SW and ST simulations, is defined as the average score of the last three cell cycles plus the standard deviation of the scores:

$$S_{WT,CT} = \sum_{c=1}^{3}\frac{S^{c}_{WT,CT}}{3} + \sigma_{S_{WT,CT}}.$$

where CT is the cell type and *c* indicates the cell cycle (of the last three cycles in the simulation) being scored. We track the last 3 cell cycles because the system's limit cycle may take more than one cell cycle to complete. In other words, the oscillatory cycle of the system may take more than one cell cycle to return to its starting point. Therefore, we average the scores of the last three cell cycles and penalize for a larger standard deviation among the individual scores. The penalty is implemented because parameter sets with consistent cell cycle oscillations tend to be more robust to parameter perturbations.

For WT simulations, we score an individual swarmer cell cycle as follows:

$$S^{c}_{WT,SW} = w_{rep}\left(\frac{t_{rep,c} - 20}{2}\right)^2 + w_{div}\left(\frac{t_{div,c} - 140}{8}\right)^2 + \sum_{j\epsilon J} w_j \bullet S_{j,c},$$

where w_{rep} and $t_{rep,c}$ are the weight and time of chromosome replication, respectively; w_{div} and $t_{div,c}$ are the weight and time of cell division, respectively. The targeted time of 20 min for chromosome replication and 140 min for cell division is consistent with experimental observations (Bastedo and Marczynski, 2009; Campos et al., 2014; Lott et al., 1987; Quon et al., 1998; Taylor et al., 2011). J is a collection of experimental time course data and j is an index for a given experiment. The data in set J is usually collected from western blots of synchronized populations and quantified using ImageJ (Schneider et al., 2012). Other quantitative data were retrieved directly from the source, such as cdG concentrations (Abel et al., 2013) and DNA synthesis (i.e. percentage of DNA that is hemi-methylation) (Quon et al., 1998). See Table S1 for a list of experiments and the corresponding protein of interest. The score $S_{j,c}$ measures the agreement between the simulation and the experimental data. We calculate $S_{j,c}$ as:

$$S_{j,c} = \sum_{t\epsilon T} \frac{\left(d_{j,t} - \lambda_j \bullet y_{j,t}\right)^2}{n},$$

where t is the time for a given experimental data point, T is the set of all experimental time points, $d_{j,t}$ is the normalized observed concentration in the jth experiment at time t, and $y_{j,t}$ is the simulated value for the corresponding variable at time t. We note that t is normalized to the length of the simulated cell cycle, as cell cycle times vary between experiments. Additionally, n is the number of data points and λ_j is the scaling coefficient that minimizes the score,

$$S_j\left(\lambda_j\right) = \min\left(S_{j*}\left(\lambda_{j*}\right)\right),$$

where S_{j*} is the score for an arbitrary scaling coefficient, λ_{j*}. We find λ_j using the MATLAB algorithm, fminsearch.

In contrast to WT swarmer simulations, we do not score WT stalked simulations in accordance with experimental time course data because there is no relevant time course data (to the best of our knowledge) for the stalked cell cycles in *C. crescentus*. For stalked WT simulations, the score is calculated as:

$$S^{c}_{WT,ST} = \left(\frac{E_{rep,c}}{4}\right)^2 + \left(\frac{t_{div,c} - 110}{6}\right)^2,$$
$$E_{rep,c} = \min\left(abs\left(t_{div,c} - 10 - t_{rep,c}\right), t_{rep,c} + 10\right).$$

$E_{rep,c}$ is the error in timing associated with initiation of chromosomal replication. As far as we know, the timing of chromosome replication has not been measured in the stalked cell, so we assume that the stalk cell should resemble the swarmer cell 30 min into the cell cycle (because the swarmer cell cycle is ~30 min longer than the stalked cell cycle (Laub et al., 2000)). Given that chromosome replication begins approximately 20 min into the swarmer cycle (Quon et al., 1998), we estimate that the chromosome should begin replication in the stalked cell approximately 10 min before cell division (which occurs 8 min after the Z-ring is completely closed).

Similar to WT simulations, we simulate mutant strains for 1600 min and calculate a score from the last three cell cycles:

$$S_{m,CT} = \sum_{c}^{3} \frac{S^{c}_{m,CT}}{3} + \sigma_{S_{m,CT}}.$$

If the cell cycle is arrested, we use a different scoring methodology depending on the strain (discussed in more detail later). We designate the cell cycle as arrested if the cell does not divide within the last 300 min of the simulation.

For strains Δ*pdeA*, Δ*popA*&P*divK*:Tn, *ctrAD51E*, *ctrA*Δ3Ω, and P*pleC*:Tn, the cell cycles are scored as:

$$S^{c}_{m,SW} = \left(\frac{t_{div,c} - 140}{5}\right)^2 + \left(\frac{t_{rep,c} - 20}{4}\right)^2 \text{ if cell cycle not arrested},$$

$$S^{c}_{m,ST} = \left(\frac{t_{div,c} - 110}{5}\right)^2 \text{ ifcellcyclenotarrested},$$
$$S_{m,CT} = \left(\frac{150}{N_{cycles}}\right)^2 \text{ ifcellcyclearrested}.$$

These mutants are described as having 'normal' cell cycles in the literature, meaning that they have relatively normal morphology and cell cycle timing. The first two equations ensure that the cell cycle time of these strains remains close to the WT. The last equation accounts for the total score for mutant, m, if the cell cycle is arrested. Here, N_{cycles} is the number of cell cycles completed successfully prior to cell-cycle arrest. We observe that arrested simulations often complete several rounds of successful cell cycles prior to arrest. A reasonable comparison would be a dampened oscillator. Therefore, if simulations are arrested, the algorithm favors parameter sets that successfully complete more cell cycles before arrest, which enables the algorithm to select parameter sets that are biased toward incremental gains in stability.

Mutant strains LS1, Δ*ccrM*, Δ*gcrA*, cdG^0, Δ*pdeA*,Δ*pleD* and *divL*(*A601L*) each have unique characteristics, and therefore have unique scoring functions. The following text describes how each mutant is scored and the reasoning behind their scoring functions.

The LS1 mutant strain, characterized by constitutive expression of *ccrM*, is a mutant of the WT LS176 strain rather than the conventional WT NA1000 strain of *C. crescentus*. The strain exhibits several defects such as elongation and the accumulation of additional chromosomes; nonetheless, the cell is viable (Zweiger et al., 1994). Given that the cell is a mutant of LS176 rather than the NA1000 strain, which the rest of our model data is based on, we do not specify any details other than that the cell cycle is not arrested. Similarly, the cdG_0 mutant strains are observed to be viable yet elongated and lacking polar organelles (Abel et al., 2013). Without any information regarding the average cell cycle time in cdG_0 mutants, we only score this strain based on viability. Thus, the LS1 and cdG_0 mutants are scored as follows:

$$S_{LS1,CT} = \left(\frac{150}{N_{cycles}}\right)^2 \text{ ifcellcyclearrested},$$
$$S^{c}_{LS1,ST} = 0 \text{ ifcellcyclenotarrested}.$$

The *ccrM* knock-out mutant, Δ*ccrM*, is viable in M2G medium, but the cells exhibit large deviations in cell cycle length with the average cell being 1.5× larger than WT (Gonzalez and Collier, 2013). Δ*ccrM* mutants in PYE medium have decreased viability, but one experiment observed a 3 h cell cycle in PYE medium (Gonzalez and Collier, 2015). Therefore, we score the cell cycle time against 180 min, and leave a large denominator of 15 min due to the large deviations in observed cell cycle length. If the stalked cell cycle is not arrested, we assign a score of zero as the literature does not distinguish between the characteristics of the swarmer and stalked cell cycles of Δ*ccrM* mutants.

$$S_{\Delta ccrM,CT} = \left(\frac{150}{N_{cycles}}\right)^2 \text{ ifcellcyclearrested},$$
$$S^{c}_{\Delta ccrM,SW} = \left(\frac{t_{div,c} - 180}{15}\right)^2 \text{ ifcellcyclenotarrested},$$
$$S^{c}_{\Delta ccrM,ST} = 0 \text{ ifcellcyclenotarrested}.$$

Δ*gcrA* mutants are observed to have a 180 min swarmer cell cycle in M2G medium (Murray et al., 2013). As the timing of the stalked cell cycle is not clear, the Δ*gcrA* mutants are scored as:

$$S_{\Delta gcrA,CT} = \left(\frac{150}{N_{cycles}}\right)^2 \text{ ifcellcyclearrested},$$
$$S^{c}_{\Delta gcrA,SW} = \left(\frac{T - 180}{8}\right)^2 \text{ ifcellcyclenotarrested},$$
$$S^{c}_{\Delta gcrA,ST} = 0 \text{ ifcellcyclenotarrested}.$$

The *divL*(*A601L*) mutant strain, defined by disrupted binding between DivK and DivL, exhibits cell-cycle arrest in G1 (Tsokos et al., 2011). Thus, we score the mutant as:

$$S^{c}_{divL(A601L),CT} = \frac{5 \times 10^4}{t_{div,c}} \text{ ifcellcyclenotarrested},$$

$$S_{divL(A601L),CT} = 5 \cdot (N_{cycles} - 1) \text{ ifcellcyclearrested.}$$

This method ensures that if the cell cycle is not arrested, the algorithm pushes the system in favor of longer *divL*(*A601L*) cell cycles, until the cell cycle is eventually arrested.

Δ*pleD* and Δ*pdeA* have observed average cdG levels of 70% and 123% of WT, respectively, while exhibiting no indication of perturbed cell cycle behavior (Abel et al., 2011, 2013; Lori et al., 2015). Thus, we score these mutants as follows:

$$S^c_{\Delta pleD,SW} = \left(\frac{t_{div,c} - 145}{5}\right)^2 + \left(\frac{t_{rep,c} - 20}{4}\right)^2 + 100 \cdot \left(\frac{cdG_{\Delta pleD,SW}}{cdG_{WT,SW}} - 0.7\right)^2 \text{ ifcellcyclenotarrested,}$$

$$S^c_{\Delta pleD,ST} = \left(\frac{t_{div,c} - 115}{5}\right)^2 + + 100 \cdot \left(\frac{cdG_{\Delta pleD,ST}}{cdG_{WT,ST}} - 0.7\right)^2 \text{ ifcellcyclenotarrested,}$$

$$S^c_{\Delta pdeA,SW} = \left(\frac{t_{div,c} - 145}{5}\right)^2 + \left(\frac{t_{rep,c} - 20}{4}\right)^2 + 100 \cdot \left(\frac{cdG_{WT,SW}}{cdG_{\Delta pdeA,SW}} - 0.81\right)^2 \text{ ifcellcyclenotarrested,}$$

$$S^c_{\Delta pdeA,ST} = \left(\frac{t_{div,c} - 115}{5}\right)^2 + 100 \cdot \left(\frac{cdG_{WT,ST}}{cdG_{\Delta pdeA,ST}} - 0.81\right)^2 \text{ ifcellcyclenotarrested,}$$

$$S_{m,CT} = \left(\frac{150}{N_{cycles}}\right)^2 \text{ ifcellcyclearrested,}$$

where $cdG_{m,CT}$ indicates the average cdG levels in strain m in cell type CT.

Manual intervention in tuning of CORI$^-$ *parameter sets.* CORI$^-$ parameter sets performed poorly, with an average cost of 12,900, compared to SLOW and QUICK parameter sets which had average costs of 850 and 540, respectively. However, despite the poor performance, these CORI$^-$ parameter sets required manual intervention in the search procedure (an intervention that the SLOW and QUICK parameter sets did not require). In our first attempts to parameterize CORI$^-$ simulations, we started with the seed SLOW parameter set, changed the parameter $\sigma_{CtrAU:Cori}$ to one, and ran the algorithm. Although we repeated this process three times, we failed to find a parameter set with viable proteolysis-null mutants, a good fit to WT time course data, and cost less than 32,000 (results not shown). Consequently, we manually tuned a CORI$^-$ parameter set that would have a viable *ctrA*Δ*3*Ω simulation and ran the parameterization algorithm in search of a suitable seed parameter set. The resulting parameter sets were a dramatic improvement over previous attempts, but, nonetheless, exhibited rapid and complete proteolysis of CtrA at the G1-S transition and predicted cell-cycle arrest of cdG^0 mutants. Again, we attempted to manually adjust parameters to correct these issues, but fixing these issues caused failures in other mutant simulations, and the parameterization algorithm forced the simulations to favor rapid CtrA proteolysis and non-viable cdG^0 mutants. After three separate attempts to find CORI$^-$ parameter sets with viable cdG^0 simulations, we chose the best overall seed parameter set and utilized it to generate the CORI$^-$ parameter sets.

Equations and simulation events governing the cell cycle model

In this section, we provide a complete list of equations governing the cell cycle model. For a list of corresponding parameter values, see File S2. Alternative parameter values utilized in mutant simulations are found in Table S2. The parameters designated by red font are specifically included to accommodate mutant simulations, and are always set to zero unless specified otherwise for a given mutant simulation. The one exception is $\sigma_{CtrAU:Cori}$, which is changed depending on whether a simulation includes $CtrA_U$:*Cori* binding or not (as specified in "General simulation methodology").

$$\begin{aligned}\frac{d[CtrA_U]}{dt} = {} & k_{s,CtrA-P1}\frac{\varepsilon_{CtrA-GcrA} \cdot J_{a,CtrA-GcrA} + [GcrA]}{J_{a,CtrA-GcrA} + [GcrA]} \cdot \frac{J^2_{i,CtrA-CtrA\sim P}}{J_{i,CtrA-CtrA} + [CtrA \sim P]^2} \cdot (1 - m_{CtrA-P1} \cdot (2M_{CtrA} - 1)) \\ & + k_{s,CtrA-P2}\frac{\varepsilon_{CtrA-CtrA} \cdot J_{a,CtrA-CtrA} + [CtrA \sim P]^2}{J^2_{a,CtrA-CtrA} + [CtrA \sim P]^2} \cdot \frac{J^2_{i,CtrA-SciP}}{J^2_{i,CtrA-SciP} + [SciP]^2} - \left(\mu + k_{d,CtrA1}\right. \\ & \left. + k_{d,CtrA2} \cdot \frac{[ClpXP]_{complex}}{J_{d,CtrA} + [CtrA_U] + [CtrA \sim P]}\right) \cdot [CtrA_U] + k_{dephos,CtrA} \cdot [CckA]_P \cdot [CtrA \sim P] \\ & - k_{phos,CtrA} \cdot [CtrA_U] \cdot [CckA]_K + k_{s,CtrA\,\Delta\,3\Omega}\end{aligned}$$

$$\frac{d[CtrA\sim P]}{dt} = -\left(\mu + k_{d,CtrA1} + k_{d,CtrA2}\cdot\frac{[ClpXP]_{Complex}}{J_{d,CtrA2} + [CtrA_U] + [CtrA\sim P]}\right)\cdot[CtrA\sim P] - k_{dephos,CtrA}\cdot[CckA]_P\cdot[CtrA\sim P]$$
$$+ k_{phos,CtrA}\cdot[CtrA_U]\cdot[CckA]_K + k_{s,CtrAD51E}$$

$$\frac{d[DnaA]_T}{dt} = k_{s,DnaA1}\frac{J_{i,DnaA-GcrA}}{J_{i,DnaA-GcrA} + [GcrA]}\cdot(1 - 2\,m_{DnaA}\cdot(1 - M_{DnaA})) - (\mu + k_{d,DnaA})\cdot[DnaA]$$

$$\frac{d[DnaA\sim ATP]}{dt} = k_{s,DnaA}\frac{J_{i,DnaA-GcrA}}{J_{i,DnaA-GcrA} + [GcrA]}\cdot(1 - 2\,m_{DnaA}\cdot(1 - M_{DnaA})) - (\mu + k_{d,DnaA} + k_{d,DnaAatp}\cdot RepSwitch)\cdot[DnaA\sim ATP]$$

$$\frac{d[GcrA]}{dt} = k_{s,GcrA}\frac{\varepsilon_{GcrA-DnaA}\cdot J_{a,GcrA-DnaA} + ([DnaA]_T - [DnaA\sim ATP])}{J_{a,GcrA-DnaA} + ([DnaA]_T - [DnaA\sim ATP])}\cdot\frac{J_{i,GcrA-CtrA}{}^2}{J_{i,GcrA-CtrA}{}^2 + [CtrA\sim P]^2} - (\mu + k_{d,GcrA})\cdot[GcrA]$$

$$\frac{d[SciP]}{dt} = k_{s,SciP}\frac{[CtrA\sim P]^2}{J_{a,SciP-CtrA}{}^2 + [CtrA\sim P]^2} - (\mu + k_{d,SciP})\cdot[SciP]$$

$$\frac{d[DivK]}{dt} = k_{s,DivK1} + k_{s,DivK2}\cdot\frac{[CtrA\sim P]^2}{J_{s,DivK-CtrA\sim P}{}^2 + [CtrA\sim P]^2} - (\mu + k_{d,DivK})\cdot[DivK] - k_{phos,DivK1}\cdot[DivJ]_A\cdot[DivK]$$
$$- k_{phos,DivK2}\cdot[PleC]_K\cdot[DivK] + k_{dephos,DivK}\cdot[PleC]\cdot[DivK\sim P] - k^+_{DivJDivK}\cdot[DivJ]\cdot[DivK] + (k^-_{DivJDivK} + k_{d,DivJ})\cdot[DivJ : DivK]$$

$$\frac{d[DivK\sim P]}{dt} = -(\mu + k_{d,DivK})\cdot[DivK\sim P] + k_{phos,DivK1}\cdot[DivJ]_A\cdot[DivK] + k_{phos,DivK2}\cdot[PleC]_K\cdot[DivK]$$
$$- k_{dephos,DivKP+}\cdot[PleC]\cdot[DivK\sim P] + 2\cdot\left((k^-_{PleCDivKP} + k_{d,PleC} + k_{d,DivK})\cdot[PleC : DivK\sim P_2]\right.$$
$$\left. - k^+_{PleCDivKP}\cdot[PleC]\cdot[DivK\sim P]^2\right) - k^+_{DivJDivKP}\cdot[DivJ]\cdot[DivK\sim P] + (k^-_{DivJDivKP} + k_{d,DivJ})\cdot[DivJ : DivK\sim P]$$
$$- k^+_{DivLDivKP}\cdot[DivL]\cdot[DivK\sim P] + (k^-_{DivLDivKP} + k_{d,DivL})\cdot[DivL : DivK\sim P]$$

$$\frac{d[DivJ]}{dt} = k_{s,DivJ} - (\mu + k_{d,DivJ})\cdot[DivJ] - k^+_{DivJDivK}\cdot[DivJ]\cdot[DivK] + (k^-_{DivJDivK} + k_{d,DivK})\cdot[DivJ : DivK]$$
$$- k^+_{DivJDivKP}\cdot[DivJ]\cdot[DivK\sim P] + (k^-_{DivJDivKP} + k_{d,DivK})\cdot[DivJ : DivK\sim P]$$

$$\frac{d[DivJ : DivK]}{dt} = k^+_{DivJDivK}\cdot[DivJ]\cdot[DivK] - (\mu + k^-_{DivJDivK} + k_{d,DivJ} + k_{d,DivK})\cdot[DivJ : DivK]$$

$$\frac{d[DivJ : DivK\sim P]}{dt} = k^+_{DivJDivKP}\cdot[DivJ]\cdot[DivK\sim P] - (\mu + k^-_{DivJDivKP} + k_{d,DivJ} + k_{d,DivK})\cdot[DivJ : DivK\sim P]$$

$$[DivJ]_A = ([DivJ : DivK\sim P] + [DivJ : DivK])\cdot([SpmX] + \theta_{DivJA})$$

$$\frac{d[DivL]}{dt} = k_{s,DivL} - (\mu + k_{d,DivL})\cdot[DivL] - k^+_{DivLDivKP}\cdot[DivL]\cdot[DivK\sim P] + (k^-_{DivLDivKP} + k_{d,DivK})\cdot[DivL : DivK\sim P]$$

$$\frac{d[DivL : DivK\sim P]}{dt} = k^+_{DivLDivKP}\cdot[DivL]\cdot[DivK\sim P] - (\mu + k^-_{DivLDivKP} + k_{d,DivK} + k_{d,DivL})\cdot[DivL : DivK\sim P]$$

$$[DivL]_T = [DivL] + [DivL : DivK\sim P]$$

$$\frac{d[CckA]_T}{dt} = k_{s,CckA} - (\mu + k_{d,CckA})\cdot[CckA]_T$$

$$\frac{d[CckA : CdG]}{dt} = k^+_{CckAcdG}\cdot[cdG]\cdot([CckA]_T - [CckA : CdG]) - k^-_{CckAcdG}\cdot[CckA : cdG] - (\mu + k_{d,CckA})\cdot[CckA : cdG]$$

$$[CckA : DivL]_T = \frac{[CckA]_T + [DivL]_T + \frac{1}{K_{CckADivL}} - \sqrt{\left([CckA]_T + [DivL]_T + \frac{1}{K_{CckA:DivL}}\right)^2 - 4\cdot[CckA]_T\cdot[DivL]_T}}{2}$$

$$[CckA]_P = \frac{[CckA : DivL]_T\cdot[DivL : DivK\sim P]}{[DivL]_T} + [CckA : cdG] - \frac{[CckA : cdG]\cdot\frac{[CckA:DivL]_T\cdot[DivL:DivK\sim P]}{[DivL]_T}}{[CckA]_T}$$

$$[CckA]_K = [CckA]_T - [CckA]_P$$

$$\frac{d[PleC]}{dt} = k_{s,PleC}\cdot(2 - 2\cdot M_{PleC}) - (\mu + k_{d,PleC})\cdot[PleC] + k^-_{PleCDivKP}\cdot[PleC : DivK\sim P_2]$$
$$- k^+_{PleCDivKP}\cdot[PleC]\cdot[DivK\sim P]^2 + 2\cdot k_{d,DivK}\cdot[PleC : DivK\sim P_2]$$

$$\frac{d[PleC : DivK\sim P_2]}{dt} = k^+_{PleCDivKP}\cdot[PleC]\cdot[DivK\sim P]^2 - (k_{d,PleC} + k^-_{PleCDivKP} + 2\cdot k_{d,DivK} + \mu)\cdot[PleC : DivK\sim P_2]$$

$$[PleC]_{tot} = [PleC] + [PleC : DivK\sim P_2]$$

$$\frac{d[PleC]_{Pole}}{dt} = k_{PleCbinding} \cdot ([PleC]_{tot} - [PleC]_{Pole}) \cdot \frac{[PodJ]}{[PodJ] \cdot [V] + J_{PleCPodJ}} - (k_{PleCunbinding} + k_{d,PleC} + \mu) \cdot [PleC]_{Pole}$$

$$\frac{d[PodJ]}{dt} = k_{s,PodJ} \cdot \frac{J_{i,PodJ-DnaA}}{J_{i,PodJ-DnaA} + [DnaA]_T} \cdot \frac{[GcrA]}{J_{a,PodJ-GcrA} + [GcrA]} \cdot (2 - 2 \cdot M_{PodJ}) - (\mu + k_{d,PodJ1}) \cdot [PodJ] - k_{d,PodJ2} \cdot \frac{[PodJ]}{J_{d,PodJ} + [PodJ]} \cdot [PerP]$$

$$\frac{d[PerP]}{dt} = k_{s,PerP} \cdot \frac{[CtrA \sim P]^2}{J_{a,PerP-CtrA}{}^2 + [CtrA \sim P]^2} \cdot (2 - 2 \cdot M_{PodJ}) - (\mu + k_{d,PerP}) \cdot [PerP]$$

$$[DNA]_F = \frac{K_{d1}}{K_{d1} + 2 \cdot [CtrA \sim P] + \frac{[CtrA \sim P]^2}{K_{d3}} + (1 - \sigma_{CtrAU:Cori}) \cdot \left(2 \cdot [CtrA_U] + \frac{[CtrA_U]^2}{K_{d2}} + 2 \cdot \frac{[CtrA_U] \cdot [CtrA \sim P]}{K_{d2}}\right)}$$

$$[DNA : CtrA \sim P_2] = \frac{[CtrA \sim P]^2 \cdot [DNA]_F}{K_{d1} \cdot K_{d3}}$$

$$\frac{d[Ini]}{dt} = (1 - 2\, m_{Ini} \cdot (1 - M_{Ini})) \cdot (1 - [DNA : CtrA \sim P_2])^5 \cdot \left(\frac{[DnaA \sim ATP]}{[DnaA \sim ATP] + J_{a,Ini-DnaA}}\right)^2 - k_{d,Ini} \cdot [Ini]$$

$$\frac{d[Elong]}{dt} = k_{elong} \cdot RepSwitch$$

$$\frac{d[CcrM]}{dt} = k_{s,CcrM} \cdot \frac{[CtrA \sim P]^2}{J_{a,CcrM-CtrA}{}^2 + [CtrA \sim P]^2} \cdot \frac{J_{I,CcrM-DnaA}}{J_{I,CcrM-DnaA} + [DnaA]} \cdot (2 - 2 \cdot M_{CcrM}) - (\mu + k_{d,CcrM}) \cdot [CcrM] + k_{s,LS1}$$

$$\frac{d[SpmX]}{dt} = k_{s,SpmX} \frac{[SpmX]^3}{c^3 + [SpmX]^3} \cdot ((1 - \theta_{DivJA}) \cdot (1 - \sigma_{\Delta SpmX}) - [SpmX])$$

$$\frac{d[Zproteins]}{dt} = k_{s,Zp} \frac{[CtrA \sim P]^2}{J_{a,Zp-CtrA}{}^2 + [CtrA \sim P]^2} - (\mu + k_{d,Zp} + k_{d,ZP2} \cdot [ClpAP]) \cdot [Zproteins]$$

$$\frac{d[Zring]}{dt} = -k_{Zconstrict} \cdot MipZswitch \cdot \frac{[Zproteins]^5}{(J_{Zring} + \theta_Z \cdot [Zring])^5 + [Zproteins]^5}$$

$$\frac{d[V]}{dt} = \mu \cdot [V]$$

$$\mu = T^{-1} \cdot \ln \frac{V_{div}}{V_{birth}}$$

$$\frac{d[CpdR]}{dt} = k_{s,CpdR} \frac{\varepsilon_{CpdR-DnaA} \cdot J_{a,CpdR-DnaA} + [DnaA]_T}{J_{a,CpdR-DnaA} + [DnaA]_T} \cdot \frac{[CtrA \sim P]}{J_{a,CpdR-CtrA} + [CtrA \sim P]} \cdot \frac{J_{i,CckAGcrA}}{J_{i,CckAGcrA} + [GcrA]} + k_{dephos,CpdR} \cdot [CpdR \sim P] \cdot [CckA]_P - k_{phos,CpdR} \cdot [CpdR] \cdot [CckA]_K - (\mu + k_{d,CpdR}) \cdot [CpdR]$$

$$\frac{d[CpdR \sim P]}{dt} = -k_{dephos,CpdR} \cdot [CpdR \sim P] \cdot [CckA]_P + k_{phos,CpdR} \cdot [CpdR] \cdot [CckA]_K - (\mu + k_{d,CpdR}) \cdot [CpdR \sim P]$$

$$\frac{d[RcdA]}{dt} = k_{s,RcdA} \cdot \frac{[CtrA \sim P]^2}{J_{a,RcdACtrA}{}^2 + [CtrA \sim P]^2} - (\mu + k_{d,RcdA}) \cdot [RcdA] - k_{d,RcdA2} \cdot ([RcdA] - [RcdA : PopA]) \cdot \frac{[CpdR]}{J_{d,CpdR} + [CpdR]}$$

$$\frac{d[PopA]}{dt} = k_{s,PopA} \cdot \frac{J_{i,PopA-GcrA}}{J_{i,PopA-GcrA} + [GcrA]} - (\mu + k_{d,PopA}) \cdot [PopA] - k^+_{PopACdG} \cdot [PopA] \cdot [cdG]^2 + k^-_{XCdG} \cdot [PopA : cdG_2]$$

$$\frac{d[PopA : cdG_2]}{dt} = k^+_{PopACdG} \cdot [PopA] \cdot [cdG]^2 - (\mu + k^-_{XCdG} + k_{d,PopA}) \cdot [PopA : cdG_2]$$

$$[PopA]_T = [PopA] + [PopA : cdG_2]$$

$$[RcdA : PopA] = \frac{[PopA]_T + [RcdA] + \frac{1}{K_{RcdAPopA}} - \sqrt{\left([PopA]_T + [RcdA] + \frac{1}{K_{RcdAPopA}}\right)^2 - 4 \cdot [PopA]_T \cdot [RcdA]}}{2}$$

$$[ClpXP]_{Complex} = \frac{[CpdR]}{[CpdR] + \frac{K_{ClpXpCpdR}}{V}} \cdot \frac{[PopA : cdG_2] \cdot [RcdA : PopA]}{[PopA : cdG_2] + [PopA]}$$

$$\frac{d[PdeA]}{dt} = k_{s,PdeA} \cdot \frac{[CtrA \sim P]}{J_{a,PdeACtrA} + [CtrA \sim P]} - k_{d,PdeA2} \cdot [CpdR] \cdot \frac{[PdeA]}{J_{d,PdeA} + [PdeA]} - (\mu + k_{d,PdeA1}) \cdot [PdeA]$$

$$[\mathrm{DgcB}]_a = \max(\mathrm{DgcB} - [\mathrm{PdeA}], 0) \cdot \frac{\mathrm{DgcB} - [\mathrm{DgcB} : \mathrm{cdG}_2]}{\mathrm{DgcB}}$$

$$\frac{d[\mathrm{cdG}]}{dt} = k_{s,\mathrm{cdG1}} \cdot [\mathrm{PleD} \sim \mathrm{P}] + k_{s,\mathrm{cdG2}} \cdot [\mathrm{DgcB}]_a - k_{d,\mathrm{cdG}} \cdot ([\mathrm{PdeA}] + \mathrm{PDE}) \cdot \frac{[\mathrm{cdG}]}{J_{d,\mathrm{cdG}} + [\mathrm{cdG}]} - \mu \cdot [\mathrm{cdG}] + 2 \cdot \left(- k^{+}_{\mathrm{PopACdG}} \cdot [\mathrm{PopA}] \cdot [\mathrm{cdG}]^2 + \left(k^{-}_{\mathrm{XCdG}} + k_{d,\mathrm{PopA}}\right) \cdot [\mathrm{PopA} : \mathrm{cdG}_2] \right) + 2 \cdot \left(- k^{+}_{\mathrm{PleDcdG}} \cdot ([\mathrm{PleD}] + [\mathrm{PleD} \sim \mathrm{P}]) \cdot [\mathrm{cdG}]^2 + \left(k_{d,\mathrm{PleD}} + k^{-}_{\mathrm{XCdG}}\right) \cdot ([\mathrm{PleD} : \mathrm{cdG}_2] + [\mathrm{PleD} \sim \mathrm{P} : \mathrm{cdG}_2]) \right) - k^{+}_{\mathrm{CckAcdG}} \cdot [cdG] \cdot ([CckA]_T - [CckA : CdG]) + k^{-}_{CckAcdG} \cdot [CckA : cdG] + 2 \cdot \left(- k^{+}_{\mathrm{DgcBcdG}} \cdot (\mathrm{DgcB} - [\mathrm{DgcB} : \mathrm{cdG}_2]) \cdot [\mathrm{cdG}]^2 + k^{-}_{\mathrm{XCdG}} \cdot [\mathrm{DgcB} : \mathrm{cdG}_2] \right)$$

$$\frac{d[\mathrm{DgcB} : \mathrm{cdG}_2]}{dt} = k^{+}_{\mathrm{DgcBcdG}} \cdot (\mathrm{DgcB} - [\mathrm{DgcB} : \mathrm{cdG}_2]) \cdot [\mathrm{cdG}]^2 - \left(\mu + k^{-}_{\mathrm{XCdG}}\right) \cdot [\mathrm{DgcB} : \mathrm{cdG}_2]$$

$$\frac{d[\mathrm{PleD}]}{dt} = k_{s,\mathrm{PleD}} \cdot \frac{[\mathrm{CtrA} \sim \mathrm{P}]^2}{J_{a,\mathrm{PleD-CtrA}}{}^2 + [\mathrm{CtrA} \sim \mathrm{P}]^2} - (\mu + k_{d,\mathrm{PleD}}) \cdot [\mathrm{PleD}] - k_{\mathrm{phos,PleD}} \cdot [\mathrm{DivJ}]_A \cdot [\mathrm{PleD}] + \left(\left(\frac{1}{10}\right) + \left(\frac{9}{10}\right) \cdot \frac{[\mathrm{PleC}]_{tot} - [\mathrm{PleC}]_{pole}}{[\mathrm{PleC}]_{tot}} \right) \cdot k_{\mathrm{dephos,PleD}} \cdot [\mathrm{PleC}] \cdot [\mathrm{PleD} \sim \mathrm{P}] - k^{+}_{\mathrm{PleDcdG}} \cdot [\mathrm{PleD}] \cdot [\mathrm{cdG}]^2 + k^{-}_{\mathrm{XCdG}} \cdot [\mathrm{PleD} : \mathrm{cdG}_2]$$

$$\frac{d[\mathrm{PleD} \sim \mathrm{P}]}{dt} = - (\mu + k_{d,\mathrm{PleD}}) \cdot [\mathrm{PleD} \sim \mathrm{P}] + k_{\mathrm{phos,PleD}} \cdot [\mathrm{DivJ}]_A \cdot [\mathrm{PleD}] - \left(\left(\frac{1}{10}\right) + \left(\frac{9}{10}\right) \cdot \frac{[\mathrm{PleC}]_{tot} - [\mathrm{PleC}]_{pole}}{[\mathrm{PleC}]_{tot}} \right) \cdot k_{\mathrm{dephos,PleD}} \cdot [\mathrm{PleC}] \cdot [\mathrm{PleD} \sim P] - k^{+}_{PleDcdG} \cdot [\mathrm{PleD} \sim \mathrm{P}] \cdot [\mathrm{cdG}]^2 + k^{-}_{\mathrm{XCdG}} \cdot [\mathrm{PleD} \sim \mathrm{P} : \mathrm{cdG}_2]$$

$$\frac{d[\mathrm{PleD} : \mathrm{cdG}_2]}{dt} = - (\mu + k_{d,\mathrm{PleD}}) \cdot [\mathrm{PleD} : \mathrm{cdG}_2] - k_{\mathrm{phos,PleD}} \cdot [\mathrm{DivJ}]_A \cdot [\mathrm{PleD} : \mathrm{cdG}_2] + \left(\left(\frac{1}{10}\right) + \left(\frac{9}{10}\right) \cdot \frac{[\mathrm{PleC}]_{tot} - [\mathrm{PleC}]_{pole}}{[\mathrm{PleC}]_{tot}} \right) \cdot k_{\mathrm{dephos,PleD}} \cdot [\mathrm{PleC}] \cdot [\mathrm{PleD} \sim \mathrm{P} : \mathrm{cdG}_2] + k^{+}_{\mathrm{PleDcdG}} \cdot [\mathrm{PleD}] \cdot [\mathrm{cdG}]^2 - k^{-}_{\mathrm{XCdG}} \cdot [\mathrm{PleD} : \mathrm{cdG}_2]$$

$$\frac{d[\mathrm{PleD} \sim \mathrm{P} : \mathrm{cdG}_2]}{dt} = - (\mu + k_{d,\mathrm{PleD}}) \cdot [\mathrm{PleD} \sim \mathrm{P} : \mathrm{cdG}_2] + k_{\mathrm{phos,PleD}} \cdot [\mathrm{DivJ}]_A \cdot [\mathrm{PleD} : \mathrm{cdG}_2] - \left(\left(\frac{1}{10}\right) + \left(\frac{9}{10}\right) \cdot \frac{[\mathrm{PleC}]_{tot} - [\mathrm{PleC}]_{pole}}{[\mathrm{PleC}]_{tot}} \right) \cdot k_{\mathrm{dephos,PleD}} \cdot [\mathrm{PleC}] \cdot [\mathrm{PleD} \sim \mathrm{P} : \mathrm{cdG}_2] + k^{+}_{\mathrm{PleDcdG}} \cdot [\mathrm{PleD} \sim \mathrm{P}] \cdot [\mathrm{cdG}]^2 - k^{-}_{\mathrm{XCdG}} \cdot [\mathrm{PleD} \sim \mathrm{P} : \mathrm{cdG}_2]$$

Events and switches

1) When [Zring] = 0 the cell volumes are split and protein concentrations shift in accordance with the equations specified below.
2) A new cell cycle begins when daughter cells separate 20 min after [Zring] = 0.
3) M_i = 0.5 when the replication fork passes through gene i (i.e. [Elong] = 0.36 for *ctrA*, [Elong] = 0.01 for *dnaA*, [Elong] = 0.25 for *ccrM*, and [Elong] = 0.75 for *perP*). M_i = 1 when [CcrM] = 0.65.
4) [Zring] = 1 at beginning of each cell cycle.
5) *MipZswitch* = 0 when [Zring] = 0; *MipZswitch* = 1 when [Elong] = 1.
6) [ClpAP] = 1 when [Zring] = 0; [ClpAP] = 0 at beginning of each cell cycle.
7) *RepSwitch* = 1 when [Ini] = 1 and [Ini] is immediately reset to 0.
8) *RepSwitch* = 0 when [Elong] = 1
9) [Elong] = 0 when [Zring] = 0.

Concentration shifts due to cytokinesis

Swarmer cell.

$$[\mathrm{PleC}]_{\mathrm{Sw}} = [\mathrm{PleC}]\cdot\frac{[\mathrm{PleC}]_{\mathrm{Pole}}}{0.46\cdot[\mathrm{PleC}]_{\mathrm{tot}}} + \left([\mathrm{PleC}]_{\mathrm{tot}} - [\mathrm{PleC}]_{\mathrm{Pole}}\right)\cdot\frac{[\mathrm{PleC}]}{[\mathrm{PleC}]_{\mathrm{tot}}}$$

$$[\mathrm{PleC}:\mathrm{DivK}\sim\mathrm{P}_2]_{\mathrm{Sw}} = [\mathrm{PleC}:\mathrm{DivK}\sim\mathrm{P}_2]\cdot\frac{[\mathrm{PleC}]_{\mathrm{Pole}}}{0.46\cdot[\mathrm{PleC}]_{\mathrm{tot}}} + \left([\mathrm{PleC}]_{\mathrm{tot}} - [\mathrm{PleC}]_{\mathrm{Pole}}\right)\cdot\frac{[\mathrm{PleC}:\mathrm{DivK}\sim\mathrm{P}_2]}{[\mathrm{PleC}]_{\mathrm{tot}}}$$

$$[\mathrm{PleC}]_{\mathrm{Pole,Sw}} = \frac{[\mathrm{PleC}]_{\mathrm{Pole}}}{0.46}$$

$$[\mathrm{PleD}\sim\mathrm{P}]_{\mathrm{Sw}} = \left(\frac{1}{10}\right)\cdot[\mathrm{PleD}\sim\mathrm{P}]$$

$$[\mathrm{PleD}\sim\mathrm{P}:\mathrm{cdG}_2]_{\mathrm{Sw}} = \left(\frac{1}{10}\right)\cdot[\mathrm{PleD}\sim\mathrm{P}:\mathrm{cdG}_2]$$

$$[\mathrm{DivJ}]_{\mathrm{Sw}} = 0$$

$$[\mathrm{DivJ}:\mathrm{DivK}]_{\mathrm{Sw}} = 0$$

$$[\mathrm{DivJ}:\mathrm{DivK}\sim\mathrm{P}]_{\mathrm{Sw}} = 0$$

$$[\mathrm{CpdR}]_{\mathrm{Sw}} = 0$$

$$[\mathrm{RcdA}]_{\mathrm{Sw}} = [\mathrm{RcdA}]\cdot\left(1 - \frac{[\mathrm{CpdR}]}{[\mathrm{CpdR}] + \frac{K_{\mathrm{ClpXpCpdR}}}{V}}\right)$$

$$[\mathrm{PopA}]_{\mathrm{Sw}} = [\mathrm{PopA}]\cdot\left(1 - \frac{[\mathrm{CpdR}]}{[\mathrm{CpdR}] + \frac{K_{\mathrm{ClpXpCpdR}}}{V}}\cdot\frac{[\mathrm{RcdA}:\mathrm{PopA}]_{\mathrm{T}}}{[\mathrm{PopA}]_{\mathrm{T}}}\right)$$

$$[\mathrm{PopA}:\mathrm{cdG}_2]_{\mathrm{Sw}} = [\mathrm{PopA}:\mathrm{cdG}_2]\cdot\left(1 - \frac{[\mathrm{CpdR}]}{[\mathrm{CpdR}] + \frac{K_{\mathrm{ClpXpCpdR}}}{V}}\cdot\frac{[\mathrm{RcdA}:\mathrm{PopA}]_{\mathrm{T}}}{[\mathrm{PopA}]_{\mathrm{T}}}\right)$$

$$[\mathrm{CckA}:\mathrm{cdG}]_{\mathrm{Sw}} = \left(\frac{[\mathrm{CckA}:\mathrm{cdG}]}{[\mathrm{CckA}]_{\mathrm{T}}}\right)\left([\mathrm{CckA}]_{\mathrm{T}} - [\mathrm{CckA}:\mathrm{DivL}]_{\mathrm{T}} + \frac{1}{0.46}\left([\mathrm{CckA}:\mathrm{DivL}]_{\mathrm{T}} - \frac{[\mathrm{CckA}:\mathrm{DivL}]_{\mathrm{T}}\cdot[\mathrm{DivL}:\mathrm{DivK}\sim\mathrm{P}]}{[\mathrm{DivL}]_{\mathrm{T}}}\right)\right)$$

$$[\mathrm{CckA}]_{\mathrm{T,Sw}} = \frac{[\mathrm{CckA}:\mathrm{DivL}]_{\mathrm{T}}}{0.46}\left(1 - \frac{[\mathrm{DivL}:\mathrm{DivK}\sim\mathrm{P}]}{[\mathrm{DivL}]_{\mathrm{T}}}\right) + [\mathrm{CckA}]_{\mathrm{T}} - [\mathrm{CckA}:\mathrm{DivL}]_{\mathrm{T}}$$

$$[\mathrm{DivL}]_{\mathrm{Sw}} = \frac{[\mathrm{DivL}]}{0.46}$$

$$[\mathrm{DivL}:\mathrm{DivK}\sim\mathrm{P}]_{\mathrm{Sw}} = 0$$

$$[\mathrm{DivL}:\mathrm{DivK}]_{\mathrm{Sw}} = \frac{[\mathrm{DivL}:\mathrm{DivK}]}{0.46}$$

$$[\mathrm{V}]_{\mathrm{Sw}} = 0.46\cdot[\mathrm{V}]$$

Stalked cell.

$$[\mathrm{PleC}]_{\mathrm{St}} = \left([\mathrm{PleC}]_{\mathrm{tot}} - [\mathrm{PleC}]_{\mathrm{Pole}}\right)\cdot\frac{[\mathrm{PleC}]}{[\mathrm{PleC}]_{\mathrm{tot}}}$$

$$[\mathrm{PleC}:\mathrm{DivK}\sim\mathrm{P}_2]_{\mathrm{St}} = \left([\mathrm{PleC}]_{\mathrm{tot}} - [\mathrm{PleC}]_{\mathrm{Pole}}\right)\cdot\frac{[\mathrm{PleC}:\mathrm{DivK}\sim\mathrm{P}_2]}{[\mathrm{PleC}]_{\mathrm{tot}}}$$

$$[\mathrm{PleC}]_{\mathrm{Pole,St}} = 0$$

$$[\mathrm{PleD}\sim\mathrm{P}]_{St} = \left(\frac{9}{10}\right)\cdot\frac{[\mathrm{PleD}\sim\mathrm{P}]}{0.54} + \left(\frac{1}{10}\right)\cdot[\mathrm{PleD}\sim\mathrm{P}]$$

$$[\mathrm{PleD}\sim\mathrm{P}:\mathrm{cdG}_2]_{\mathrm{ST}} = \left(\frac{9}{10}\right)\cdot\frac{[\mathrm{PleD}\sim\mathrm{P}:\mathrm{cdG}_2]}{0.54} + \left(\frac{1}{10}\right)\cdot[\mathrm{PleD}\sim\mathrm{P}:\mathrm{cdG}_2]$$

$$[\mathrm{DivJ}]_{\mathrm{St}} = \frac{[\mathrm{DivJ}]}{0.54}$$

$$[\mathrm{DivJ}:\mathrm{DivK}]_{\mathrm{St}} = \frac{[\mathrm{DivJ}:\mathrm{DivK}]}{0.54}$$

$$[\mathrm{DivJ}:\mathrm{DivK}\sim\mathrm{P}]_{\mathrm{St}} = \frac{[\mathrm{DivJ}:\mathrm{DivK}\sim\mathrm{P}]}{0.54}$$

$$[\mathrm{CpdR}]_{St} = \frac{[\mathrm{CpdR}]}{0.54}$$

$$[\mathrm{RcdA}]_{St} = [\mathrm{RcdA}] \cdot \left(1 - \frac{[\mathrm{CpdR}]}{[\mathrm{CpdR}] + \frac{K_{\mathrm{ClpXpCpdR}}}{V}}\right) + \frac{1}{0.54} \cdot \frac{[\mathrm{RcdA}] \cdot [\mathrm{CpdR}]}{[\mathrm{CpdR}] + \frac{K_{\mathrm{ClpXpCpdR}}}{V}}$$

$$[\mathrm{PopA}]_{St} = [\mathrm{PopA}] \cdot \left(1 - \frac{[\mathrm{CpdR}]}{[\mathrm{CpdR}] + \frac{K_{\mathrm{ClpXpCpdR}}}{V}} \cdot \frac{[\mathrm{RcdA} : \mathrm{PopA}]_T}{[\mathrm{PopA}]_T} + \frac{1}{0.54} \cdot \frac{[\mathrm{CpdR}]}{[\mathrm{CpdR}] + \frac{K_{\mathrm{ClpXpCpdR}}}{V}} \cdot \frac{[\mathrm{RcdA} : \mathrm{PopA}]_T}{[\mathrm{PopA}]_T}\right)$$

$$[\mathrm{PopA} : \mathrm{cdG}_2]_{St} = [\mathrm{PopA} : \mathrm{cdG}_2] \cdot \left(1 - \frac{[\mathrm{CpdR}]}{[\mathrm{CpdR}] + \frac{K_{\mathrm{ClpXpCpdR}}}{V}} \cdot \frac{[\mathrm{RcdA} : \mathrm{PopA}]_T}{[\mathrm{PopA}]_T} + \frac{1}{0.54} \cdot \frac{[\mathrm{CpdR}]}{[\mathrm{CpdR}] + \frac{K_{\mathrm{ClpXpCpdR}}}{V}} \cdot \frac{[\mathrm{RcdA} : \mathrm{PopA}]_T}{[\mathrm{PopA}]_T}\right)$$

$$[\mathrm{CckA} : \mathrm{cdG}]_{St} = \left(\frac{[\mathrm{CckA} : \mathrm{cdG}]}{[\mathrm{CckA}]_T}\right)\left([\mathrm{CckA}]_T - [\mathrm{CckA} : \mathrm{DivL}]_T + \frac{1}{0.56}\left(\frac{[\mathrm{CckA} : \mathrm{DivL}]_T \cdot [\mathrm{DivL} : \mathrm{DivK} \sim \mathrm{P}]}{[\mathrm{DivL}]_T}\right)\right)$$

$$[\mathrm{CckA}]_{T,St} = \frac{1}{0.56}\left(\frac{[\mathrm{CckA} : \mathrm{DivL}]_T \cdot [\mathrm{DivL} : \mathrm{DivK} \sim \mathrm{P}]}{[\mathrm{DivL}]_T}\right) + [\mathrm{CckA}]_T - [\mathrm{CckA} : \mathrm{DivL}]_T$$

$$[\mathrm{DivL}]_{St} = 0$$

$$[\mathrm{DivL} : \mathrm{DivK} \sim \mathrm{P}]_{St} = \frac{[\mathrm{DivL} : \mathrm{DivK} \sim \mathrm{P}]}{0.54}$$

$$[\mathrm{DivL} : \mathrm{DivK}]_{St} = 0$$

$$[V]_{St} = 0.54 \cdot [V]$$

QUANTIFICATION AND STATISTICAL ANALYSIS

All western blots retrieved from the literature were analyzed by ImageJ (Schneider et al., 2012) to produce normalized, quantitative data for protein expression levels over time. A simulated 'cell' was determined to be arrested if it did not initiate chromosome replication or divide in the last 300 min of the simulation. All statistical analyses were performed utilizing built-in MATLAB functions. The distribution of scores for each collection of parameter sets was plotted utilizing MATLAB's boxplot function, which automatically calculates the median and interquartile range (IQR) while defining outliers as scores that deviate from the median by more than 1.5 times the IQR. We note that parameter sets that are considered outliers in the box plot (Figure 5D) are not precluded from result simulations and analysis.

For our analysis of the timing of cell cycle events (i.e., t^{cr} and t^{div}), we removed times that were identified as outliers utilizing the MATLAB function, rmoutliers, which defines an outlier as any time point that is more than three scaled median absolute deviations from the median time. Standard deviations are calculated utilizing the MATLAB function, std.